Numerical Issues Arising in the Simulations of Transient Water Flow in Layered Unsaturated Soils

by

Ruowen Liu

A Dissertation Presented in Partial Fulfillment
of the Requirements for the Degree
Doctor of Philosophy

Approved April 2017 by the
Graduate Supervisory Committee:

Bruno Welfert, Chair
Sandra Houston
Zdzislaw Jackiewicz
Christian Ringhofer
Claudia Zapata

ARIZONA STATE UNIVERSITY

May 2017

ABSTRACT

The geotechnical community typically relies on recommendations made from numerical simulations. Commercial software exhibits (local) numerical instabilities in layered soils across soil interfaces. This research work investigates unsaturated moisture flow in layered soils and identifies a possible source of numerical instabilities across soil interfaces and potential improvement in numerical schemes for solving the Richards' equation. The numerical issue at soil interfaces is addressed by a (nonlinear) interface problem. A full analysis of the simplest soil hydraulic model, the Gardner model, identifies the conditions of ill-posedness of the interface problem. Numerical experiments on various (more advanced and practical) soil hydraulic models show that the interface problem can also be ill-posed under certain circumstances. Spurious numerical ponding and/or oscillations around soil interfaces are observed consequently. This work also investigates the impact of different averaging schemes for cell-centered conductivities on the propensity of ill-posedness of the interface problem and concludes that smaller averaging conductivities are more likely to trigger numerical instabilities. In addition, an agent-based stochastic soil model, with hydraulic properties defined at the finite difference cell level, results in a large number of interface problems. This research compares sequences of stochastic realizations in heterogeneous unsaturated soils with the numerical solution using homogenized soil parameters. The mean of stochastic realizations is not identical to the solution obtained from homogenized soil parameters.

ACKNOWLEDGMENTS

I would like to express my deepest appreciation to my advisor Dr. Bruno Welfert, who provided insightful guidance and persistent help during my whole Ph.D. study. Without him, this dissertation would not have been possible.

I am also deeply grateful to Professor Sandra Houston, to expose me to the world of unsaturated soil mechanics. I also give thanks to my committee members, Professor Zdzislaw Jackiewicz, Professor Christian Ringhofer and Dr. Claudia Zapata for their invaluable support.

I would like to thank the School of Mathematical & Statistical Sciences at ASU for their financial and professional support, including the Summer Research Block Grant (2012). I would like to thank the National Sciences Foundation for partially funding my research under grant CMMI-0825089 and for their continued dedication to the advancement of science. The opinions, conclusion, and interpretations expressed in this dissertation are those of the author and not necessarily of the National Science Foundation.

I would like to thank my friends at Arizona State University who make my school life colorful. Thanks to their help and discussions throughout my study program.

I am also very grateful to the outstanding female faculty at Arizona State University, including Dr. Houston, Dr. Zapata, Dr. Marilyn Carlson, Dr. Katie Kolossa and many more, for being female role models in science, technology, engineering, and mathematics (STEM). Their contributions and achievements amplify my STEM career aspirations.

Finally, I would like to express my deepest thanks to all my loved ones for their companion and encouragement. Thanks to my parents who always support me to chase my dreams. Special thanks to Fangfei Li who never hesitates to help and inspire me.

TABLE OF CONTENTS

Page

LIST OF TABLES v

LIST OF FIGURES vi

LIST OF SYMBOLS x

CHAPTER

1 INTRODUCTION 1

1.1 Background 1

1.2 Literature Review 2

1.3 Outline of This Work 5

2 MATHEMATICAL MODEL 6

2.1 Richards' Equation 6

2.2 Soil Hydraulic Relations 8

2.3 Interface Problem 10

2.3.1 Formulation of the Interface Equation 10

2.3.2 Ill-posedness of the Interface Equation 14

2.4 Averaging Methods for Cell-Centered Conductivities 20

2.5 A Reduced Model for Stochastic Soil Hydraulic Parameters 25

3 NUMERICAL SIMULATIONS 34

3.1 Investigation on Interface Problems in Two-Layer Soils 34

3.1.1 Two-Layer Case Using Gardner Model 34

3.1.2 Two-Layer Case Using MvG Model 41

3.1.3 Two-Layer Case Using FXLR Model 43

3.2 Comparison of Averaging Methods for Cell-Centered Conductivities 45

3.2.1 Comparison in a Two-Layer Soil 45

CHAPTER Page

3.2.2 Comparison of Geometric Mean and Log-Mean with Mesh Refinement 48
3.2.3 Comparison in Multi-Layer Soils 51
3.3 Numerical Results with Stochastic Soil Hydraulic Parameters 61
4 CONCLUSIONS AND FUTURE WORK 71
4.1 Conclusions 71
4.2 Future Work 74
4.2.1 2D Cracked Soil 74
4.2.2 Fingering Effect 74
REFERENCES 77
APPENDIX
A EXPLICIT CRITERIA FOR GARDNER MODEL WITH GEOMETRIC MEAN 81
A.1 Number of Roots of Equation (2.24) 82
A.2 Stability of Fixed-Point Iteration 83
B REDUCTION IN STOCHASTIC EQUATIONS 84
B.1 Reduction in Equation (2.44) 85
B.2 Reduction in Equation (2.63) 86
C NUMERICAL IMPLEMENTATIONS 88
C.1 Non-Dimensionalization Method 89
C.2 Indexing for Various Boundary Conditions 90
C.3 Solving the Interface Equation by Iterative Methods 91
C.4 Using DVODE 92
C.5 Using OpenMP 93

LIST OF TABLES

Table Page

2.1 The MvG Parameters of Five Example Soils from van Genuchten (1980) and the Equivalent α for the Gardner Model According to Equation (2.10). 11

2.2 Soil Parameters for Two-Cell Cases (in Figure 2.6) to Exhibit Multiple Solutions to the Interface Equation. 16

3.1 Dimensionless Soil Hydraulic Parameters for the Two-Layer Case Using the Gardner Model. 35

3.2 Dimensionless Soil Hydraulic Parameters for the Two-Layer Case Using the MvG Model. 41

3.3 Dimensionless Soil Hydraulic Parameters for the Two-Layer Case Using the FXLR Model (Transparent Interface) 43

3.4 Gardner Model: Well-Posedness of the Interface Problem Using Different Conductivity Averaging Methods. 46

LIST OF FIGURES

Figure Page

2.1 The Richards' Equation Is Solved Numerically in an n-Layer Soil Column. 7

2.2 Staggered Finite Difference Water Content θ and Flux q Grids. 8

2.3 A Soil Interface and the (Staggered) Finite Difference Scheme at the Interface. 11

2.4 Fictitious Nodes in Extended Layers. 12

2.5 Examples of Stability Issues in Various Software a) Suction Oscillation with Depth, b) Actual Flux Oscillation at Soil Surface, and c) Suction with Depth Increased Monotonically to Unreasonable Values (Excerpt from PhD Dissertation of Dye, Heather Beate, April 2008, Arizona State University). Copy Right 2008 by ProQuest LLC. 15

2.6 Multiple Solutions of $r = g(r)$ Exist While Equation (2.22) Is Satisfied. 16

2.7 The (μ, λ)-Space Criteria for the Gardner Model with The Geometric Mean. 18

2.8 Fixed-Point Iteration and Newton Iteration for Interface Problem under the Gardner Model and the Geometric Mean for Cell-Centered Hydraulic Conductivities. 19

2.9 Arithmetic Mean as a Parallel Flow and Harmonic Mean as a Serial Flow in Layered Soils. 21

2.10 Comparison of Values of Four Averaging Means from the Smallest (Left) to the Largest (Right). 23

2.11 ω_g/ω_{total} and ω_l/ω_{total} as Functions of $\ln(\tau)$. 23

3.1 Gardner Model Case 1. 37

3.2 Numerical Solutions of the Gardner Model Case 1 38

3.3 Gardner Model Case 2. 39

Figure Page

3.4 Numerical Solutions for the MvG Model 42
3.5 Numerical Solutions for the FXLR Model with a Transparent Interface ($z = 0.5$) Forcing $r = 1$. 44
3.6 Numerical Solutions for the FXLR Model with a Transparent Interface ($z = 0.5$) Using the Root Larger Than 1. 45
3.7 Numerical Solutions of Unsaturated Flow in a Two-Layer Soil Using Different Averaging Methods for Cell-Centered Hydraulic Conductivities When $N = 100$. 47
3.8 Local Mesh Refinement Around a Soil Interface. New Grid Points Are the Trisection Points of the Previous Interface Cell, $\Delta_{j-1} = \Delta_j = \Delta_{j+1}$. 49
3.9 Comparison of Numerical Solutions Using the Geometric Mean and the Log-Mean, with Spatial Mesh Refinements at the Interface ($z = 0.5$). 50
3.10 Finite Difference Scheme in an n-Layer Soil. 51
3.11 Numerical Simulations at Different Times of a 1D Infiltration Process in a Five-Layer Soil Using the Gardner Model. Soil Interfaces Are $z = 0.2, 0.4, 0.6, 0.8$. 53
3.12 Depth vs Time Relation for Where and When a Given Pressure Head Value Is Reached in a 1D Infiltration Process in a Ten-Layer Soil Setting Using the MvG Model. 54
3.13 Numerical Simulations at Different Times of a 1D Infiltration Process in a Ten-Layer Soil Using the MvG Model – (1). 54
3.14 Numerical Simulations at Different Times of a 1D Infiltration Process in a Ten-Layer Soil Using the MvG Model – (2). 55

3.15 Numerical Simulations at Different Times of a 1D Infiltration Process in a Ten-Layer Soil Using the MvG Model – (3). 56
3.16 Numerical Simulations at Different Times of a 1D Infiltration Process in a Ten-Layer Soil Using the MvG Model – (4). 57
3.17 Numerical Simulations at Different Times of a 1D Infiltration Process in a Ten-Layer Soil Using the MvG Model – (5). 58
3.18 Numerical Simulations at Different Times of a 1D Infiltration Process in a Ten-Layer Soil Using the MvG Model – (6). 59
3.19 Depth vs Time Relation for Where and When a Given Pressure Head Value Is Reached in a 1D Infiltration Process in a Ten-Layer Soil Setting Using the FXLR Model. 60
3.20 Numerical Simulations at Different Times of a 1D Infiltration Process in a Ten-Layer Soil Using the FXLR Model. 61
3.21 Comparison of Mean of DNS (Solid), Solution Using Homogenized Parameters (Dashed), and Solution of the Reduced Model (Circle), for $\sigma_b = 0.2, 0.4$. 64
3.22 Comparison of Mean of DNS (Solid), Solution Using Homogenized Parameters (Dashed), and Solution of the Reduced Model (Circle), for $\sigma_b = 0.8, 1.2$. 65
3.23 Four DNS Realizations (Solid Curves) for $\sigma_b = 0.8$, Compared with the Solution Using Homogenized Parameters (Dashed Curves), Corresponding to Figure 3.22(a). 66

Figure Page

3.24 Histogram and PDF of DNS When $\sigma_b = 0.2$. The Mean of DNS Is Compared with the Solution Using Homogenized Soil Parameters or the Reduced Model. 67
3.25 Histogram and PDF of DNS When $\sigma_b = 0.4$. The Mean of DNS Is Compared with the Solution Using Homogenized Soil Parameters or the Reduced Model. 68
3.26 Histogram and PDF of DNS When $\sigma_b = 0.8$. The Mean of DNS Is Compared with the Solution Using Homogenized Soil Parameters or the Reduced Model. 69
3.27 Histogram and PDF of DNS When $\sigma_b = 1.2$. The Mean of DNS Is Compared with the Solution Using Homogenized Soil Parameters or the Reduced Model. 70
C.1 Mesh Indexing for Various Boundary Conditions. 90

LIST OF SYMBOLS

α	soil hydraulic model parameter [L^{-1}]
A	an arbitrary matrix
b	natural logarithm of β
β	non-dimensionalized saturated conductivity (soil model parameter)
D	differentiation notation, e.g., $D_{\boldsymbol{b}}$, $D_{\boldsymbol{\theta}}$, etc.
δh	difference between the actual and the fictitious nodal conductivity [L]
Δ	one-dimensional spatial cell size [L]
E	expectation
$\boldsymbol{\eta}$	a vector in the reduced model for stochastic soil hydraulic parameters
f	function notation in Netwon iteration solving the interface equation
g	function notation in Picard iteration solving the interface equation
G	a difference operator acting on vector
G_c	a column difference operator acting on matrix
G_r	a row difference operator acting on matrix
h	capillary pressure head [L]
H	a matrix in the reduced model for stochastic soil hydraulic parameters
i, j, k	integer index
K	soil hydraulic conductivity [L/T]
K_s	saturated hydraulic conductivity [L/T]
κ	a vector in the reduced model for stochastic soil hydraulic parameters
L	a lower shift matrix
λ	interface equation parameter
m	soil hydraulic model parameter
μ	interface equation parameter

n	soil hydraulic model parameter or an integer index
N	number of interior grid points
ω_{g}	difference between the geometric mean and the harmonic mean
ω_{l}	difference between the log-mean and the harmonic mean
ω_{total}	difference between the arithmetic mean and the harmonic mean
p	soil hydraulic model parameter
P	a matrix in the reduced model for stochastic soil hydraulic parameters
q	infiltration flux [L/T]
r	ratio of interface conductivities in extended layers
S_e	effective saturation
t	time [T]
τ	ratio of adjacent nodal conductivities
θ	volumetric water content
θ_r	residual volumetric water content
θ_s	saturated volumetric water content
U	an upper shift matrix
V	an identical matrix with reduced dimensions
z	depth (positive downward) [L]
$\boldsymbol{\zeta}$	a vector in the reduced model for stochastic soil hydraulic parameters

Chapter 1

INTRODUCTION

1.1 Background

The soil between the land surface and the water table of groundwater, known as the vadose zone, is unsaturated and often made up of distinct horizontal layers. Soil layers can form naturally (such as sedimentation) or due to human activities (such as agricultural practices and remove-and-replace techniques in construction). The prediction of moisture movement in the vadose zone is of great importance in many fields, such as environmental management, geotechnical engineering, agriculture engineering, contaminant control and flood control. The laboratory experiments on soil hydraulic properties may take days or weeks, and are still subject to errors resulting from response hysteresis and limitations of testing methods, among others. In situ data are more difficult to obtain consistently not only because of long periods of time for measurements but also because of change of climates, human activities, etc. Therefore, the geotechnical community refers to numerical simulations to make large-scale strategies with considerable financial stakes. However, current numerical implementations for unsaturated flow in heterogeneous (layered) soils have the following defects: (1) they often employ homogenization of parameters and conditions, (2) they often produce numerical oscillations in layered (heterogeneous) soils due to discontinuity of soil hydraulic properties. The purpose of this research is to address variations in soil hydraulic properties across soil interfaces more appropriately from a mathematical and physical point of view.

1.2 Literature Review

The Richards' equation, a nonlinear partial differential equation, is used to model moisture movement in porous media. It was formulated by Richardson (1922) and Richards (1931). In general, there is no closed-form analytical solution of the Richards' equation. The Richards' equation is stiff, and its numerical simulation is computationally expensive, characterized by stability and convergence difficulties. In unsaturated layered soils, Srivastava and Yeh (1991) derive the analytical solutions of the one-dimensional Richards' equation using the simplest soil hydraulic constitutive model – the Gardner model. However, they point out that the analytical solution is possible for varying only the saturated conductivities when other parameters are isotropic. For a general case associated with more varying soil parameters or for more complicated soil hydraulic constitutive models, analytical solutions are impossible to achieve in layered soils.

Numerical simulations of water infiltration in homogeneous soils have been well studied (Celia *et al.*, 1990; van Dam and Feddes, 2000; Fredlund *et al.*, 2012) and many studies on water infiltration in heterogeneous soils use similar methodologies by homogenizing soil parameters. Very few papers have addressed water movement in heterogeneous soils by imposing the continuity of both flux and pressure head at soil layer interfaces. Historically, simulations of water flow across interfaces in layered soils have been obtained using head-based nodal averaging. The majority of the work uses the arithmetic average of pressure heads (Kirkland *et al.*, 1992) or the (weighted) average of water contents (Zha *et al.*, 2013) for the soil interfaces without imposing the continuity of flux. This typically results in water imbalance around the interface, although Schaudt and Morrill (2002) argue that refining the spatial discretization can compensate for this defect. The commonly used commercial software products

do not address the interface problem by imposing the continuity of flux. For example, HYDRUS smoothes the dissimilarity of soil materials by smoothly changing the soil parameters (Simunek *et al.*, 1998). Dye (2008) studies the numerical oscillations using various commercial codes HYDRUS, SVFlux and Vadose/W.

Hills *et al.* (1989) first point out that the flux must be continuous across the interface of two soil types. However, they do not propose any algorithm to impose the continuity of flux but use an explicit approximation of the interface pressure head, which does not satisfy the continuity of flux. Romano *et al.* (1998) propose an algorithm to enforce the continuity of both flux and pressure head numerically. Schaudt and Morrill (2002) impose the continuity of flux across the interface by using one-sided approximations on either side of the interface without proposing any numerical scheme to solve the interface problem. Matthews *et al.* (2004) also establish an interface equation by comparing one-sided approximations of flux, but solve it via a Newton iteration. They also use one-sided differences to approximate the pressure head gradients at the interface. Liu *et al.* (2016b) show that multiple solutions of the nonlinear interface equation may exist in certain soil parameter regimes, especially when sharp wetting fronts pass through the interface between highly dissimilar materials.

Averaging methods of hydraulic conductivities are required for most numerical methods for solving the Richards' equation. The choice of averaging method impacts the determination of interface conductivities in layered soils. Haverkamp and Vauclin (1979) present a summary of averaging methods for cell-centered hydraulic conductivities in finite difference schemes. They test nine different methods of weighting cell-centered hydraulic conductivity values in homogeneous unsaturated soil and test the influence of averaging methods upon numerical solutions. Baker (2006) uses a three-point grid test to validate some common averaging means. Previous studies

show that the geometric mean produces better numerical solutions (Haverkamp and Vauclin, 1979; Schnabel and Richie, 1984; Belfort and Lehmann, 2005). Szymkiewicz and Helmig (2011) compare conductivity averaging methods in one-dimensional unsaturated flow in layered soils using two finite difference scheme (vertex-centered and cell-centered). An and Noh (2014) proposes a high-order averaging method of hydraulic conductivities to improve the accuracy of numerical simulations of moisture movement in a heterogeneous soil. Liu *et al.* (2016a) investigate the impact of different averaging methods for cell-centered hydraulic conductivities on the interface problem of unsaturated flow in layered soils.

Field studies in the vadose zone have demonstrated extensive variability in characteristics of soil hydraulic properties. Many results in the literature describe statistics of parameters in various soil hydraulic constitutive models (Biggar and Nielsen, 1976; Carsel and Parrish, 1988; Russo and Bouton, 1992; Haskett *et al.*, 1995). Field studies have shown significant variability in saturated hydraulic conductivities (Wierenga *et al.*, 1991) and suggest that the cross-correlation between saturated hydraulic conductivity and soil texture is rather small (Nielsen *et al.*, 1973). Due to uncertainty of soil hydraulic properties, it is significant to develop a stochastic model of moisture flow in the vadose zone regarding the large-scale variations. Many stochastic approaches treat the actual heterogeneous medium as an equivalent homogeneous system with a set of effective properties (Yeh *et al.*, 1985a,b,c; Mantoglou and Gelhar, 1987; Zhu and Mohanty, 2002; Severino and Santini, 2005; Liu *et al.*, 2016c), for example, Liu *et al.* (2016c) express large-scale parameters by the mean parameters plus correction terms using the θ-based form of the Richards' equation. Other studies apply the perturbation method in heterogeneous soils and compare to Monte Carlo simulations (Andersson and Shapiro, 1983; Ünlü *et al.*, 1990; Foussereau *et al.*, 2000). This research work presents a reduced method on the stochastic governing equations

which has not been found in the literature.

1.3 Outline of This Work

The issues addressed in this research work are threefold: (1) the mathematical formulation of the interface problem in unsaturated flow across soil layers, (2) impacts of different averaging methods of cell-centered conductivities on the ill-posedness of the interface problem, (3) a reduced model for stochastic soil hydraulic parameters in heterogeneous soils compared with the solution of homogenized soil parameters and sequences of stochastic realizations.

Chapter 2 presents all mathematical formulations and analysis in this research work. Chapter 3 provides illustrations and numerical evidence via numerical simulations. Conclusions and future work are discussed in Chapter 4.

Chapter 2

MATHEMATICAL MODEL

2.1 Richards' Equation

The moisture movement in unsaturated soils is described by the one-dimensional Richards' equation (Richardson, 1922; Richards, 1931). This equation is often written in three forms, which are identified as the "h-based" form, the "θ-based" form, and the "mixed form":

h-based form

$$C(h)\frac{\partial h}{\partial t} = -\frac{\partial q}{\partial z}, \quad q = K\left(1 - \frac{\partial h}{\partial z}\right), \tag{2.1}$$

θ-based form

$$\frac{\partial \theta}{\partial t} = -\frac{\partial q}{\partial z}, \quad q = K\left(1 - D(\theta)\frac{\partial \theta}{\partial z}\right), \tag{2.2}$$

mixed form

$$\frac{\partial \theta}{\partial t} = -\frac{\partial q}{\partial z}, \quad q = K\left(1 - \frac{\partial h}{\partial z}\right), \tag{2.3}$$

where $\theta = \theta(z,t)$ represents volumetric water content, z is depth (positive downwards), t is time, q is infiltration flux, K is soil hydraulic conductivity, and h is capillary pressure head. In Equations (2.1) and (2.2), $C(h) \equiv \partial\theta/\partial h$ and $D(\theta) \equiv K(\theta)/C(\theta)$. In this research, these quantities are non-dimensionalized in numerical simulations (see Appendix C.1). The Richards' equation is augmented with specific Dirichlet or Neumann boundary conditions as shown in Figure 2.1, as well as an initial profile of pressure head. In particular, the 1D (vertical) soil column is made up of multiple layers.

For the following reasons, only the mixed form is considered in this research.

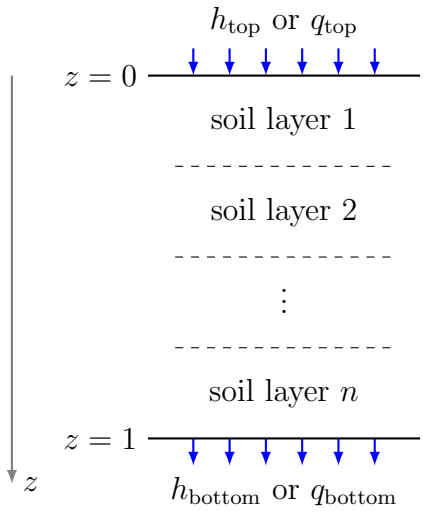

Figure 2.1: The Richards' Equation Is Solved Numerically in an n-Layer Soil Column.

1. In the h-based form of the Richards' equation, the value of $C(h)$ is close to zero when soil is near saturation. It has been reported that the h-based form generally yields poor results, characterized by large mass balance errors and erroneous estimates of infiltration depth (Celia *et al.*, 1990).

2. The θ-based form is not commonly used in layered soils because the water content profile is usually discontinuous at interfaces between different soil materials, thus introduces difficulties in evaluating the gradient of water content, $\partial\theta/\partial z$.

3. The mixed form is consistently reliable and robust with respect to mass balance.

In this work, the mixed form of the Richards' equation is solved numerically in a staggered difference scheme (Figure 2.2). The spatial derivatives are approximated via standard second-order central finite differences and the mixed form Richards' equation yields a system of ordinary differential equations (ODEs)

$$\frac{d\theta_j}{dt} = -\frac{q_{j+\frac{1}{2}} - q_{j-\frac{1}{2}}}{\frac{1}{2}(\Delta_{j-1} + \Delta_j)} \tag{2.4}$$

with

$$q_{j+\frac{1}{2}} = K_{j+\frac{1}{2}} \left(1 - \frac{h_{j+1} - h_j}{\Delta_j} \right). \tag{2.5}$$

The cell-centered conductivity $K_{j+\frac{1}{2}}$ in Equation (2.5) is estimated by an average of adjacent nodal conductivities K_j and K_{j+1}. Formulations and numerical solutions associated with four common averaging schemes (the harmonic mean, the geometric mean, the log-mean, and the arithmetic mean) are presented in Sections 2.4 and 3.2.

A uniform difference scheme is used in numerical simulations, i.e., $\Delta_j = \Delta$ for all j, except those in Section 3.2.2 when a finer mesh is required in the vicinity of the soil layer interface.

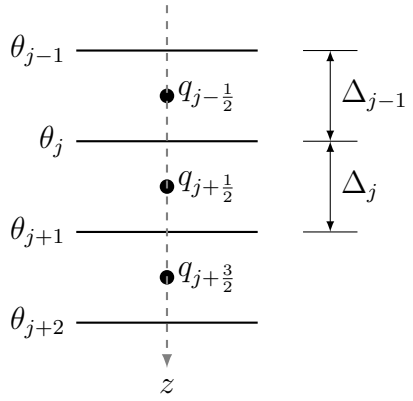

Figure 2.2: Staggered Finite Difference Water Content θ and Flux q Grids.

2.2 Soil Hydraulic Relations

Soil hydraulic properties are described by a set of physical equations relating volumetric water content θ, pressure head h, hydraulic conductivity K and effective saturation S_e,

$$0 \le S_e = \frac{\theta - \theta_r}{\theta_s - \theta_r} \le 1, \tag{2.6}$$

where θ_r and θ_s are residual and saturated volumetric water contents, respectively.

A soil hydraulic constitutive model consists of two relations, the soil-water characteristic curve (SWCC) and the hydraulic conductivity function. The SWCC provides a relation between volumetric water content (or effective saturation) and pressure head. The saturated and residual water contents used in computation of effective saturation are obtained from the SWCC. The hydraulic conductivity (or permeability) function, describes soil hydraulic conductivity as a function of pressure head.

A large number of closed-form empirical soil hydraulic models can be found in the literature (Fredlund *et al.*, 2012). The soil hydraulic parameters in those models can be fitted by data from direct laboratory and field measurements. This research investigates three commonly used models:

1. The Gardner model (Gardner, 1958)

$$\begin{aligned} S_e &= \begin{cases} e^{\alpha h} & \text{if } h < 0, \\ 1 & \text{if } h \geq 0, \end{cases} \\ K &= \beta S_e, \end{aligned} \tag{2.7}$$

   with $\alpha > 0$, $\beta > 0$,

2. the Mualem-van Genuchten model (MvG) (van Genuchten, 1980)

$$\begin{aligned} S_e &= \begin{cases} (1 + (-\alpha h)^n)^{-m} & \text{if } h < 0, \\ 1 & \text{if } h \geq 0, \end{cases} \\ K &= \beta \sqrt{S_e} \left(1 - \left(1 - (S_e)^{\frac{1}{m}}\right)^m\right)^2, \end{aligned} \tag{2.8}$$

   with $\alpha > 0$, $\beta > 0$, $n > 1$, and $0 < m = 1 - 1/n < 1$,

3. the Fredlund & Xing-Leong & Rahardjo model (FXLR) (Fredlund and Xing, 1994; Leong and Rahardjo, 1997)

$$\begin{aligned} S_e &= \begin{cases} [\ln(e + (-\alpha h)^n)]^{-m} & \text{if } h < 0, \\ 1 & \text{if } h \geq 0, \end{cases} \\ K &= \beta (S_e)^p, \end{aligned} \tag{2.9}$$

with $\alpha > 0$, $\beta > 0$, $n > 0$, $m > 0$, and $p > 0$.

The parameters associated to a common letter do not necessarily carry the same physical meaning in different models. Because the Gardner model is simple (quasi-linear) and sufficient for describing flow characteristics in many situations, it is often considered in numerical tests and mathematical analysis. In the MvG model, $n > 1$ and $0 < m < 1$ are related to the pore size distribution in the soil. In the FXLR model, $1/\alpha$ relates to the air-entry value (increasing $1/\alpha$ increases the air-entry value), whereas in the other two models α is a curve-fitting parameter. In the FXLR model m, n are independent positive curve-fitting parameters. The exponent p is determined by fitting the hydraulic conductivity data with typical values in the range 2.5–24.5. Larger values of p are also observed but not common (Fredlund and Xing, 1994). The parameter β in all three models is simply a non-dimensionalized form of the saturated hydraulic conductivity. It is also interesting to note that Zhu *et al.* (2004) establish parameter equivalence of α for the Gardner model (α_{G}) and the MvG model (α_{MvG}) based on preserving macroscopic capillary lengths and predicting the same vertical water flux:

$$\frac{\alpha_{\mathrm{MvG}}}{\alpha_{\mathrm{G}}} = \frac{0.046m + 2.07m^2 + 19.5m^3}{1 + 4.7m + 16m^2}. \tag{2.10}$$

Table 2.1 lists the MvG parameters and corresponding α_{G} values for five example soils from van Genuchten (1980).

2.3 Interface Problem

2.3.1 Formulation of the Interface Equation

This work presents a local numerical scheme for the interface problem. Assume a vertical soil column is partitioned into several layers with different hydraulic properties. The soil hydraulic parameters adjacent to a soil interface are represented as

Table 2.1: The MvG Parameters of Five Example Soils from van Genuchten (1980) and the Equivalent α for the Gardner Model According to Equation (2.10).

Soil	θ_s	θ_r	$\beta \propto K_s$	n	m	α_{MvG}	α_{G}
	(cm^3/cm^3)		(cm/day)			(cm^{-1})	(cm^{-1})
Hygiene sandstone	0.250	0.153	108.0	10.4	0.9038	0.0079	0.0090
Touchet Silt Loam	0.469	0.190	303.0	7.09	0.8590	0.0050	0.0060
Silt Loam	0.396	0.131	4.96	2.06	0.5146	0.00423	0.01003
Guelph Loam (drying)	0.520	0.218	31.6	2.03	0.5074	0.0115	0.0278
Beit Netofa Clay	0.446	0.0	0.082	1.17	0.1453	0.00152	0.02787

superscripted $-$ (upper) and $+$ (lower) (Figure 2.3).

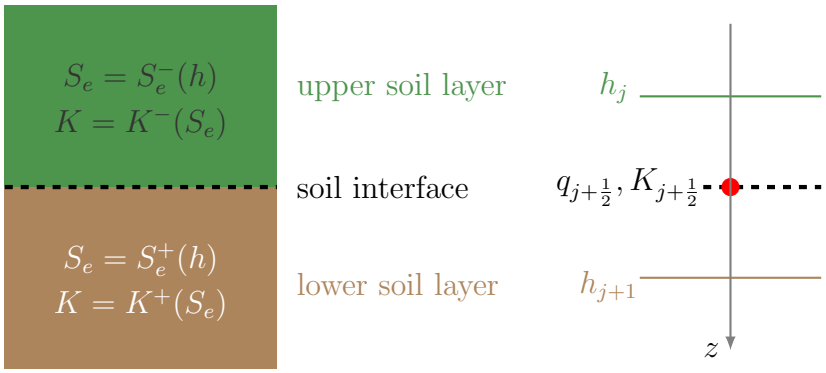

Figure 2.3: A Soil Interface and the (Staggered) Finite Difference Scheme at the Interface.

To ensure mass conservation across the soil interface, Equation (2.4) remains valid. However, Equation (2.5) no longer holds because it involves hydraulic relations associated with different hydraulic parameters for both sides of the interface. The soil hydraulic conductivity at the interface, $K_{j+\frac{1}{2}}$, cannot be estimated as an average of K_j and K_{j+1} due to the discontinuity of conductivity across the interface.

The interface problem must be formulated by the continuity of both pressure head

and flux at the soil interface. The continuity of pressure head at the soil interface is applied implicitly via linear extrapolations,

$$\begin{aligned} h^-_{j+1} &= 2h_{j+\frac{1}{2}} - h_j &&= h_{j+1} - \delta h, \\ h^+_j &= 2h_{j+\frac{1}{2}} - h_{j+1} &&= h_j - \delta h, \end{aligned} \tag{2.11}$$

with $\delta h := h_{j+1} + h_j - 2h_{j+\frac{1}{2}}$. The quantities h^-_{j+1}, h^+_j represent pressure heads at "fictitious" or "ghost" nodes (Romano *et al.*, 1998) in extended layers (Figure 2.4). Conductivities K^-_{j+1} and K^+_j are evaluated from extrapolated pressure head values h^-_{j+1} and h^+_j using the hydraulic properties of the associated layer, i.e., $K^-_{j+1} = K^-(h^-_{j+1})$ and $K^+_j = K^+(h^+_j)$.

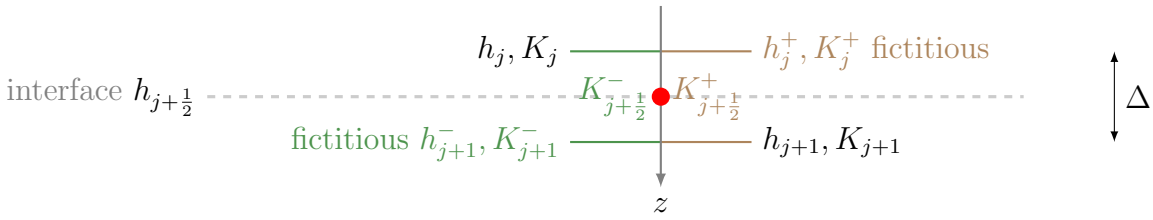

Figure 2.4: Fictitious Nodes in Extended Layers.

Local enforcement of the continuity of flux at the interface yields a nonlinear equation,

$$q_{j+\frac{1}{2}} := K^-_{j+\frac{1}{2}} \left(1 - \frac{h^-_{j+1} - h_j}{\Delta}\right) = K^+_{j+\frac{1}{2}} \left(1 - \frac{h_{j+1} - h^+_j}{\Delta}\right). \tag{2.12}$$

The interface conductivities can then be defined as averages of the nodal conductivities in the extended layer, for example, using the geometric mean,

$$\begin{aligned} K^-_{j+\frac{1}{2}} &= \sqrt{K_j K^-_{j+1}}, \\ K^+_{j+\frac{1}{2}} &= \sqrt{K^+_j K_{j+1}}. \end{aligned} \tag{2.13}$$

Define the ratio of the interface conductivities in extended layers by $r := K^-_{j+\frac{1}{2}} / K^+_{j+\frac{1}{2}}$. Substituting Equation (2.11) into Equation (2.12) yields

$$\delta h = (\Delta - (h_{j+1} - h_j)) \frac{1-r}{1+r}, \tag{2.14}$$

and the expression of r becomes a nonlinear equation of r, for example, using the geometric mean for conductivities,

$$r := \frac{K^-_{j+\frac{1}{2}}}{K^+_{j+\frac{1}{2}}} = \sqrt{\frac{K_j K^-(h_{j+1} - \delta h)}{K^+(h_j - \delta h) K_{j+1}}} = g(r). \tag{2.15}$$

Equation (2.15) must be solved iteratively, for example, using a fixed-point (Picard) iteration

$$r_{n+1} = g(r_n), \quad r_0 \text{ given}, \tag{2.16}$$

or a Newton iteration

$$r_{n+1} = r_n - \frac{g(r_n) - r_n}{g'(r_n) - 1} := f(r_n), \quad r_0 \text{ given}. \tag{2.17}$$

Once r is determined, the quantities associated with extended layers in Equation (2.12) are computed in order by Equations (2.14), (2.11) and (2.13). Notice that altering the averaging method for cell-centered conductivities changes the averaging formula in Equations (2.13) and (2.15).

It is worth noting that a local scheme is used here to estimate interface conductivities $K_{j\pm\frac{1}{2}}$ in Equation (2.13) (with a geometric averaging scheme). There are many other strategies using forward/backward estimates of conductivities, for example, by using $K_j = \sqrt{K_{j-1} K^-_{j+1}}$ and $K_{j+1} = \sqrt{K^+_j K_{j+2}}$, the interface conductivities are estimated by

$$K^-_{j+\frac{1}{2}} = \sqrt{\frac{(K_j)^3}{K_{j-1}}}, \quad K^+_{j+\frac{1}{2}} = \sqrt{\frac{(K_{j+1})^3}{K_{j+2}}}. \tag{2.18}$$

The approach (2.18) involves four nodal values around a soil interface, therefore cannot be applied to cell-wise layers with stochastic soil parameters. Moreover, computing interface conductivities directly from one-sided cells instead of solving an interface equation (2.12) may lead to water balance errors because it does not guarantee flux continuity at the interface.

The local approach described here [e.g., Equation (2.13)] only involves nodal values adjacent to soil layer interfaces, thus has two advantages: (1) it is consistent with the approach within each layer; (2) the local scheme for $K_{j\pm\frac{1}{2}}$ can be applied to heterogeneous soils with cell-wise stochastic soil parameters (e.g., direct numerical simulations in Section 3.3).

2.3.2 Ill-posedness of the Interface Equation

Numerical oscillations are reported using commercial software, for example, in Figure 2.5 (Dye, 2008). The interface equation (2.15) may be ill-posed in certain soil parameter regimes due to its nonlinearity. This research addresses numerical issues when solving the interface problem.

Fictitious Pressure Heads in Extended Layers

When solving the interface equation, either fictitious (extrapolated) pressure head h_j^+ or h_{j+1}^- may be positive despite both $h_j, h_{j+1} < 0$. It leads to erroneous or non-physical interface pressure head and introduces a lack of regularity which further complicates the analysis and the convergence properties of the Picard (2.16) and Newton (2.17) iterations. For example, if

$$h_{j+1} - 2h_j < \Delta < -h_j \tag{2.19}$$

(as $h_{j+1} < h_j < 0$ corresponding to a wetting front moving downward) then

$$|\delta h| < \Delta - (h_{j+1} - h_j) < -h_{j+1} \quad \Rightarrow \quad h_{j+1}^- < 0 \tag{2.20}$$

but

$$h_j^+ \geq 0 \quad \text{for} \quad r \geq \frac{\Delta - h_{j+1}}{\Delta - h_{j+1} + 2h_j} > 1, \tag{2.21}$$

in which case $K^+(h_j - \delta h) = \beta^+$ in Equation (2.15). Although $h_j^+, h_{j+1}^- \geq 0$ may be physically unrealistic, given that $h_j, h_{j+1} < 0$, it may still occur during the finite

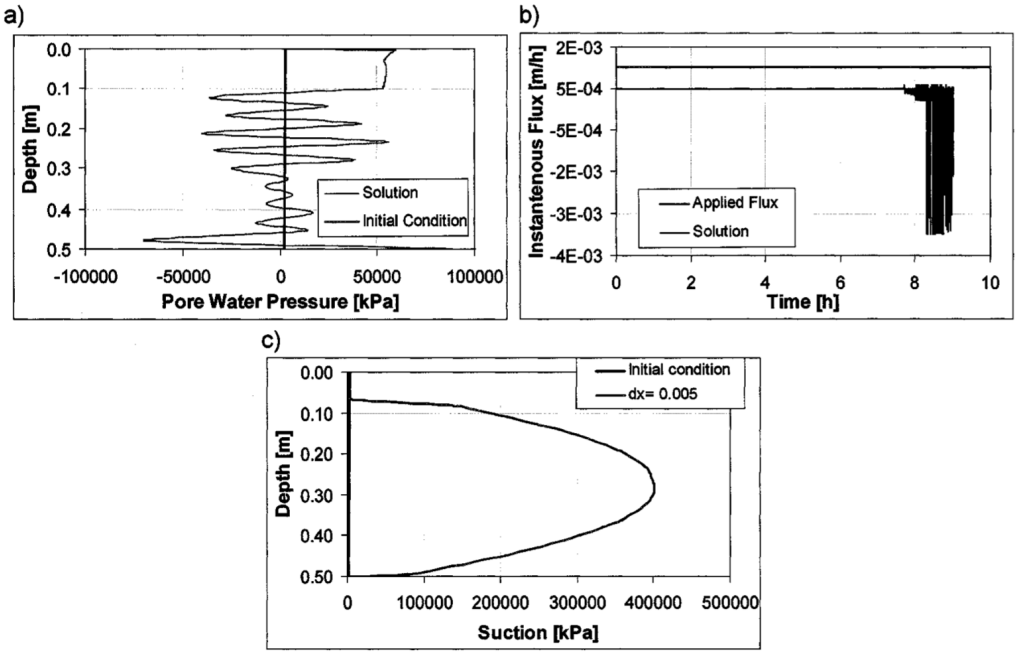

Figure 2.5: Examples of Stability Issues in Various Software a) Suction Oscillation with Depth, b) Actual Flux Oscillation at Soil Surface, and c) Suction with Depth Increased Monotonically to Unreasonable Values (Excerpt from PhD Dissertation of Dye, Heather Beate, April 2008, Arizona State University). Copy Right 2008 by ProQuest LLC.

difference numerical solution process when the grid size Δ is too large. The condition

$$0 < \Delta < \min\left(-h_{j+1}, -h_j\right) - |h_{j+1} - h_j| \tag{2.22}$$

guarantees that

$$|\delta h| < |\Delta - (h_{j+1} - h_j)| \leq \Delta + |h_{j+1} - h_j| < \min\left(-h_{j+1}, -h_j\right), \tag{2.23}$$

for any $r > 0$, i.e., that the fictitious pressure heads (2.11) are negative (unsaturated). The continuity of h across the interface ensures that (2.22) holds for Δ sufficiently small. In the presence of a very sharp wetting front, condition (2.22) may impose a very small upper bound on Δ to avoid $h_{j+1} \ll h_j < 0$.

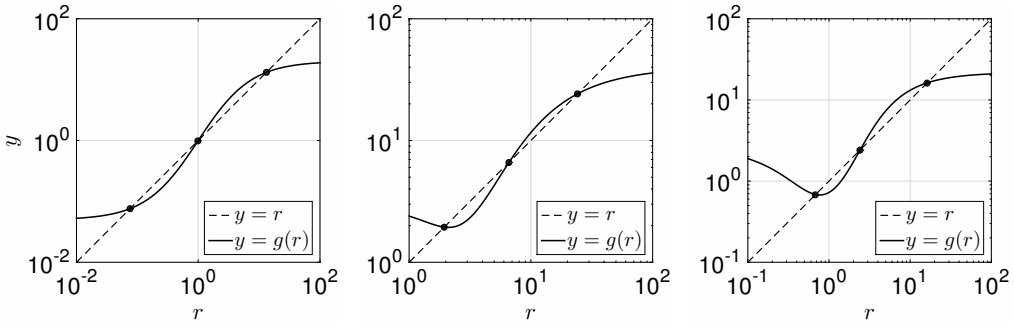

(a) Gardner (b) MvG (c) FXLR

Figure 2.6: Multiple Solutions of $r = g(r)$ Exist While Equation (2.22) Is Satisfied.

Multiple Solutions of The Interface Equation

Unfortunately, Equation (2.22) does not in general guarantee the uniqueness of the solution to the interface equation (2.15). Figure 2.6 illustrates such a situation in two-cell examples with $\Delta = 10$ cm for the Gardner, MvG, and FXLR models. Soil parameters used for the two-cell cases are listed in Table 2.2. While both the failure of Equation (2.22) to hold and the multiplicity of solutions to the interface problem are consequences of a too coarse spatial discretization, it is unclear how the two issues are related or how they interact.

Table 2.2: Soil Parameters for Two-Cell Cases (in Figure 2.6) to Exhibit Multiple Solutions to the Interface Equation.

Model	h_j (cm)	h_{j+1} (cm)	α^- (cm^{-1})	α^+ (cm^{-1})	β^-	β^+	n^-	n^+	m^-	m^+	p^-	p^+
Gardner	-60	-100	0.13	0.01	14765	1						
MvG	-56	-101	0.022	0.031	0.9	1	7.5	5				
FXLR	-60	-100	0.015	0.0148	1	1.2	4.98	4.7	0.78	0.81	15	15

Suppose that the extrapolated pressure heads h_j^+, h_{j+1}^- are always negative (by

refining grids if needed). For the simplest Gardner model with the geometric mean for conductivities, Equation (2.15) reduces to

$$r = g(r) = \lambda \exp\left(\mu \frac{1-r}{1+r}\right) \tag{2.24}$$

with

$$\lambda = \frac{\beta^-}{\beta^+} \exp\left(\left(\alpha^- - \alpha^+\right) \frac{h_{j+1} + h_j}{2}\right) > 0 \tag{2.25}$$

and

$$\mu = \frac{1}{2}\left(\alpha^+ - \alpha^-\right)\left(\Delta - \left(h_{j+1} - h_j\right)\right). \tag{2.26}$$

Figure 2.7 shows analytical criteria for the existence of multiple roots of (2.24) using either the Picard iteration or the Newton iteration. For (μ, λ) in the white region the Picard iteration converges to a unique single root for any choice of r_0 (locally). For (μ, λ) in the shaded region, the Picard iteration converges to a 2-cycle (oscillates between two distinct values), while the Newton iteration converges to a single root. For (μ, λ) in the hatched region Equation (2.24) has multiple roots and using either iteration method converges to a solution which may be non-physical. The precise characterization of the shaded and hatched regions is formulated in Appendix A.

It is shown in Appendix A that the Picard iteration converges to the unique root of (2.24) provided $|\mu| < 2$, which can always be achieved by selecting Δ small enough. Note that this requirement on Δ is not associated with the condition (2.22). Particularly, if $\alpha^+ = \alpha^-$, then $\mu = 0$ and the solution $r = \lambda = \beta^-/\beta^+$ of (2.24) is unique. Previous researches (Romano *et al.*, 1998; Srivastava and Yeh, 1991; Brunone *et al.*, 2003) do not realize the multiplicity of roots of the interface equation because they use the same α value for the Gardner model throughout all soil layers.

Figure 2.8 shows $g(r)$ and $f(r)$ vs r in scaled logarithmic axes. For fixed μ, changes in λ correspond to horizontal translations. For $\mu < -2$ Equation (2.24) has multiple roots for a range $1/\lambda^* \leq \lambda \leq \lambda^*$ ($\lambda \approx 13.6$ for $\mu = -6$). When $\lambda = 1$ the value

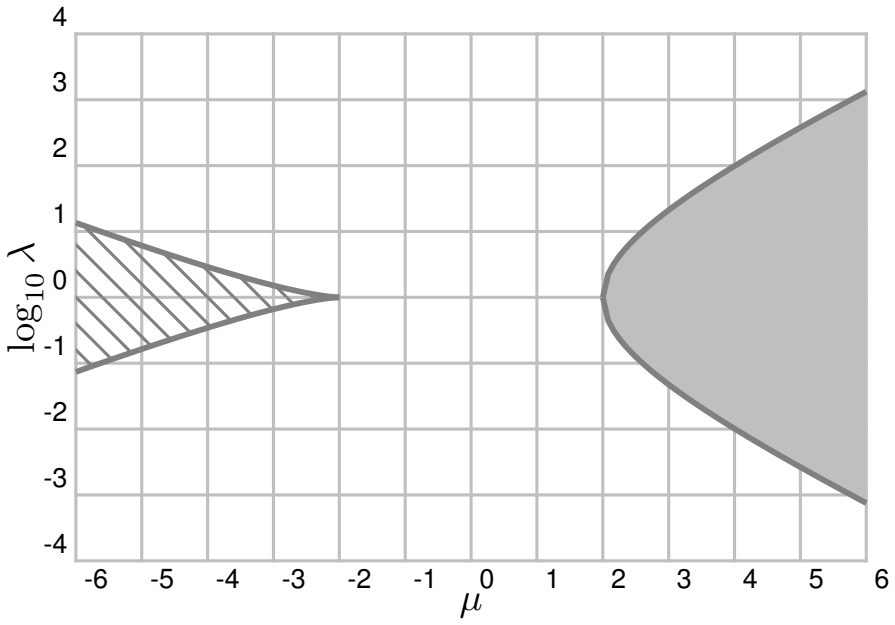

Figure 2.7: The (μ, λ)-Space Criteria for the Gardner Model with The Geometric Mean.

$r = 1$ is a root of (2.24) for any μ, represented by a $\bullet$. For $\mu \geq -2$ the Newton iteration converges globally, quadratically for $\mu > -2$ but only linearly (with rate $\frac{2}{3}$) for $\mu = -2$ due to $r = 1$ having multiplicity 3. For $\mu < -2$ the iteration function f may become negative (shaded areas), leading to non-physical iterated values r_n and potentially creating problems in the convergence. In each case the root $r = 1$ is represented by a $\bullet$.

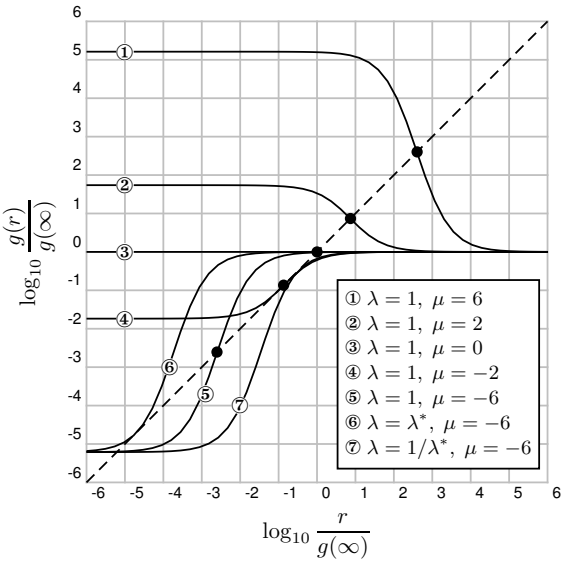

(a) Fixed-Point Iteration Function $g(r)$ vs. r.

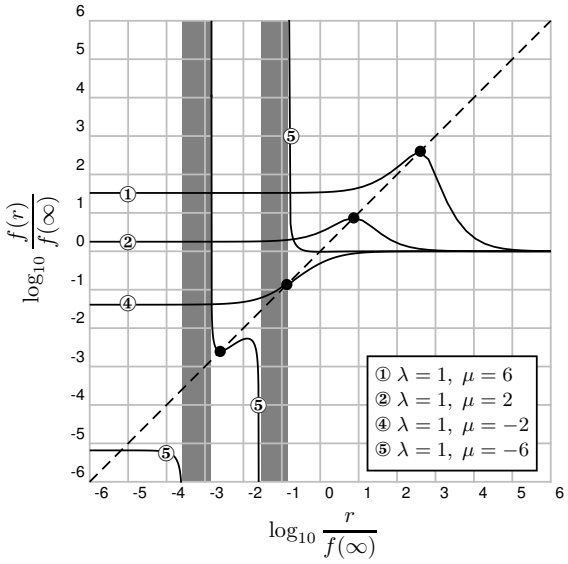

(b) Newton Iteration Function $f(r)$ vs. r. Notice $f(\infty) = g(\infty)$.

Figure 2.8: Fixed-Point Iteration and Newton Iteration for Interface Problem under the Gardner Model and the Geometric Mean for Cell-Centered Hydraulic Conductivities.

For more sophisticated model, e.g. the MvG and FXLR models, the interface equation (2.15) cannot be reduced to a simple equation with only a small number of parameters, such as (μ, λ) for the Gardner model. In general the solution(s) depend(s) on h_j, h_{j+1}, Δ, α^-, α^+, β^-/β^+, n^-, n^+, m^-, m^+ (and p^-, p^+). Hence, ill-posedness of the interface equation using the MvG or FXLR model cannot be analytically determined. However, numerical simulations (shown in Chapter 3) conducted for those models support the potential existence of multiple solutions of the interface problem.

2.4 Averaging Methods for Cell-Centered Conductivities

In the interface equation (2.15), the form of averaging scheme for interface conductivities determines the expression of $g(r)$, and consequently affects the numerical solutions of water flow in unsaturated layered soils. Four commonly used averaging methods are investigated in this work:

$$\text{harmonic mean:} \quad K^{(h)}_{j+\frac{1}{2}} = \frac{2K_jK_{j+1}}{K_j + K_{j+1}}, \tag{2.27}$$

$$\text{geometric mean:} \quad K^{(g)}_{j+\frac{1}{2}} = \sqrt{K_jK_{j+1}}, \tag{2.28}$$

$$\text{log-mean:} \quad K^{(l)}_{j+\frac{1}{2}} = \begin{cases} \dfrac{K_{j+1} - K_j}{\ln(K_{j+1}/K_j)} & \text{if } K_j \neq K_{j+1}, \\ K_j & \text{if } K_j = K_{j+1}, \end{cases} \tag{2.29}$$

$$\text{arithmetic mean:} \quad K^{(a)}_{j+\frac{1}{2}} = \frac{1}{2}(K_j + K_{j+1}). \tag{2.30}$$

In a one-dimensional vertical soil setting, the arithmetic mean can be interpreted by a parallel flow, and the harmonic mean can be interpreted by a serial flow in one spatial cell (Figure 2.9). When the two neighboring nodal hydraulic conductivities K_j and K_{j+1} are very different, the arithmetic mean tends to yield an average closer to the larger nodal value, as if the water flow chooses the faster route among the parallel channels. The harmonic mean results in an average closer to the smaller nodal value

because the lower conductivity behaves like a bottleneck for the flow.

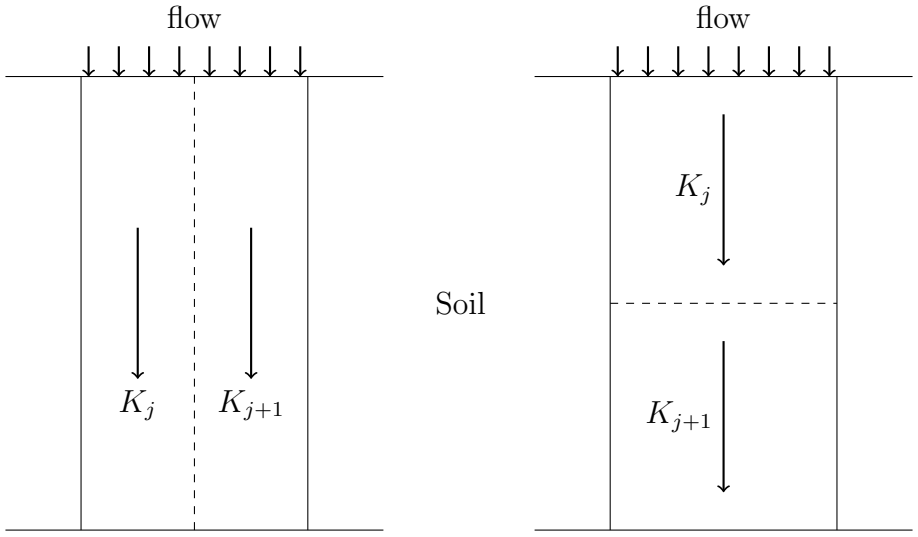

(a) Arithmetic Mean (b) Harmonic Mean

Figure 2.9: Arithmetic Mean as a Parallel Flow and Harmonic Mean as a Serial Flow in Layered Soils.

The geometric mean is based on the arithmetic mean of pressure heads using the Gardner model. Suppose the saturated conductivity is non-dimensionalizated ($\beta = 1$), the hydraulic function in the Gardner model then reduces to $K = e^{\alpha h}$. Since the average of pressure head is $\bar{h} = (h_j + h_{j+1})/2 = (\ln K_j + \ln K_{j+1})/(2\alpha)$, the average conductivity as $K_{j+\frac{1}{2}} = e^{\alpha \bar{h}}$ yields the geometric mean.

The log-mean is also based on the Gardner model, i.e., $K = e^{\alpha h}$, but derived from the average conductivity as a function of pressure head in the cell,

$$K_{j+\frac{1}{2}} = \frac{1}{h_{j+1} - h_j} \int_{h_j}^{h_{j+1}} K(h)\, dh = \frac{K_{j+1} - K_j}{\ln\left(K_{j+1}/K_j\right)}. \tag{2.31}$$

Notice that in the log-mean formula (2.31), $K_j \neq K_{j+1}$ is assumed. As $K_{j+1} \to K_j$, the limit of the log-mean (K_{j+1} as a variable) is K_j, as expected.

It can be easily verified that

$$K^{(h)}_{j+\frac{1}{2}} \leq K^{(g)}_{j+\frac{1}{2}} \leq K^{(l)}_{j+\frac{1}{2}} \leq K^{(a)}_{j+\frac{1}{2}} \tag{2.32}$$

with equality when $K_j = K_{j+1}$.

When the two nodal conductivities have a large difference, especially when a wetting front is passing through a cell in a coarse spatial grid, variations of different averaging methods significantly impact the convergency and accuracy of the numerical simulation.

To compare the values of different averaging methods more precisely, suppose that $K_j \neq K_{j+1}$. Define the ratio of the two neighboring nodal conductivities by $\tau = K_j/K_{j+1}$. For simplicity, the subscript $j + \frac{1}{2}$ (for the average conductivity) in Equations (2.27)–(2.30) is dropped.

Denote the total difference between the arithmetic mean and the harmonic mean by $\omega_{\text{total}} = K^{(a)} - K^{(h)}$, the deviation from the geometric mean to the harmonic mean by $\omega_{\text{g}} = K^{(g)} - K^{(h)}$, and the deviation from the log-mean to the harmonic mean by $\omega_{\text{l}} = K^{(l)} - K^{(h)}$. Then

$$\frac{\omega_{\text{g}}}{\omega_{\text{total}}} = \frac{2\sqrt{\tau}}{(\tau+1)^2} \leq \frac{1}{2}, \tag{2.33}$$

and

$$\frac{\omega_{\text{l}}}{\omega_{\text{total}}} = \frac{2\left(\tau^2 - 1 - 2\tau\ln(\tau)\right)}{(\tau-1)^2\ln(\tau)} \leq \frac{2}{3}. \tag{2.34}$$

As $\tau \to 1$ ($K_{j+1} \to K_j$), $\omega_{\text{g}}/\omega_{\text{total}} \to 1/2$ and $\omega_{\text{l}}/\omega_{\text{total}} \to 2/3$.

To visualize a comparison of these four means, Figure 2.10 shows the distances of these means in general, as the harmonic mean is the smallest and the arithmetic mean the largest, the geometric mean is smaller than the middle of the segment and the log-mean is closer to the geometric mean than to the arithmetic mean. Figure 2.11 shows how the ratio of distances changes when the ratio of the two nodal conductivities varies. The geometric mean approaches to zero faster than the log-mean when the

difference between K_j and K_{j+1} increases. This implies that the geometric mean may underestimate the average conductivity when the gradient of K is large, as a result, it may also impact the well-posedness of the interface problem.

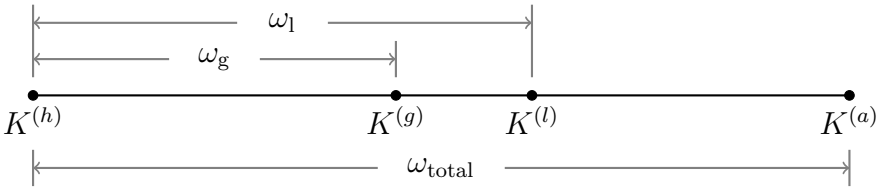

Figure 2.10: Comparison of Values of Four Averaging Means from the Smallest (Left) to the Largest (Right).

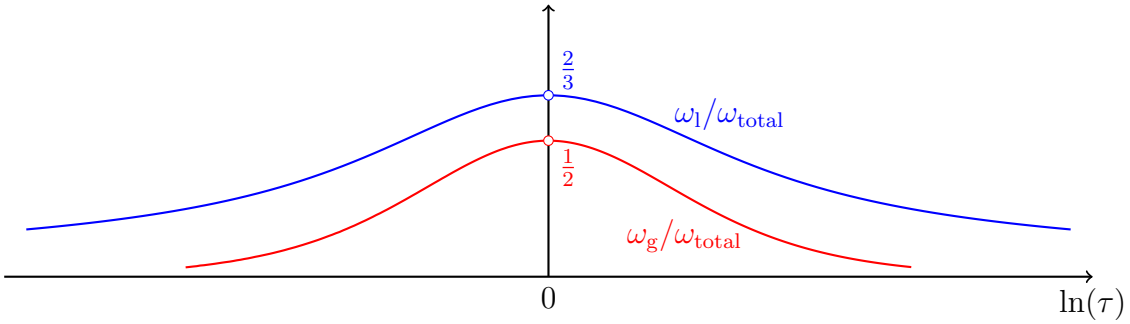

Figure 2.11: ω_g/ω_{total} and ω_l/ω_{total} as Functions of $\ln(\tau)$.

The following facts can be drawn from the comparison of four averaging methods:

(1) The harmonic mean yields the smallest average value and it approximates the physical reality of serial flows in 1D layered soil.

(2) The arithmetic mean is the linear approximation to the log-mean, however, the arithmetic mean overestimates the average conductivity (perhaps not physical) when the difference between K_j and K_{j+1} is large, extremely if either of them is zero. In such a scenario, the much lower conductivity value should dominates the mean value because it is impervious. The other three average means (log-mean,

geometric mean and harmonic mean) all yield zero if one of the conductivities is zero, which is more realistic, especially for a 1D simulation..

(3) The log-mean is between the geometric mean and the arithmetic mean. It is closer to the geometric mean than to the arithmetic mean. It has been known that the geometric mean produces better numerical solutions (Haverkamp and Vauclin, 1979; Schnabel and Richie, 1984; Belfort and Lehmann, 2005). It is also reported in numerical simulations that the arithmetic means of K overestimate the soil water fluxes, while geometric means of K underestimate these fluxes (van Dam and Feddes, 2000). Therefore, the log-mean of conductivities is recommended in numerical simulations.

It is worth noting that the upstream mean and the modified upstream mean as in Baker (2006) are even larger than the arithmetic mean, since they use the conductivity of the lower suction (higher pressure head) as the average, and unsaturated soil conductivity decreases with decreasing pressure head. Other averaging methods in Haverkamp and Vauclin (1979) are established on averaging nodal pressure heads and then evaluate the conductivity by plugging in the hydraulic conductivity function. However, this type of averaging methods should be addressed more carefully because the hydraulic conductivity function $K(h)$ is highly nonlinear, and averaging pressure heads can introduce large deviation from the appropriate average of conductivities. Notice that the geometric mean is also formulated on averaging pressure heads, however, the quasi-linearity of the Gardner model compensates for the error from nonlinearity of $K(h)$.

The robustness of the four averaging methods is investigated by performing numerical experiments in multi-layer soils in Section 3.2. In a layered soil, using different averaging methods for cell-centered conductivities affects the ill-posedness of the in-

terface problem. Numerical simulations in Section 3.2 show that a relatively large average conductivity is less likely to trigger multiple solutions of the interface problem because it potentially smoothes sharp wetting front.

2.5 A Reduced Model for Stochastic Soil Hydraulic Parameters

It is known that the vadose zone has large variability in characterization of soil hydraulic properties. The parameters in soil hydraulic models are considered as random fields. Many studies show that soil hydraulic conductivity is the key characterization of variability of soil (Wierenga *et al.*, 1991; Nielsen *et al.*, 1973). In general, the natural logarithm of saturated soil hydraulic conductivity follows normal distributions (Russo and Bouton, 1992). As a result, water content (pressure head) follows certain probability distributions in an infiltration/evaporation process in heterogeneous soils. The probability distributions of water content then determine the probability distributions of soil hydraulic conductivity and flux. For statistical analysis of water content profiles in transient water flow, numerical solutions of expectation and standard deviation (variance) of water content are desired. This section presents a reduced model on one-dimensional Richards' equation in stochastic soils. The reduced model is a coupled system including expectations of water contents as well as covariances of water contents and soil parameters, taking into account stochastic saturated hydraulic conductivities.

The following assumptions are made:

(1) the Gardner model is used for soil hydraulic relations,

(2) the geometric mean is employed for estimation of cell-centered conductivities,

(3) the soil is always unsaturated, i.e., $h < 0$,

(4) the 1D soil column is discretized into uniform spatial cells,

(5) the natural logarithm of saturated hydraulic conductivity has a normal distribution, i.e. $\ln \beta = b \sim \mathcal{N}(\bar{b}, \sigma_b^2)$,

(6) b, as a random variable, is independent for each (uniform) spatial cell and has the same distribution throughout the soil,

(7) b value is fixed (no hysteretic response) in each cell,

(8) other soil parameters are assumed to be isotropic.

In the ODE system (2.4)-(2.5), denote the quantities in each (uniform) spatial cell of the finite difference scheme as vectors,

$$\boldsymbol{\theta} = \begin{bmatrix} \theta_1 \\ \vdots \\ \theta_n \end{bmatrix}, \quad \boldsymbol{b} = \begin{bmatrix} b_1 \\ \vdots \\ b_n \end{bmatrix}, \quad \boldsymbol{q} = \begin{bmatrix} q_1 \\ \vdots \\ q_n \end{bmatrix},$$

$$\boldsymbol{S}_e = \begin{bmatrix} (S_e)_1 \\ \vdots \\ (S_e)_n \end{bmatrix} = \begin{bmatrix} \frac{\theta_1 - \theta_r}{\theta_s - \theta_r} \\ \vdots \\ \frac{\theta_n - \theta_r}{\theta_s - \theta_r} \end{bmatrix}, \quad \boldsymbol{h} = \begin{bmatrix} h_1 \\ \vdots \\ h_n \end{bmatrix} = \begin{bmatrix} \frac{\ln(S_e)_1}{\alpha} \\ \vdots \\ \frac{\ln(S_e)_n}{\alpha} \end{bmatrix}.$$

The letter n used in this section, without specification, is an integer index related to the total number of cells, not a soil parameter in models MvG and FXLR. Note that all vector indices fall on the nodal grid except $\boldsymbol{q}$ on the cell-centered grid (Figure 2.2). For simplicity of vector notations, $i + \frac{1}{2}$ is not used for cell-centered grids, instead, q_i indeed means $q_{i+\frac{1}{2}}$. Boundary conditions are treated by setting the first and/or last entry in $\boldsymbol{\theta}$ and/or $\boldsymbol{q}$ accordingly. Also, each vector dimension can change (by one or two) according to the boundary conditions. See Appendix C.2 for the treatment of boundary conditions.

Then the original ODE system (2.4)-(2.5) is written as

$$\frac{d\boldsymbol{\theta}}{dt} = -G\left(\boldsymbol{q}(\boldsymbol{b}, \boldsymbol{\theta})\right), \tag{2.35}$$

with

$$q_i(\boldsymbol{b}, \boldsymbol{\theta}) = \exp\left\{\frac{b_i + b_{i+1}}{2}\right\} \sqrt{(S_e)_i (S_e)_{i+1}} \left(1 - \frac{h_{i+1} - h_i}{\Delta}\right), \tag{2.36}$$

and G is a difference operator,

$$\begin{aligned} G : \mathbb{R}^n &\rightarrow \mathbb{R}^{n-1} \\ x &\mapsto Gx \end{aligned}$$

with

$$G = \frac{1}{\Delta} \begin{bmatrix} -1 & 1 & 0 & \cdots & 0 & 0 \\ 0 & -1 & 1 & \cdots & 0 & 0 \\ \vdots & \vdots & \vdots & & \vdots & \vdots \\ 0 & 0 & 0 & \cdots & -1 & 1 \end{bmatrix}. \tag{2.37}$$

For a staggered (dual) finite difference scheme used here, the operator G calculates the central difference.

Since $\boldsymbol{b}$ characterizes the variability of soil properties and results in the variability of other variables ($\boldsymbol{\theta}$, etc.), it is considered as the primary variable in Equation (2.35). Using the properties of normal distributions for $\boldsymbol{b}$, the Taylor expansion of $\boldsymbol{q}(\boldsymbol{b}, \boldsymbol{\theta})$ in terms of $\boldsymbol{b}$ has a closed-form formula (see Appendix B.1). Also notice that the probability distribution of $\boldsymbol{\theta}$ is unknown and the reduced model only intends to involve the first and second moments (i.e., expectation and variance) of $\boldsymbol{\theta}$, thus $\boldsymbol{\theta}$ is considered as the secondary variable in Equation (2.35) and the higher order (> 2) terms involving $\boldsymbol{\theta}$ in the Taylor expansion are truncated.

Let $\bar{\boldsymbol{b}} = E[\boldsymbol{b}]$ and $\bar{\boldsymbol{\theta}} = E[\boldsymbol{\theta}]$ denote the expectations of $\boldsymbol{b}$ and $\boldsymbol{\theta}$, respectively. Denote $\boldsymbol{\delta b} = \boldsymbol{b} - \bar{\boldsymbol{b}}$ and $\boldsymbol{\delta\theta} = \boldsymbol{\theta} - \bar{\boldsymbol{\theta}}$. Then $E[\boldsymbol{\delta b}] = E[\boldsymbol{\delta\theta}] = 0$. The Taylor expansion

of q_i about $(\bar{\boldsymbol{b}}, \bar{\boldsymbol{\theta}})$ (truncated as stated above) is,

$$\begin{aligned} q_i(\boldsymbol{b}, \boldsymbol{\theta}) \;\approx\; & q_i(\bar{\boldsymbol{b}}, \bar{\boldsymbol{\theta}}) + \sum_{k_1+\cdots+k_n \geq 1} \frac{1}{k_1! k_2! \cdots k_n!} \left(D_{b_1^{k_1} \ldots b_n^{k_n}} q_i(\bar{\boldsymbol{b}}, \bar{\boldsymbol{\theta}}) \right) (\delta b_1)^{k_1} \cdots (\delta b_n)^{k_n} \\ & + \sum_{k=1}^{n} \left(D_{\theta_k} q_i(\bar{\boldsymbol{b}}, \bar{\boldsymbol{\theta}}) \right) (\delta \theta_k) + \sum_{k=1}^{n} \sum_{l=1}^{n} \frac{1}{2} \left(D_{\theta_k \theta_l} q_i(\bar{\boldsymbol{b}}, \bar{\boldsymbol{\theta}}) \right) (\delta \theta_k)(\delta \theta_l) \\ & + \sum_{k=1}^{n} \sum_{l=1}^{n} \left(D_{b_k \theta_l} q_i(\bar{\boldsymbol{b}}, \bar{\boldsymbol{\theta}}) \right) (\delta b_k)(\delta \theta_l). \end{aligned} \tag{2.38}$$

For simplicity of notation, denote

$$D_{\boldsymbol{b}} q_i = (D_{b_1} q_i, D_{b_2} q_i, \ldots, D_{b_n} q_i), \tag{2.39}$$

$$D_{\boldsymbol{\theta}} q_i = (D_{\theta_1} q_i, D_{\theta_2} q_i, \ldots, D_{\theta_n} q_i), \tag{2.40}$$

$$D_{\boldsymbol{\theta\theta}} q_i = \begin{bmatrix} \frac{\partial^2 q_i}{\partial \theta_1 \partial \theta_1} & \frac{\partial^2 q_i}{\partial \theta_1 \partial \theta_2} & \cdots & \frac{\partial^2 q_i}{\partial \theta_1 \partial \theta_n} \\ \frac{\partial^2 q_i}{\partial \theta_2 \partial \theta_1} & \frac{\partial^2 q_i}{\partial \theta_2 \partial \theta_2} & \cdots & \frac{\partial^2 q_i}{\partial \theta_2 \partial \theta_n} \\ \vdots & \vdots & \ddots & \vdots \\ \frac{\partial^2 q_i}{\partial \theta_n \partial \theta_1} & \frac{\partial^2 q_i}{\partial \theta_n \partial \theta_2} & \cdots & \frac{\partial^2 q_i}{\partial \theta_n \partial \theta_n} \end{bmatrix}, \tag{2.41}$$

$$D_{\boldsymbol{b\theta}} q_i = \begin{bmatrix} \frac{\partial^2 q_i}{\partial b_1 \partial \theta_1} & \frac{\partial^2 q_i}{\partial b_1 \partial \theta_2} & \cdots & \frac{\partial^2 q_i}{\partial b_1 \partial \theta_n} \\ \frac{\partial^2 q_i}{\partial b_2 \partial \theta_1} & \frac{\partial^2 q_i}{\partial b_2 \partial \theta_2} & \cdots & \frac{\partial^2 q_i}{\partial b_2 \partial \theta_n} \\ \vdots & \vdots & \ddots & \vdots \\ \frac{\partial^2 q_i}{\partial b_n \partial \theta_1} & \frac{\partial^2 q_i}{\partial b_n \partial \theta_2} & \cdots & \frac{\partial^2 q_i}{\partial b_n \partial \theta_n} \end{bmatrix}. \tag{2.42}$$

Then Equation (2.38) can be written in the following matrix form

$$\begin{aligned} q_i(\boldsymbol{b}, \boldsymbol{\theta}) \;\approx\; & q_i(\bar{\boldsymbol{b}}, \bar{\boldsymbol{\theta}}) + \sum_{k_1+\cdots+k_n \geq 1} \frac{1}{k_1! k_2! \cdots k_n!} \left(D_{b_1^{k_1} \ldots b_n^{k_n}} q_i(\bar{\boldsymbol{b}}, \bar{\boldsymbol{\theta}}) \right) (\delta b_1)^{k_1} \cdots (\delta b_n)^{k_n} \\ & + \left(D_{\boldsymbol{\theta}} q_i(\bar{\boldsymbol{b}}, \bar{\boldsymbol{\theta}}) \right) \cdot (\boldsymbol{\delta\theta}) + \frac{1}{2} (\boldsymbol{\delta\theta})^T \cdot \left(D_{\boldsymbol{\theta\theta}} q_i(\bar{\boldsymbol{b}}, \bar{\boldsymbol{\theta}}) \right) \cdot (\boldsymbol{\delta\theta}) \\ & + (\boldsymbol{\delta b})^T \cdot \left(D_{\boldsymbol{b\theta}} q_i(\bar{\boldsymbol{b}}, \bar{\boldsymbol{\theta}}) \right) \cdot (\boldsymbol{\delta\theta}) \,. \end{aligned} \tag{2.43}$$

The probability distribution of q_i depends on the distributions of $\boldsymbol{b}$ and $\boldsymbol{\theta}$. Using

Equation (2.43) to estimate the expectation of q_i,

$$\begin{aligned}
& E\left[q_i(\boldsymbol{b},\boldsymbol{\theta})\right] \\
\approx\ & q_i(\bar{\boldsymbol{b}},\bar{\boldsymbol{\theta}}) + \sum_{k_1+\cdots+k_n\geq 1} \frac{1}{k_1!k_2!\cdots k_n!}\left(D_{b_1^{k_1}\cdots b_n^{k_n}} q_i(\bar{\boldsymbol{b}},\bar{\boldsymbol{\theta}})\right) E\left[(\delta b_1)^{k_1}\cdots(\delta b_n)^{k_n}\right] \\
& + \left(D_{\boldsymbol{\theta}} q_i(\bar{\boldsymbol{b}},\bar{\boldsymbol{\theta}})\right)\cdot E\left[\boldsymbol{\delta\theta}\right] + \frac{1}{2}E\left[(\boldsymbol{\delta\theta})^T\cdot\left(D_{\boldsymbol{\theta\theta}} q_i(\bar{\boldsymbol{b}},\bar{\boldsymbol{\theta}})\right)\cdot(\boldsymbol{\delta\theta})\right] \\
& + E\left[(\boldsymbol{\delta b})^T\cdot\left(D_{\boldsymbol{b\theta}} q_i(\bar{\boldsymbol{b}},\bar{\boldsymbol{\theta}})\right)\cdot(\boldsymbol{\delta\theta})\right] \\
=\ & q_i(\bar{\boldsymbol{b}},\bar{\boldsymbol{\theta}})e^{\sigma_b^2/4} \\
& + \frac{1}{2}\operatorname{trace}\left(\left(D_{\boldsymbol{\theta\theta}} q_i(\bar{\boldsymbol{b}},\bar{\boldsymbol{\theta}})\right)\cdot\Sigma_{\boldsymbol{\theta\theta}}\right) + \operatorname{trace}\left(\left(D_{\boldsymbol{b\theta}} q_i(\bar{\boldsymbol{b}},\bar{\boldsymbol{\theta}})\right)\cdot\Sigma_{\boldsymbol{b\theta}}^T\right). \qquad (2.44)
\end{aligned}$$

A detailed derivation for $q_i(\bar{\boldsymbol{b}},\bar{\boldsymbol{\theta}})e^{\sigma_b^2/4}$ in Equation (2.44) can be found in Appendix B.1. Here Σ denotes the covariance matrices:

$$\Sigma_{\boldsymbol{\theta\theta}} = \begin{bmatrix} \overline{\delta\theta_1\delta\theta_1} & \overline{\delta\theta_1\delta\theta_2} & \cdots & \overline{\delta\theta_1\delta\theta_n} \\ \overline{\delta\theta_2\delta\theta_1} & \overline{\delta\theta_2\delta\theta_2} & \cdots & \overline{\delta\theta_2\delta\theta_n} \\ \vdots & \vdots & \ddots & \vdots \\ \overline{\delta\theta_n\delta\theta_1} & \overline{\delta\theta_n\delta\theta_2} & \cdots & \overline{\delta\theta_n\delta\theta_n} \end{bmatrix}, \qquad (2.45)$$

$$\Sigma_{\boldsymbol{b\theta}} = \begin{bmatrix} \overline{\delta b_1\delta\theta_1} & \overline{\delta b_1\delta\theta_2} & \cdots & \overline{\delta b_1\delta\theta_n} \\ \overline{\delta b_2\delta\theta_1} & \overline{\delta b_2\delta\theta_2} & \cdots & \overline{\delta b_2\delta\theta_n} \\ \vdots & \vdots & \ddots & \vdots \\ \overline{\delta b_n\delta\theta_1} & \overline{\delta b_n\delta\theta_2} & \cdots & \overline{\delta b_n\delta\theta_n} \end{bmatrix}. \qquad (2.46)$$

Equation (2.44) then reduces to,

$$\frac{d\bar{\boldsymbol{\theta}}}{dt} \approx -G\left(\boldsymbol{q}(\bar{\boldsymbol{b}},\bar{\boldsymbol{\theta}})e^{\sigma_b^2/4} + \boldsymbol{\eta} + \boldsymbol{\zeta}\right), \qquad (2.47)$$

with

$$\eta_i = \frac{1}{2}\operatorname{trace}\left(\left(D_{\boldsymbol{\theta\theta}} q_i(\bar{\boldsymbol{b}},\bar{\boldsymbol{\theta}})\right)\cdot\Sigma_{\boldsymbol{\theta\theta}}\right), \qquad (2.48)$$

$$\zeta_i = \operatorname{trace}\left(\left(D_{\boldsymbol{b\theta}} q_i(\bar{\boldsymbol{b}},\bar{\boldsymbol{\theta}})\right)\cdot\Sigma_{\boldsymbol{b\theta}}^T\right). \qquad (2.49)$$

Since the covariance matrices $\Sigma_{\boldsymbol{b\theta}}$ and $\Sigma_{\boldsymbol{\theta\theta}}$ are both involved in Equation (2.47), a coupled system is required to compute them. By the chain rule,

$$\frac{d}{dt}\Sigma_{\boldsymbol{\theta\theta}} = E\left[\frac{d\boldsymbol{\delta\theta}}{dt}\cdot(\boldsymbol{\delta\theta})^T\right] + E\left[(\boldsymbol{\delta\theta})\cdot\left(\frac{d\boldsymbol{\delta\theta}}{dt}\right)^T\right], \tag{2.50}$$

$$\frac{d}{dt}\Sigma_{\boldsymbol{b\theta}} = E\left[(\boldsymbol{\delta b})\cdot\left(\frac{d\boldsymbol{\delta\theta}}{dt}\right)^T\right]. \tag{2.51}$$

In Equation (2.51), note the fact that $\boldsymbol{b}$ does not change over time, that is, $d\boldsymbol{\delta b}/dt \equiv 0$.

Since

$$\frac{d\boldsymbol{\delta\theta}}{dt} = \frac{d\boldsymbol{\theta}}{dt} - \frac{d\bar{\boldsymbol{\theta}}}{dt},$$

by Equations (2.35) and (2.47), the i-th entry is

$$\left(\frac{d\boldsymbol{\delta\theta}}{dt}\right)_i \approx -\frac{1}{\Delta}(\kappa_{i+1}-\kappa_i) \tag{2.52}$$

with

$$\kappa_i = q_i(\boldsymbol{b},\boldsymbol{\theta}) - \left(q_i(\bar{\boldsymbol{b}},\bar{\boldsymbol{\theta}})e^{\sigma_b^2/4} + \eta_i + \zeta_i\right). \tag{2.53}$$

Then the i-th row of $E\left[\frac{d\boldsymbol{\delta\theta}}{dt}\cdot(\boldsymbol{\delta\theta})^T\right]$ is

$$E\left[\left(\frac{d\boldsymbol{\delta\theta}}{dt}\right)_i(\boldsymbol{\delta\theta})^T\right] \approx -\frac{1}{\Delta}\left(E\left[\kappa_{i+1}(\boldsymbol{\delta\theta})^T\right] - E\left[\kappa_i(\boldsymbol{\delta\theta})^T\right]\right). \tag{2.54}$$

Substitute Equation (2.43) to (2.53), estimate the expectations in Equation (2.54), and truncate the higher order terms involving $\boldsymbol{\delta\theta}$, then

$$E\left[\kappa_i(\boldsymbol{\delta\theta})^T\right] \approx \left(D_{\boldsymbol{b}}q_i(\bar{\boldsymbol{b}},\bar{\boldsymbol{\theta}})\right)\cdot\Sigma_{\boldsymbol{b\theta}} + \left(D_{\boldsymbol{\theta}}q_i(\bar{\boldsymbol{b}},\bar{\boldsymbol{\theta}})\right)\cdot\Sigma_{\boldsymbol{\theta\theta}}. \tag{2.55}$$

To write the entire matrix for $E\left[\frac{d\boldsymbol{\delta\theta}}{dt}\cdot(\boldsymbol{\delta\theta})^T\right]$, define a row difference operator,

$$\begin{aligned} G_r : \mathbb{R}^{n\times m} &\to \mathbb{R}^{(n-1)\times m} \\ A_{n\times m} &\mapsto \frac{1}{\Delta}\left(V_{(n-1)\times n}U_{n\times n} - V_{(n-1)\times n}\right)A_{n\times m} \end{aligned}$$

with matrix $(V)_{i,j} = \delta_{i,j}$ and $(U)_{i,j} = \delta_{i+1,j}$. U with ones on the super-diagonal is usually called an upper shift matrix. Also, denote

$$G_r = \frac{1}{\Delta}\left(V_{(n-1)\times n}U_{n\times n} - V_{(n-1)\times n}\right) \tag{2.56}$$

and the linear map is equivalent to left-multiplication by G_r.

Denote the Jacobian matrices of $\boldsymbol{q}$ by $(D_{\boldsymbol{b}}\boldsymbol{q})_{i,j} = D_{b_j}q_i$, $(D_{\boldsymbol{\theta}}\boldsymbol{q})_{i,j} = D_{\theta_j}q_i$, then

$$E\left[\frac{d\boldsymbol{\delta\theta}}{dt}\cdot(\boldsymbol{\delta\theta})^T\right] \approx -G_r\left(\left(D_{\boldsymbol{b}}\boldsymbol{q}(\bar{\boldsymbol{b}},\bar{\boldsymbol{\theta}})\right)\cdot\Sigma_{\boldsymbol{b\theta}} + \left(D_{\boldsymbol{\theta}}\boldsymbol{q}(\bar{\boldsymbol{b}},\bar{\boldsymbol{\theta}})\right)\cdot\Sigma_{\boldsymbol{\theta\theta}}\right) \tag{2.57}$$

Notice that $E\left[(\boldsymbol{\delta\theta})\cdot\left(\frac{d\boldsymbol{\delta\theta}}{dt}\right)^T\right]$ is the transpose of $E\left[\frac{d\boldsymbol{\delta\theta}}{dt}\cdot(\boldsymbol{\delta\theta})^T\right]$, Equation (2.50) thus reduces to

$$\frac{d}{dt}\Sigma_{\boldsymbol{\theta\theta}} \approx H + H^T, \tag{2.58}$$

with

$$H = -G_r\Big(\left(D_{\boldsymbol{b}}\boldsymbol{q}(\bar{\boldsymbol{b}},\bar{\boldsymbol{\theta}})\right)\cdot\Sigma_{\boldsymbol{b\theta}} + \left(D_{\boldsymbol{\theta}}\boldsymbol{q}(\bar{\boldsymbol{b}},\bar{\boldsymbol{\theta}})\right)\cdot\Sigma_{\boldsymbol{\theta\theta}}\Big). \tag{2.59}$$

For Equation (2.51), using (2.52), the i-th column of $(\boldsymbol{\delta b})\cdot\left(\frac{d\boldsymbol{\delta\theta}}{dt}\right)^T$ is

$$(\boldsymbol{\delta b})\left(\frac{d\boldsymbol{\delta\theta}}{dt}\right)^T_i \approx -\frac{1}{\Delta}(\kappa_{i+1}-\kappa_i)\boldsymbol{\delta b}. \tag{2.60}$$

Its expectation yields

$$E\left[\boldsymbol{\delta b}\left(\frac{d\boldsymbol{\delta\theta}}{dt}\right)^T_i\right] \approx -\frac{1}{\Delta}\left(E\left[\kappa_{i+1}(\boldsymbol{\delta b})\right] - E\left[\kappa_i(\boldsymbol{\delta b})\right]\right). \tag{2.61}$$

The above expression is more complicated than Equation (2.55) because in (2.55) all higher order terms involve $\boldsymbol{\delta\theta}$ are truncated. In contrast, Equation (2.61) has terms that only contain $\boldsymbol{\delta b}$ and all orders for pure $\boldsymbol{\delta b}$ must be maintained. Higher order terms involving $\boldsymbol{\delta\theta}$ are again truncated. By Equation (2.53) and $E\left[\boldsymbol{\delta b}\right] = 0$,

$$E\left[\kappa_i(\boldsymbol{\delta b})\right] \approx E\left[q_i(\boldsymbol{b},\boldsymbol{\theta})(\boldsymbol{\delta b})\right]. \tag{2.62}$$

Then by Equation (2.43),

$$E\left[\kappa_i(\boldsymbol{\delta b})\right] \approx \sum_{k_1+\cdots+k_n\geq 1} \frac{1}{k_1!k_2!\cdots k_n!}\left(D_{b_1^{k_1}\ldots b_n^{k_n}} q_i(\bar{\boldsymbol{b}},\bar{\boldsymbol{\theta}})\right) E\left[(\delta b_1)^{k_1}\cdots(\delta b_n)^{k_n}(\boldsymbol{\delta b})\right] + \Sigma_{\boldsymbol{b\theta}}\cdot\left(D_{\boldsymbol{\theta}} q_i(\bar{\boldsymbol{b}},\bar{\boldsymbol{\theta}})\right)^T \tag{2.63}$$

The first term in the above equation has a closed-form expression in terms of σ_b and partial derivatives of $\boldsymbol{q}$ (see Appendix B.2).

Similarly, define a column difference operator,

$$\begin{aligned} G_c : \mathbb{R}^{m\times n} &\to \mathbb{R}^{m\times(n-1)} \\ A_{m\times n} &\mapsto \frac{1}{\Delta} A_{m\times n}\left(L_{n\times n}V_{n\times(n-1)} - V_{n\times(n-1)}\right) \end{aligned}$$

with matrix $(V)_{i,j} = \delta_{i,j}$ and $(L)_{i,j} = \delta_{i,j+1}$. Notice that L is often called a lower shift matrix with ones on the sub-diagonal. When a matrix is right-multiplied by L, it performs a right shift on the matrix entries. Also, denote

$$G_c = \frac{1}{\Delta}\left(L_{n\times n}V_{n\times(n-1)} - V_{n\times(n-1)}\right) \tag{2.64}$$

and the linear map is equivalent to right-multiplication by G_c.

Then Equation (2.51) reduces to,

$$\frac{d}{dt}\Sigma_{\boldsymbol{b\theta}} \approx -\left(\frac{\sigma_b^2}{2}\left(1+e^{\sigma_b^2/4}-e^{\sigma_b^2/8}\right)P + \Sigma_{\boldsymbol{b\theta}}\cdot\left(D_{\boldsymbol{\theta}}\boldsymbol{q}(\bar{\boldsymbol{b}},\bar{\boldsymbol{\theta}})\right)^T\right) G_c, \tag{2.65}$$

with

$$P = \operatorname{diag}(\boldsymbol{q}(\bar{\boldsymbol{b}},\bar{\boldsymbol{\theta}})) + L_{n\times n}\operatorname{diag}(\boldsymbol{q}(\bar{\boldsymbol{b}},\bar{\boldsymbol{\theta}})). \tag{2.66}$$

Here $\operatorname{diag}(\boldsymbol{q}(\bar{\boldsymbol{b}},\bar{\boldsymbol{\theta}}))$ is a diagonal matrix with the diagonal $\boldsymbol{q}(\bar{\boldsymbol{b}},\bar{\boldsymbol{\theta}})$. In fact, for the Gardner model with the geometric mean of conductivities in Equation (2.36), $P = 2\left(D_{\boldsymbol{b}}\boldsymbol{q}(\bar{\boldsymbol{b}},\bar{\boldsymbol{\theta}})\right)^T$.

As a result, a (coupled) system of ODEs is formulated by

$$\begin{cases} \dfrac{d\bar{\boldsymbol{\theta}}}{dt} & \approx & -G\left(\boldsymbol{q}(\bar{\boldsymbol{b}},\bar{\boldsymbol{\theta}})e^{\sigma_b^2/4}+\boldsymbol{\eta}+\boldsymbol{\zeta}\right), \\ \dfrac{d}{dt}\Sigma_{\boldsymbol{\theta\theta}} & \approx & H+H^T, \\ \dfrac{d}{dt}\Sigma_{\boldsymbol{b\theta}} & \approx & -\left(\frac{\sigma_b^2}{2}\left(1+e^{\sigma_b^2/4}-e^{\sigma_b^2/8}\right)P+\Sigma_{\boldsymbol{b\theta}}\cdot\left(D_{\boldsymbol{\theta}}\boldsymbol{q}(\bar{\boldsymbol{b}},\bar{\boldsymbol{\theta}})\right)^T\right)G_c. \end{cases} \tag{2.67}$$

The coupled system (2.67), as a reduced model for stochastic soil hydraulic parameters, consists of the expectation equations of soil water contents and the covariance equations of water contents and soil hydraulic parameters. Section 3.3 presents the numerical solution of this reduced model. The reduced model is also compared to two other approaches: (1) direct numerical simulations using agent-based (cell-wise) random parameters, and (2) the numerical solution using homogenized soil parameters.

Chapter 3

NUMERICAL SIMULATIONS

The numerical experiments in this research are coded in Fortran90, performed on either the Intel Xeon CPU E5-2620 (2.00 GHz) or the Intel Core i7 (2.7 GHz). All the numerical experiments can fit in the cache size. Appendix C shows more details about the implementation of numerical simulations.

3.1 Investigation on Interface Problems in Two-Layer Soils

Numerical simulations of transient flow in two-layer soils using three hydraulic models (Gardner, MvG, FXLR) are presented here. The purpose of these numerical experiments is to demonstrate the possible existence of multiple solutions to the interface problem for all three hydraulic models with specific soil parameters or conditions and how the ill-posedness of the interface problem impacts the numerical solution.

3.1.1 Two-Layer Case Using Gardner Model

Since the Gardner model has been analyzed analytically in Equations. (2.24)–(2.26), two cases are demonstrated in which the (μ, λ) path falls into the hatched or shaded region in Figure 2.7 during the numerical simulation: (1) for the hatched region that multiple solutions to the interface problem exist, (2) for the shaded region that a fixed-point iteration converges to a 2-cycle.

Case 1 – Hatched Region

For a specific infiltration process in a two-layer soil, the boundary pressure heads are fixed as $h_{\text{top}} = -0.6, h_{\text{bottom}} = -1$ (non-dimensionalized) using the parameters in

Table 3.1. The initial pressure head profile is assumed to be constant within the range $0.55 \leq z \leq 1$ (lower layer) and linear within the range $0 \leq z \leq 0.55$ (upper layer plus a small piece of the lower layer). This initial steady state can be interpreted as a forced drainage at the bottom of the soil. Notice that the initial/boundary conditions can affect the ill-posedness of the interface problem, thus, this research work only uses conditions that can trigger the existence of multiple solutions.

Table 3.1: Dimensionless Soil Hydraulic Parameters for the Two-Layer Case Using the Gardner Model.

Case No.	Layer	α	β	θ_s	θ_r
Case 1	upper	13	1	0.4	0.06
	lower	1	0.0006	0.4	0.06
Case 2	upper	10	1	0.4	0.06
	lower	130	1476	0.4	0.06

When the number of interior grid points $N = 50$ (a description of indexing can be found in Appendix C.2), multiple solutions to the interface problem exist at certain time steps during the numerical simulation. Figure 3.1(a) shows the trajectories in (μ, λ)-space computed at the interface during each numerical run. It shows how this trajectory moves out of the hatched region as the grid is refined, i.e., N is increased, from $t = 0$ (I) to $t = 100$ (T) with $N = 50$ (crosses), $N = 100$ (asterisks) and $N = 200$ (dots). Figure 3.1(b) indicates that multiple solutions can introduce strong deviation or non-physical oscillations in pressure head under the interface (at $z \approx 0.5098$). In a multi-layer soil, errors from multiple interfaces may compound and possibly lead to greater oscillations or instabilities.

Figure 3.2 shows the pressure head profiles at different time steps corresponding to the (three) different values of N used. In the cases $N = 50, 100$, multiple solutions

exist during the numerical simulation, while for $N = 200$, the interface problem always admits a unique solution. Non-physical pressure heads can be observed in Figure 3.2(a) and Figure 3.2(b), in particular as the wetting front passes through the interface or shortly thereafter. When $N = 50$, multiple solutions do not disappear once they appear, leading to an unrecoverable wrong profile. When $N = 100$, multiple solutions exist only when the gradient of pressure head at the interface is large, the pressure head profile becomes inaccurate due to the impact of multiple solutions from $t \approx 1.04$ to $t \approx 4.15$. After the front has passed through the interface, multiple solutions disappear when $N = 100$. Because of the natural diffusion process, the profile may autocorrect itself only if the interface problem ceases to have multiple roots after the front passes the interface.

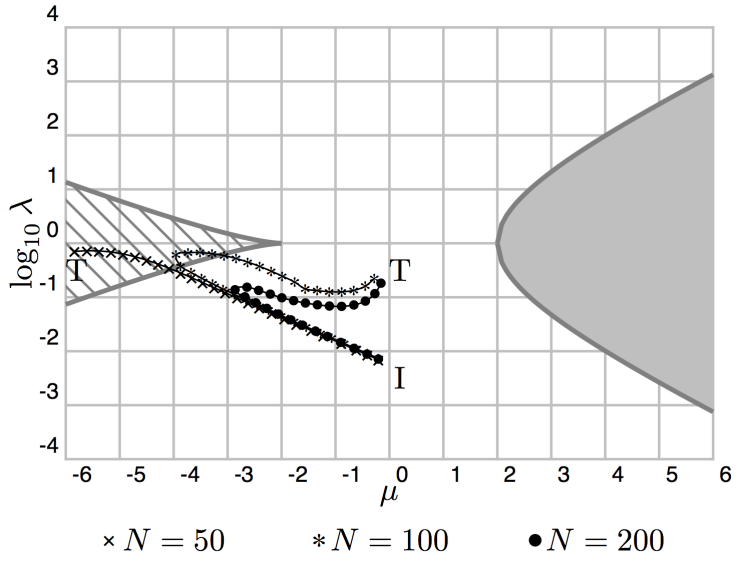

(a) (μ, λ) Trajectories at the Interface.

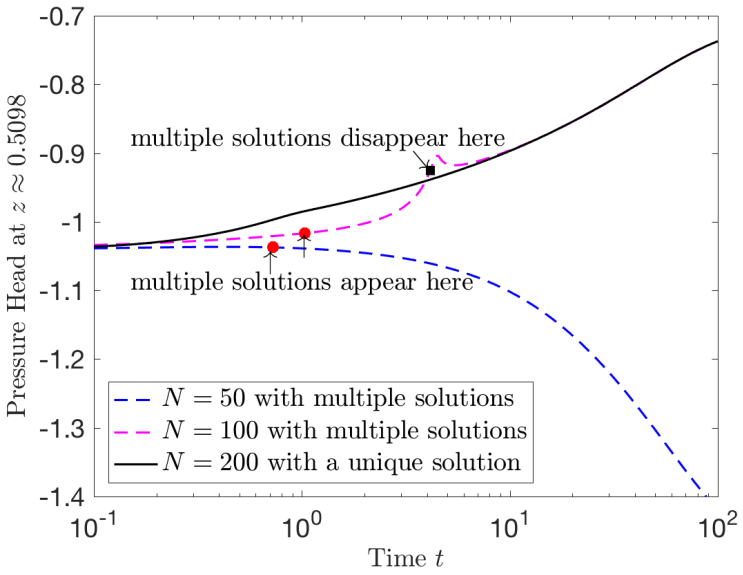

(b) Pressure Head below the Interface.

Figure 3.1: Gardner Model Case 1.

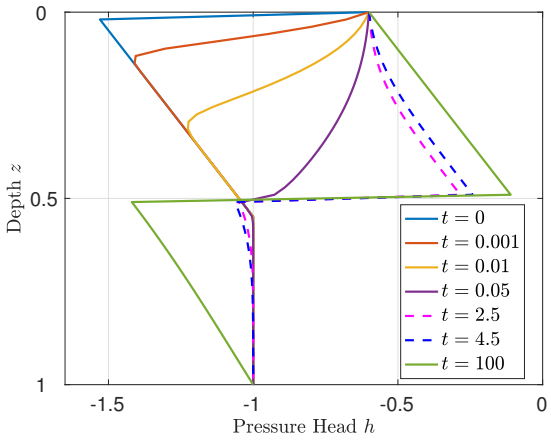

(a) Pressure Head Profile for $N = 50$

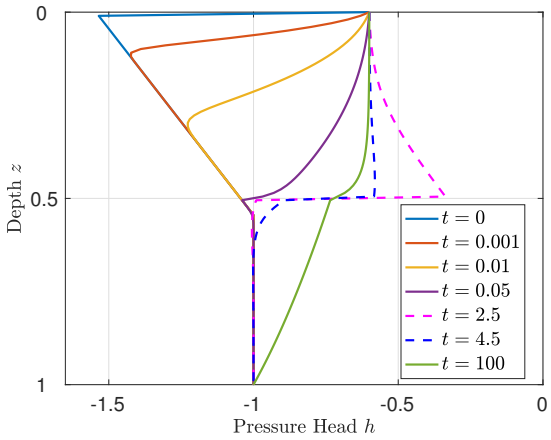

(b) Pressure Head Profile for $N = 100$

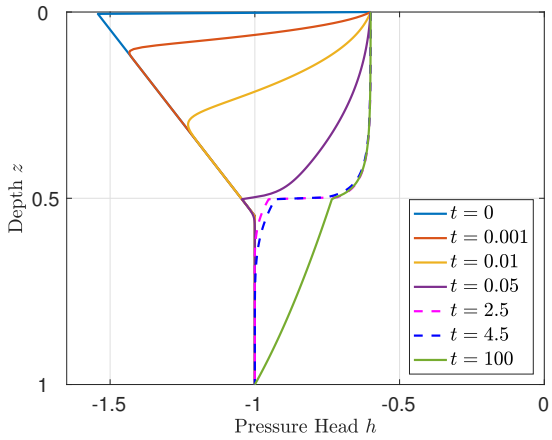

(c) Pressure Head Profile for $N = 200$

Figure 3.2: Numerical Solutions of the Gardner Model Case 1

Case 2 – Shaded Region

This case occurs when the fixed-point iteration converges to a 2-cycle. It can be avoided by switching to a different iterative method for solving the interface problem (2.15), for example, using a Newton iteration instead.

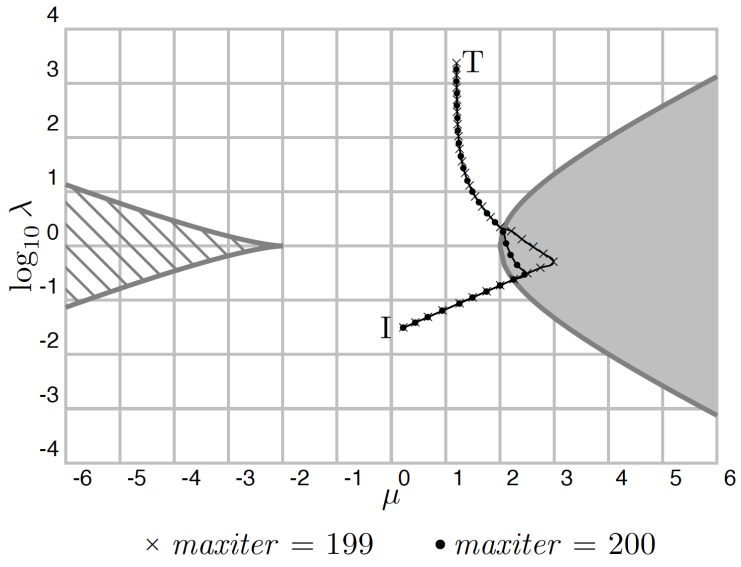

(a) (μ, λ) Trajectories at the Interface.

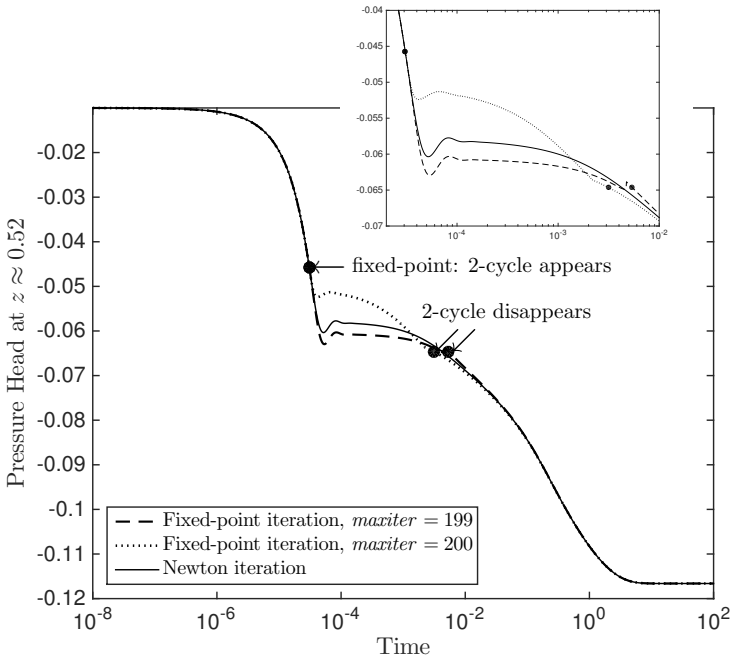

(b) Pressure Head below the Interface.

Figure 3.3: Gardner Model Case 2.

The solution process is illustrated in Figure 3.3 when such a situation arises in the numerical simulation using the fixed-point iteration. The (μ, λ) trajectories at the interface during the numerical run $0 \leq t \leq 100$ with $N = 24$ using the fixed-point iteration (2.16) is shown in Figure 3.3(a). For different maximum iteration number (*maxiter*), 199 (crosses) or 200 (dots), the trajectories are apart from each other in the shaded region due to alternating roots in 2-cycles of the fixed-point iteration.

In this case, the 2-cycle oscillates between two values, neither of which satisfies Equation (2.15). The resulting fluxes appearing on each side of the rightmost equality in (2.12) are not equal anymore. Instead of (2.12), the arithmetic average of these fluxes is considered,

$$q_{j+\frac{1}{2}} \approx \frac{1}{2}\left[K^{-}_{j+\frac{1}{2}}\left(1 - \frac{h^{-}_{j+1} - h_j}{\Delta}\right) + K^{+}_{j+\frac{1}{2}}\left(1 - \frac{h_{j+1} - h^{+}_{j}}{\Delta}\right)\right]. \tag{3.1}$$

The non-dimensionalized boundary pressure heads are set to $h_{\text{top}} = -0.6$ and $h_{\text{bottom}} = -0.01$, corresponding to an evaporation process. The initial pressure head profile is linear in the upper layer and constant in the lower layer. The fixed-point iteration exhibits a 2-cycle only for relatively coarse grids. Figure 3.3(b) shows the pressure head at $z = 0.52$, which is the first grid point below the interface, when $N = 24$. The simulation is compared with the numerical solution obtained via a Newton iteration. As in case 1, these results also indicate that non-convergence of the fixed-point iteration is temporary and has no long-lasting impact on the solution at later times. The evaporation process in the whole soil column is not shown here because the difference in the entire pressure head profile is not much visible.

Considering the risk of a 2-cycle of a fixed-point iteration, a Newton iteration is used by default in further implementation when using more advanced models (MvG and FXLR).

3.1.2 Two-Layer Case Using MvG Model

For the MvG model, multiple solutions of the interface problem also exist, for example, when using parameters given in Table 3.2 and (non-dimensionalized) boundary conditions $h_{\text{top}} = -1$ and $h_{\text{bottom}} = -135$. The initial pressure head profile is set linear throughout the soil column, i.e., $h_{\text{initial}}(z) = h_{\text{bottom}} - (1 - z)$ for $0 \leq z \leq 1$.

Table 3.2: Dimensionless Soil Hydraulic Parameters for the Two-Layer Case Using the MvG Model.

Layer	α	β	n	θ_s	θ_r
upper	0.13	0.8	2.5	0.368	0.001
lower	0.29	1	2.72	0.368	0.001

Figure 3.4(a) shows the overall infiltration process for $N = 104$ and $N = 110$. When $N = 104$ the interface problem exhibits multiple solutions during the simulation, while $N = 110$ the interface problem always has a unique solution. The impact of the multiplicity of solutions can be seen in Figure 3.4(b) to remain local in time (around $t \approx 0.015$) and in the vicinity of the soil interface at $z = 0.5$. Although the two values of N are very close, Figure 3.4(b) demonstrates numerical ponding (as the solid curve for $t = 0.0149$ crosses the other two curves) due to the existence of multiple solutions to the interface problem when using $N = 104$.

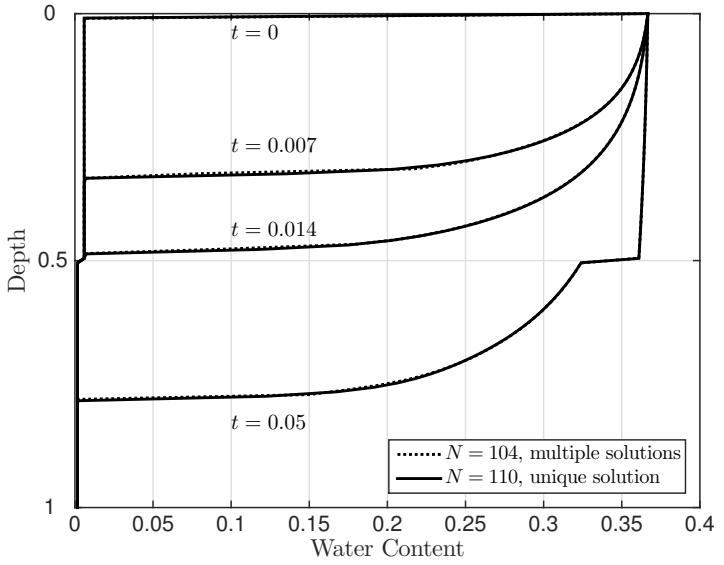

(a) Water Content Profiles of an Infiltration Process

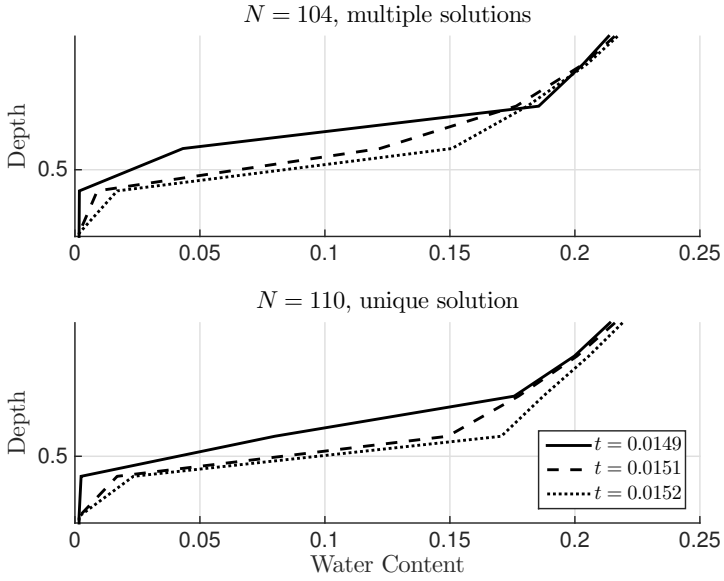

(b) Water Content Profiles near the Interface

Figure 3.4: Numerical Solutions for the MvG Model

3.1.3 Two-Layer Case Using FXLR Model

For the FXLR model, the numerical solution of a "transparent" interface problem is presented here. The purpose of this numerical experiment is to demonstrate the possibility for highly nonlinear models to introduce numerical issues with the interface problem even across very similar soil types.

When upper and lower layers have identical hydraulic properties ($K^+ = K^- = K$), the interface equation (2.15) yields

$$g(1) = \sqrt{\frac{K_j K(h_{j+1})}{K_{j+1} K(h_j)}} = \sqrt{\frac{K_j K_{j+1}}{K_{j+1} K_j}} = 1, \tag{3.2}$$

i.e., $r = 1$ is a root of Equation (2.15) and $K^+_{j+\frac{1}{2}} = K^-_{j+\frac{1}{2}} = K_{j+\frac{1}{2}}$. In other words, the interface is transparent in a homogeneous soil. In the case of the Gardner model, for which identical layers lead to a unique root ($\lambda = 1$ and $\mu = 0$ in Equations (2.25) and (2.26)), the interface problem is guaranteed a unique solution. However, even in the case of a transparent interface, the interface problem may admit multiple (three) solutions for certain advanced hydraulic model. This work presents a case of the FXLR model for the interface problem to have other roots $r \neq 1$ under such transparent condition, typically one greater than 1 and one smaller than 1.

One example of such instance is obtained for the parameters listed in Table 3.3 (used in both layers) and (non-dimensionalized) boundary pressure heads $h_{\text{top}} = -40$ and $h_{\text{bottom}} = -70$. The initial pressure head profile is linear throughout the soil.

Table 3.3: Dimensionless Soil Hydraulic Parameters for the Two-Layer Case Using the FXLR Model (Transparent Interface)

Layer	α	β	n	m	p	θ_s	θ_r
upper and lower	0.015	1	2.5	5	18	0.4	0.01

If multiple solutions exist for the transparent interface, forcing $r = 1$ is equivalent to solving (2.3) in a single layer. Figure 3.5 shows general convergence in the numerical water profiles as Δ decreases and $r = 1$ is fixed. Under this situation, multiple solutions only exist for a short period as the wetting fronts passes through the interface.

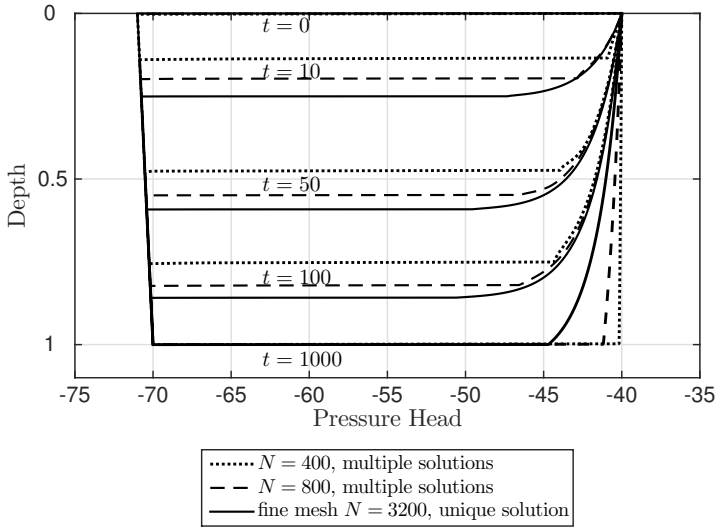

Figure 3.5: Numerical Solutions for the FXLR Model with a Transparent Interface ($z = 0.5$) Forcing $r = 1$.

Because $r = 1$ is typically an unstable solution for the fixed-point iteration (but stable for the Newton iteration), it is still possible for the fixed-point iteration to converge to a root $r \neq 1$ even when starting from a value of r close to 1. In such a situation, let the simulation force to select the root larger than 1. Figure 3.6 illustrates the resulting pressure head profile in the soil with $N = 500$. Once the wetting front arrives at the interface, the numerical flow nonphysically accumulates at the interface. Since r is overestimated, the hydraulic conductivities of the upper layer are unrealistically larger than conductivities in the lower layer, and the lower layer

behaves like a numerical impervious block. Multiple roots of the interface equation do not disappear under this situation. It is worth noting that positive extrapolated pressure heads $h_j^+, h_{j+1}^- > 0$ and numerical instabilities occur when using the largest root of the interface problem.

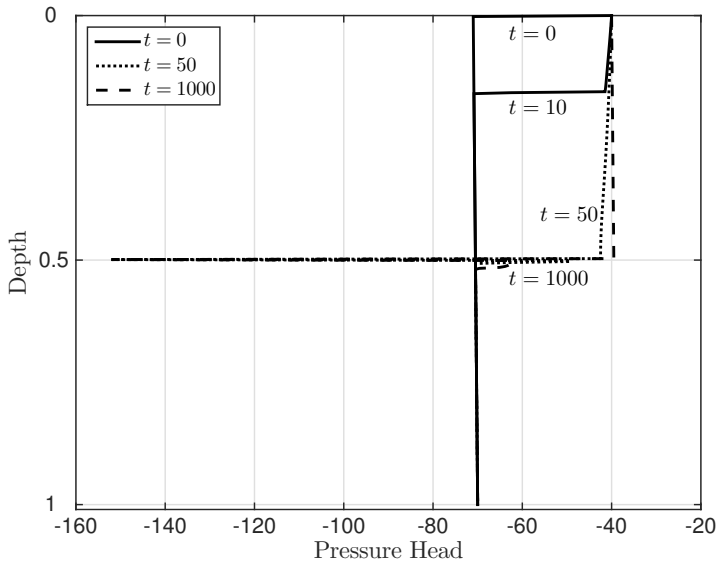

Figure 3.6: Numerical Solutions for the FXLR Model with a Transparent Interface ($z = 0.5$) Using the Root Larger Than 1.

3.2 Comparison of Averaging Methods for Cell-Centered Conductivities

3.2.1 Comparison in a Two-Layer Soil

Numerical simulations of one-dimensional infiltration flow in a two-layer soil are used here to compare four hydraulic conductivity averaging methods and their impact on the interface problem. Numerical experiments are conducted using the same parameters and conditions in Section 3.1.1.

Table 3.4 lists whether physical numerical simulations are obtained and whether the uniqueness of the solution to the interface problem is guaranteed for different N

values.

Table 3.4: Gardner Model: Well-Posedness of the Interface Problem Using Different Conductivity Averaging Methods.

Harmonic Mean	$N = 50$ Physical Solution: ✗ Uniqueness: ✗	$N = 100$ Physical Solution: ✗ Uniqueness: ✗
	$N = 200$ Physical Solution: ✗ Uniqueness: ✗	$N = 1000$ Physical Solution: ✗ Uniqueness: ✗
Geometric Mean	$N = 50$ Physical Solution: ✗ Uniqueness: ✗	$N = 100$ Physical Solution: Partially Uniqueness: Temporarily
	$N = 200$ Physical Solution: ✓ Uniqueness: ✓	$N = 1000$ Physical Solution: ✓ Uniqueness: ✓
Log-Mean	$N = 50$ Physical Solution: ✓ Uniqueness: ✓	$N = 100$ Physical Solution: ✓ Uniqueness: ✓
	$N = 200$ Physical Solution: ✓ Uniqueness: ✓	$N = 1000$ Physical Solution: ✓ Uniqueness: ✓
Arithmetic Mean	$N = 50$ Physical Solution: ✓ Uniqueness: ✓	$N = 100$ Physical Solution: ✓ Uniqueness: ✓
	$N = 200$ Physical Solution: ✓ Uniqueness: ✓	$N = 1000$ Physical Solution: ✓ Uniqueness: ✓

Figure 3.7 shows the numerical infiltration process, when $N = 100$, using the four hydraulic conductivities averaging methods described in Section 2.4 (used throughout the domain and not simply at the interface).

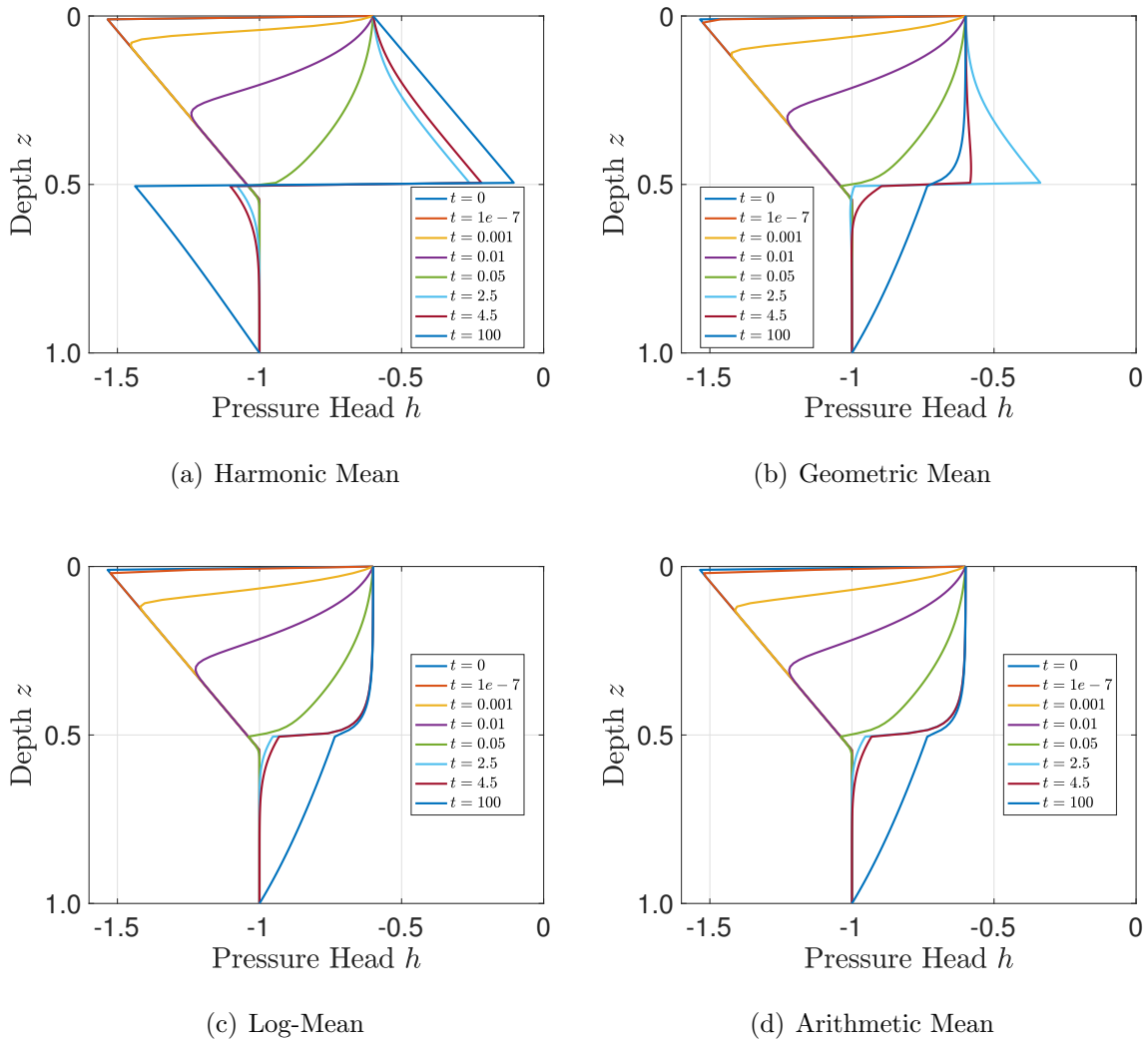

(a) Harmonic Mean

(b) Geometric Mean

(c) Log-Mean

(d) Arithmetic Mean

Figure 3.7: Numerical Solutions of Unsaturated Flow in a Two-Layer Soil Using Different Averaging Methods for Cell-Centered Hydraulic Conductivities When $N = 100$.

The harmonic mean leads to a non-physical solution as soon as the water front reaches the interface, and numerical ponding occuring at the interface persists later on because of the underestimated interface conductivity. The source of the problem can be attributed to the existence of multiple solutions to the interface problem when the gradient of pressure head starts increasing at the passage of the wetting front, a larger than physical root being selected in the numerical iteration. The

simulation with the geometric mean temporarily exhibits a similar behavior, with the existence of multiple solutions, but the ponding issue is only temporary as the pressure head profile seems to correctly adjust itself once the interface problem ceases to have multiple solutions(after the wetting front passes). Both the log-mean and the arithmetic mean lead, in this example, to an interface problem with a unique root at all times. The corresponding head profiles can be verified to be correct by using a finer spatial discretization.

For the MvG model and the FXLR model, numerical experiments using different conductivity averaging methods are compared in multi-layer soils in Section 3.2.3.

3.2.2 Comparison of Geometric Mean and Log-Mean with Mesh Refinement

As shown in previous simulations in a two-layer soil, using the geometric mean for conductivities leads to multiple roots of the interface problem, while using the log-mean guarantees a unique root. In this section, a local mesh refinement strategy is proposed in order to show the critical discretization size needed for the geometric mean to cease multiplicity issue of the interface problem compared with the log-mean. It is worth noting that refining the mesh locally around a soil interface requires much less computational cost to solve the Richards' equation than refining the mesh globally, except in an agent-based heterogenous soil (i.e., each cell is a distinct soil layer). As mentioned before, this mesh refinement strategy is feasible only when a local scheme for estimating interface conductivities is employed. Notice that the grid around an interface is not uniform but symmetric about the interface, thus the value of Δ in Equation (2.12) is the cell size that straddles the interface.

Figure 3.8 shows the local mesh refinement around a soil interface. Several iterations of refinements are applied until the interface problem ceases to have multiple roots. Each refinement adds two trisection points of the cell containing the interface

to the original grid points and keeps all the rest grid points as in the last iteration. In the numerical implementation, the index of grid points should be updated and numbered sequentially after each iteration refinement.

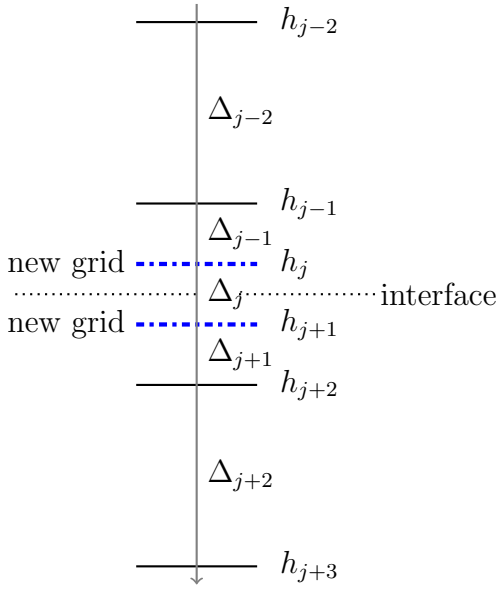

Figure 3.8: Local Mesh Refinement Around a Soil Interface. New Grid Points Are the Trisection Points of the Previous Interface Cell, $\Delta_{j-1} = \Delta_j = \Delta_{j+1}$.

The numerical experiments are conducted using the Gardner model with the geometric mean and the log-mean for conductivities. The initial number of (uniform) finite difference cells, N, is 100. Soil hydraulic parameters for the Gardner model used here are $\alpha^- = 5, \alpha^+ = 3, \beta^{\pm} = 1, \theta_r = 0.01, \theta_s = 0.5$ (non-dimensionalized). The boundary conditions are fixed pressure heads $h_{\text{top}} = -0.5$ and $h_{\text{bot}} = -5$ (non-dimensionalized). Figure 3.9 shows that, using the geometric mean, multiple solutions of the interface problem vanish after four levels of refinements. The uniqueness of solution is always guaranteed using the log-mean, that is, no mesh refinement is needed for the log-mean. Compared to the log-mean, using the geometric mean requires a much finer mesh (1/27 of the size for the log-mean in this example) to ensure good

numerical performance around the soil layer interface. Since the Richards' equation is very stiff, this defect of the geometric mean can lead to unaffordable computational cost.

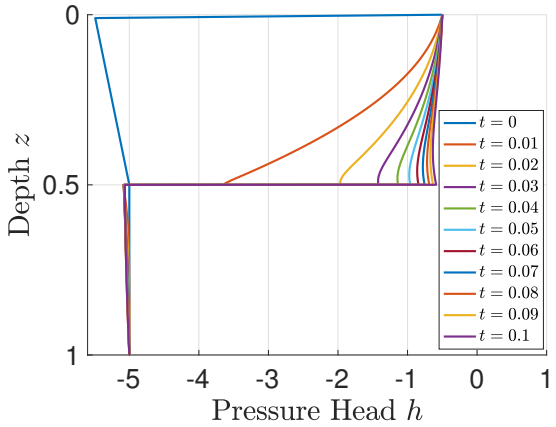

(a) Geometric Mean with 3 Levels of Refinements at the Interface. Multiple Solutions Exist.

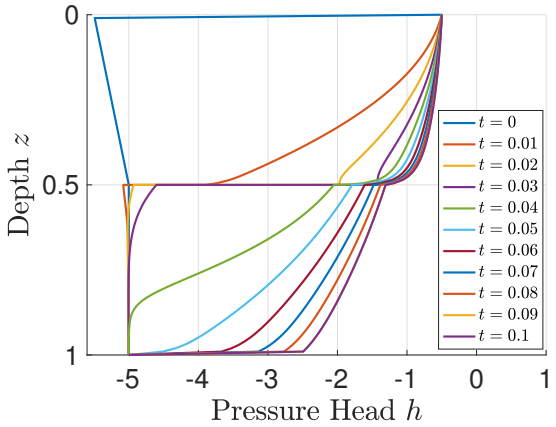

(b) Geometric Mean with 4 Levels of Refinements at the Interface. A Unique Solution Is Guaranteed.

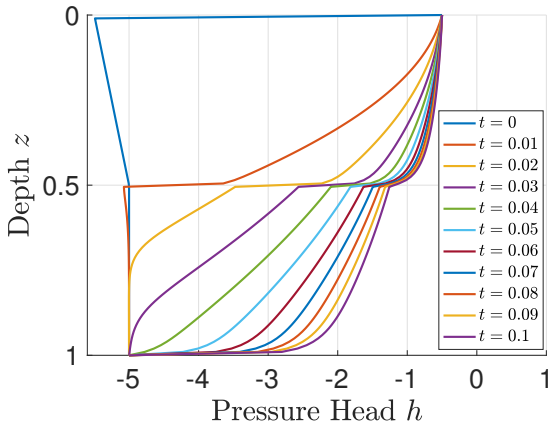

(c) Log-Mean with No Refinement at the Interface. A Unique Solution Is Guaranteed.

Figure 3.9: Comparison of Numerical Solutions Using the Geometric Mean and the Log-Mean, with Spatial Mesh Refinements at the Interface ($z = 0.5$).

3.2.3 Comparison in Multi-Layer Soils

Considering a vertical soil column of several layers, each layer is associated with a set of soil hydraulic parameters. The discrete scheme for an n-layer soil with a uniform spatial discretization is shown in Figure 3.10.

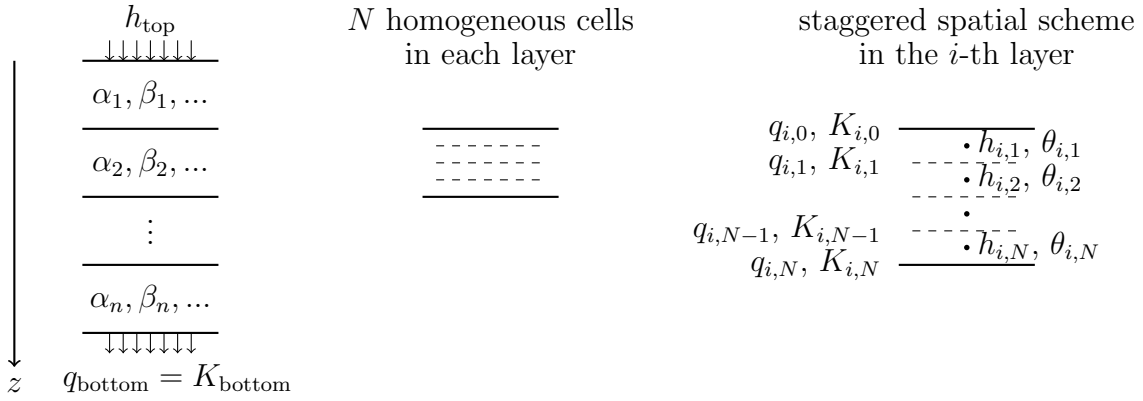

Figure 3.10: Finite Difference Scheme in an n-Layer Soil.

Multi-Layer Case Using the Gardner Model

Five alternating layers with uniform thickness is set for the Gardner model case. Each layer is discretized into 20 uniform spatial cells. The odd layers (layer 1, 3 and 5) are assigned non-dimensionalized soil parameters $\alpha = 13, \beta = 1$, and the even layers (layer 2 and 4) with $\alpha = 1, \beta = 0.0006$. The residual and saturated water contents are the same for the entire soil, $\theta_r = 0.06, \theta_s = 0.4$. The initial pressure head profile is $h_{\text{initial}} = -1$ (non-dimentionalized). The boundary conditions are $h_{\text{top}} = -0.4$ (fixed pressure head) and $q_{\text{bottom}} = K_{\text{bottom}}$ (free drainage). Figure 3.11 shows the numerical solutions of pressure head at different times using the four averaging methods for cell-centered conductivities. The occurrence of multiple solutions of the interface problems is triggered across the interfaces at $z = 0.2$ and 0.6, when using the harmonic mean and the geometric mean. At $t = 1$, there is numerical ponding near

the interface $z = 0.2$ for the harmonic and geometric means. For the geometric mean, the multiple solutions of the interface problem disappear shortly after the wetting front has passed through this interface, then the numerical result autocorrects itself at $t = 3$ due to the diffusive nature of the flow (and the Richards' equation). However, the multiple solutions subsist after they first occur for the harmonic mean, and an incorrect infiltration process persists because of low conductivities at the interfaces from a high conductivity layer to a low conductivity layer. Similar behavior is shown for the harmonic mean and the geometric mean due to the existence of multiple solutions across the interface $z = 0.6$ at $t = 10, 100$. The log-mean and the arithmetic mean in this case always admit a unique solution to the interface problems.

Multi-Layer Case Using the MvG Model

Numerical simulation for the MvG model in a ten-layer soil is investigated here. Each layer with uniform thickness is discretized into 20 uniform spatial cells. The odd layers (1, 3, 5, 7 and 9) are assigned with non-dimensionalized soil parameters $\alpha = 0.13, \beta = 1, n = 2.5$, and the even layers (2, 4, 6, 8 and 10) with $\alpha = 0.29, \beta = 1, n = 2.72$. The residual and saturated water contents are $\theta_r = 0.001, \theta_s = 0.368$ for the entire soil column. The boundary conditions are fixed pressure head values for the top and the bottom of the soil, $h_{\text{top}} = -1$ and $h_{\text{bottom}} = -135$. The initial pressure head profile is $h_{\text{initial}}(z) = -136 + z$.

Figure 3.12 shows the space-time relation representing where and when a given pressure head, $h = \ln\left((e^{h_{\text{top}}} + e^{h_{\text{bottom}}})/2\right)$, is obtained. Figures 3.13–3.18 shows the infiltration process (as water content profiles) at different times. When using the harmonic mean, the cell-centered conductivities are extremely underestimated so the numerical water infiltration is too slow to be acceptable. The wetting front has not reached the top-most interface at $z = 0.1$ when $t = 0.1$. The other three averaging

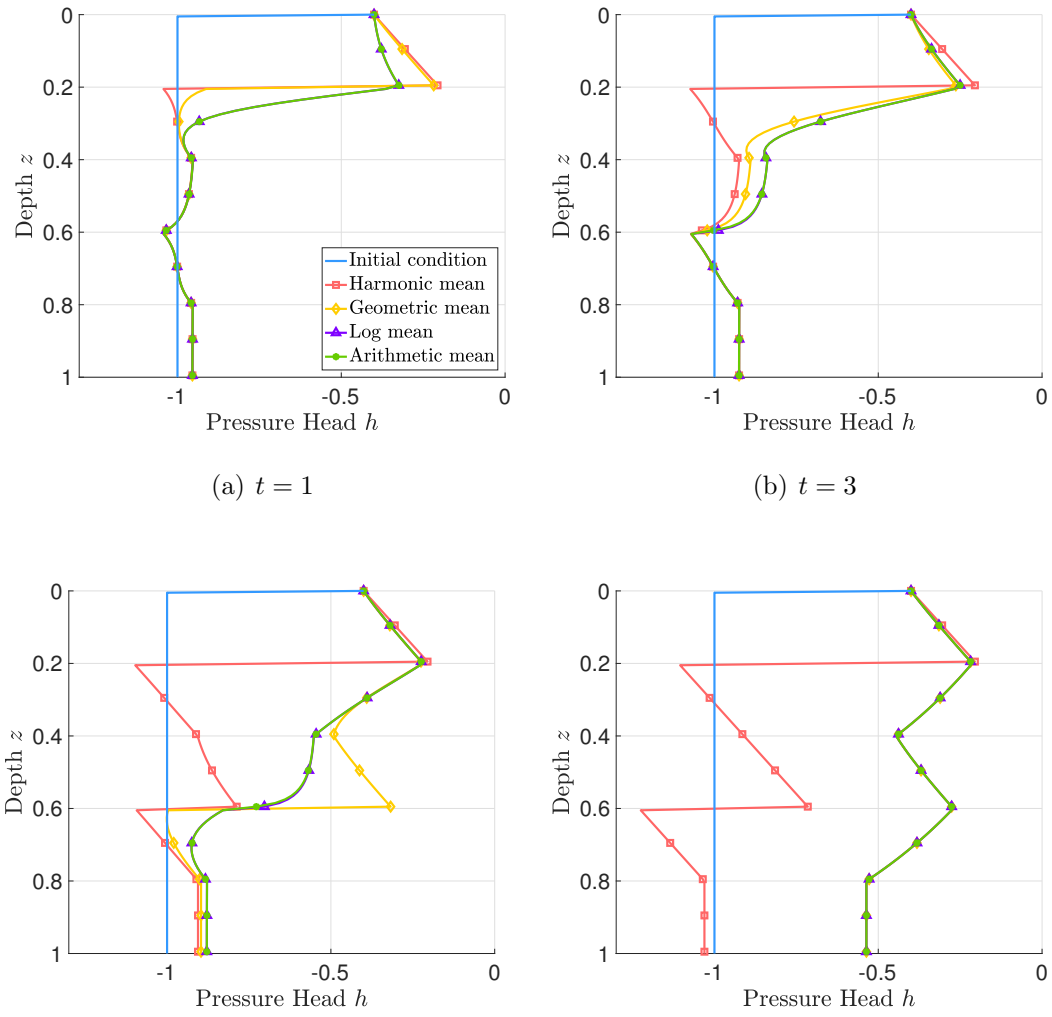

(a) $t = 1$ (b) $t = 3$

(c) $t = 10$ (d) $t = 1000$

Figure 3.11: Numerical Simulations at Different Times of a 1D Infiltration Process in a Five-Layer Soil Using the Gardner Model. Soil Interfaces Are $z = 0.2, 0.4, 0.6, 0.8$.

methods yield more acceptable results. However, using the geometric mean triggers multiple solutions to the interface problems, leading to oscillations (in Figure 3.12 and 3.13–3.18). These oscillations are in the vicinity of soil interfaces ($z = 0.1, 0.2, 0.3$, etc.). In this experiment, the log-mean and the arithmetic mean always admit a unique solution to the interface problems, as desired.

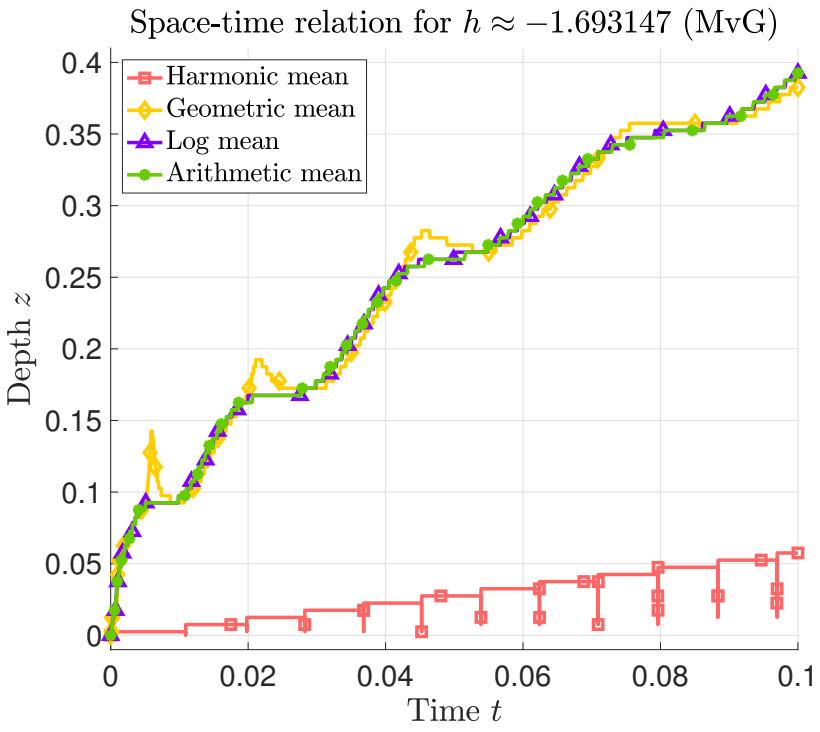

Figure 3.12: Depth vs Time Relation for Where and When a Given Pressure Head Value Is Reached in a 1D Infiltration Process in a Ten-Layer Soil Setting Using the MvG Model.

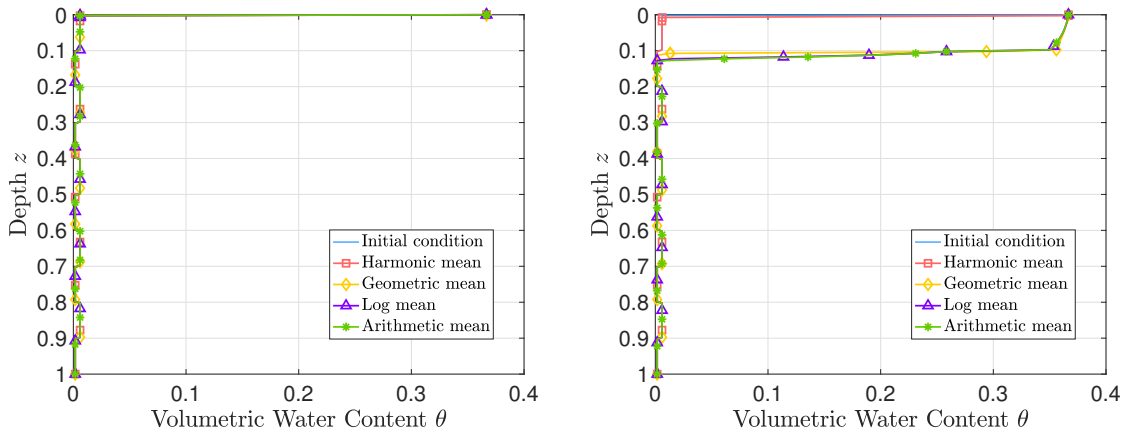

(a) $t = 0$ (b) $t = 0.001$

Figure 3.13: Numerical Simulations at Different Times of a 1D Infiltration Process in a Ten-Layer Soil Using the MvG Model – (1).

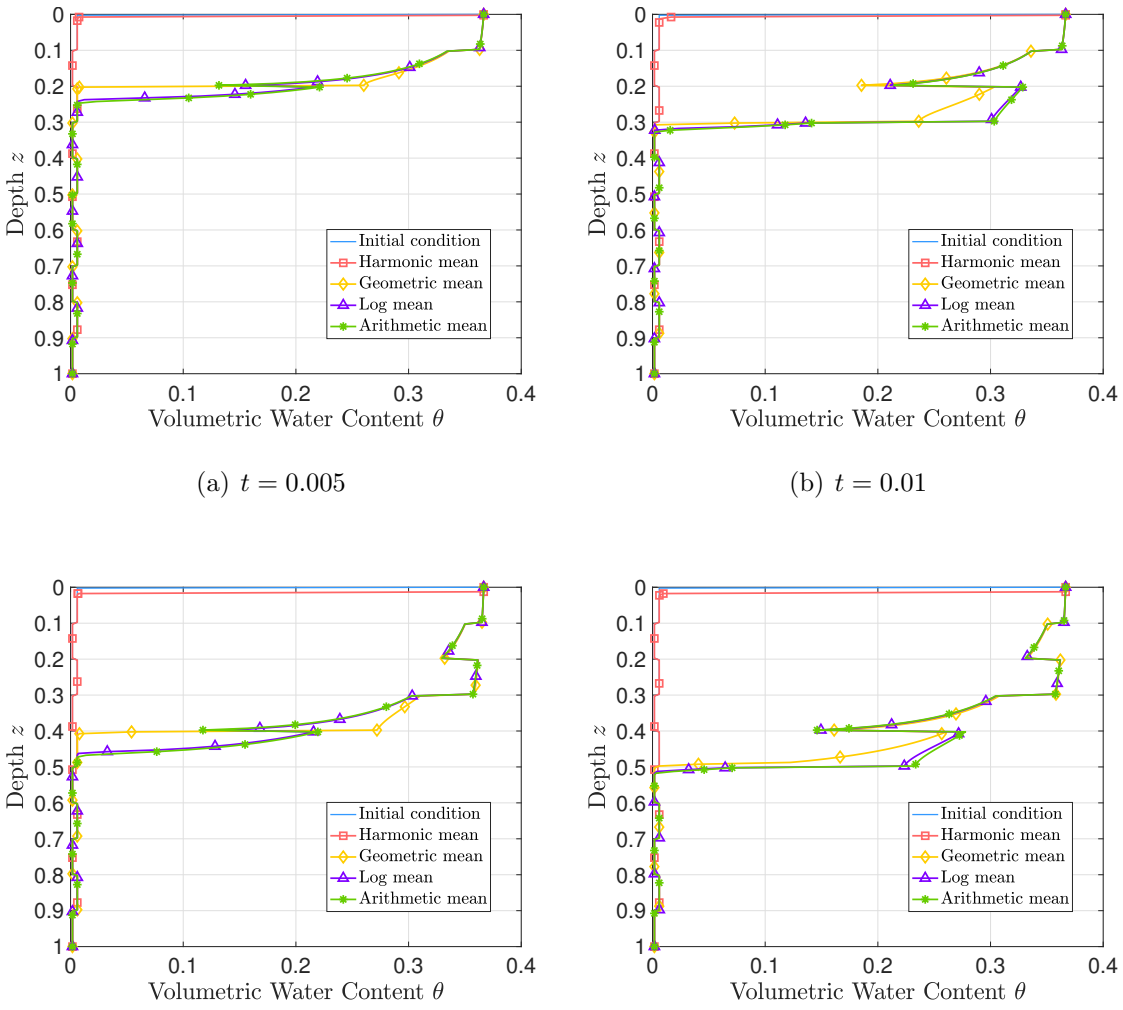

(a) $t = 0.005$ (b) $t = 0.01$

(c) $t = 0.02$ (d) $t = 0.025$

Figure 3.14: Numerical Simulations at Different Times of a 1D Infiltration Process in a Ten-Layer Soil Using the MvG Model – (2).

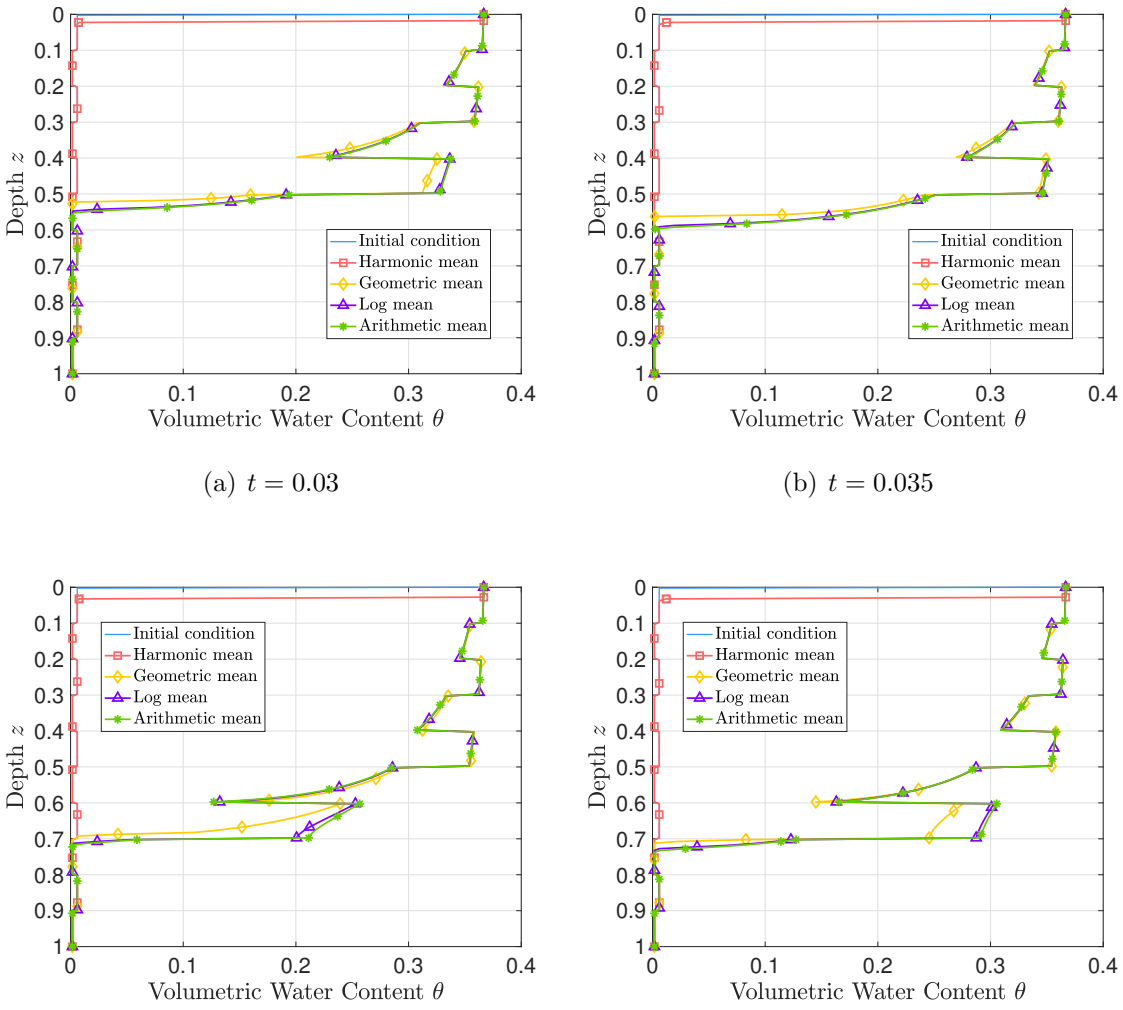

(a) $t = 0.03$ (b) $t = 0.035$

(c) $t = 0.048$ (d) $t = 0.052$

Figure 3.15: Numerical Simulations at Different Times of a 1D Infiltration Process in a Ten-Layer Soil Using the MvG Model – (3).

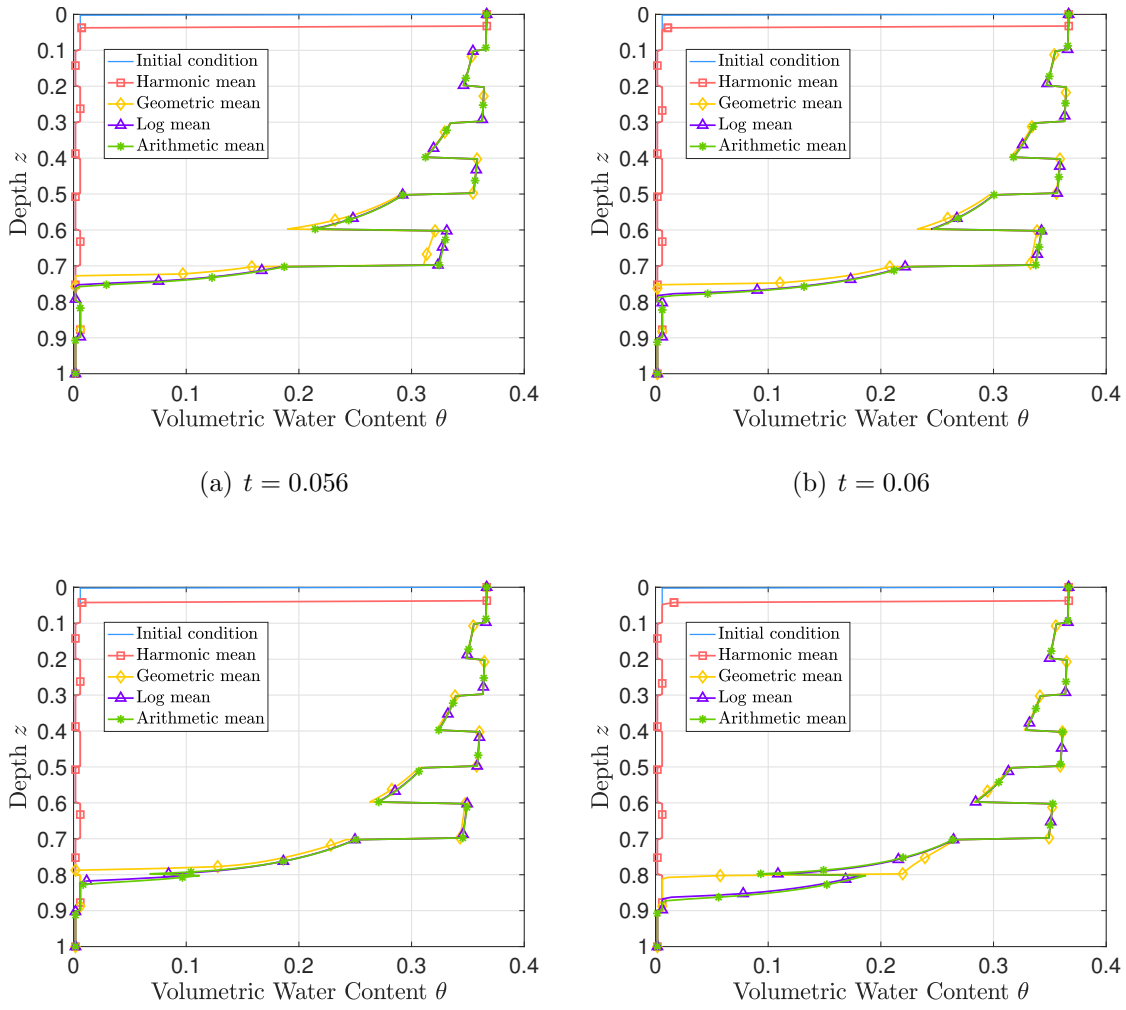

(a) $t = 0.056$ (b) $t = 0.06$

(c) $t = 0.065$ (d) $t = 0.07$

Figure 3.16: Numerical Simulations at Different Times of a 1D Infiltration Process in a Ten-Layer Soil Using the MvG Model – (4).

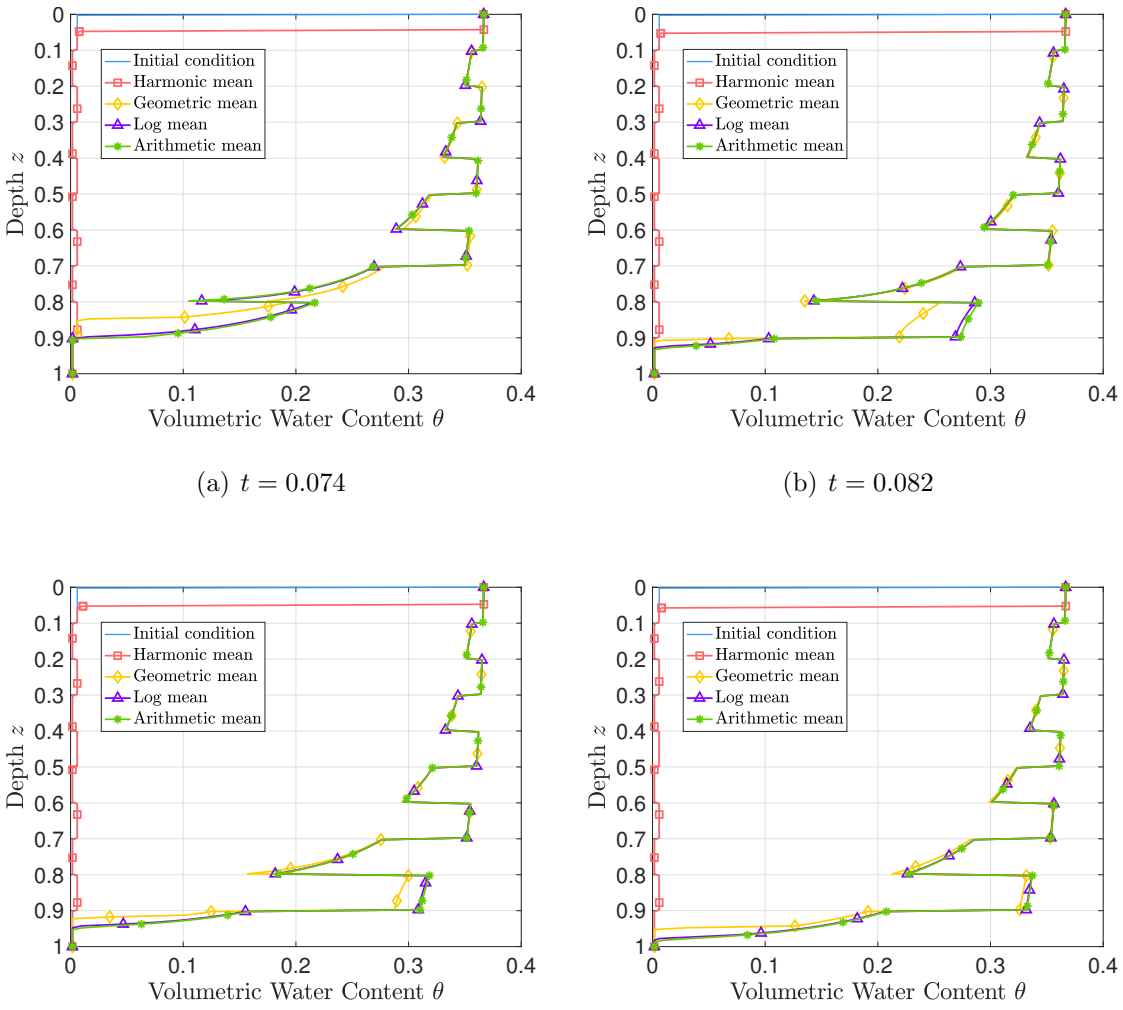

(a) $t = 0.074$

(b) $t = 0.082$

(c) $t = 0.086$

(d) $t = 0.092$

Figure 3.17: Numerical Simulations at Different Times of a 1D Infiltration Process in a Ten-Layer Soil Using the MvG Model – (5).

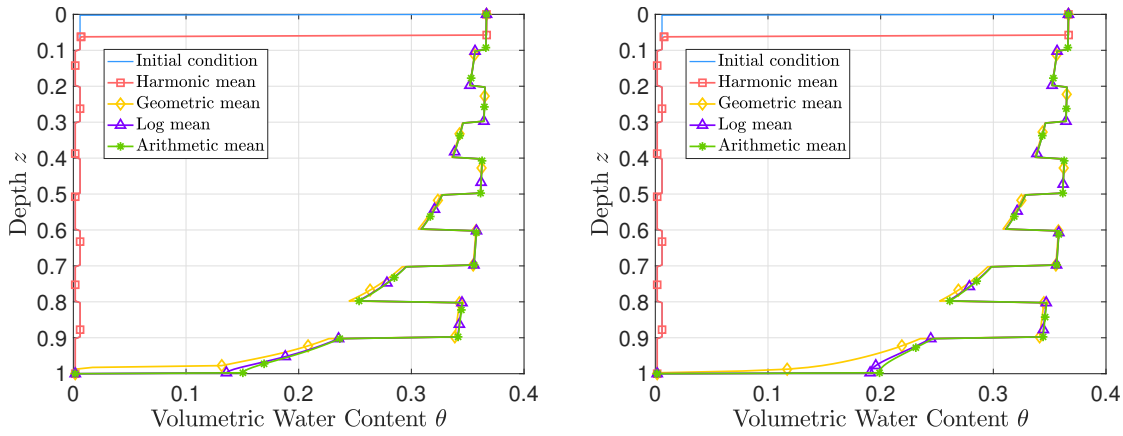

(a) $t = 0.098$ (b) $t = 0.1$

Figure 3.18: Numerical Simulations at Different Times of a 1D Infiltration Process in a Ten-Layer Soil Using the MvG Model – (6).

Multi-Layer Case Using the FXLR Model

A soil column with ten uniform layers discretized into 20 uniform cells each is used again for the FXLR model. Soil hydraulic parameters $\alpha = 0.015, m = 2.5, m = 5, p = 18$ are used for all the layers. The odd layers are assigned with $\beta = 1$ and the even layers $\beta = 0.9$. The initial/boundary conditions are $h_{\text{top}} = -70$ and $h_{\text{bottom}} = -40$ (non-dimensionalized).

Figure 3.19 shows the space-time relation representing where and when a given pressure head, $h = \ln\left((e^{h_{\text{top}}} + e^{h_{\text{bottom}}})/2\right)$, is obtained. Figure 3.20 shows the infiltration process (as water content profiles) at time $t = 1, 10, 60, 100$. The numerical infiltration using the harmonic mean is too slow as shown in Figure 3.20, similar to the numerical result using the MvG model. Oscillations are observed for the geometric mean due to the existence of multiple roots to the interface problems. Numerical ponding occurs at soil interfaces despite the relatively small dissimilarity between the saturated conductivities of even and odd layers, due to the ill-posedness of the inter-

face problems when using the geometric mean. It is noticed that multiple solutions still exist in a homogeneous soil column (i.e., the same β value is used for all these layers), but the oscillations disappear for the geometric mean (between $t \approx 50$ and $t \approx 450$ in Figure 3.19) because $r = 1$ is always obtained for the interface equations. In this experiment, the log-mean and the arithmetic mean again admit a unique solution and exhibit similar behavior of the infiltration process. Also notice that the infiltration process using the geometric mean is much slower than log-mean and arithmetic mean, and the downward flow is hindered at interfaces due to the existence of multiple roots of the interface problem. Numerical oscillations due to the multiplicity issue of the interface problems when using the geometric mean are dramatically visible in Figure 3.19. Compared with Figure 3.12, similar behaviors of the four means are observed for the FXLR model.

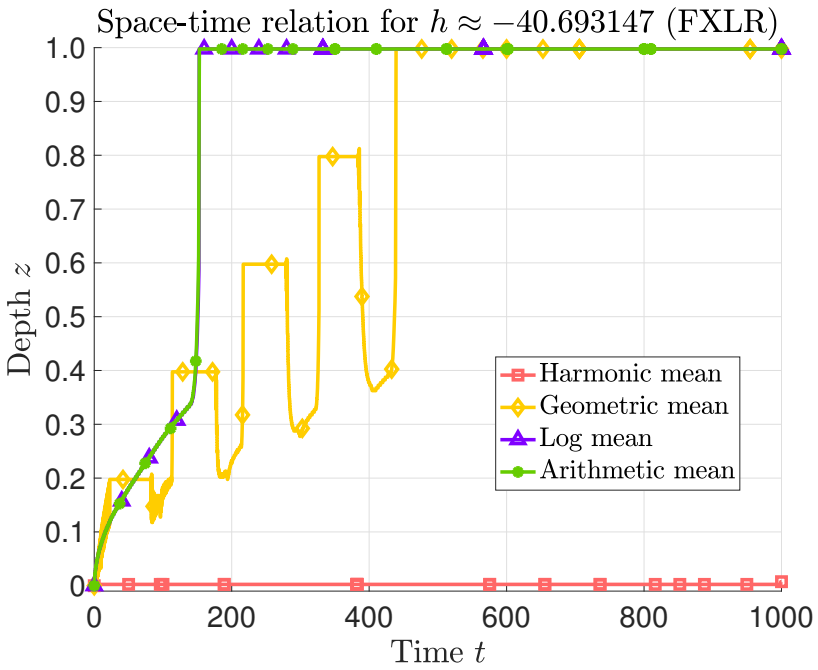

Figure 3.19: Depth vs Time Relation for Where and When a Given Pressure Head Value Is Reached in a 1D Infiltration Process in a Ten-Layer Soil Setting Using the FXLR Model.

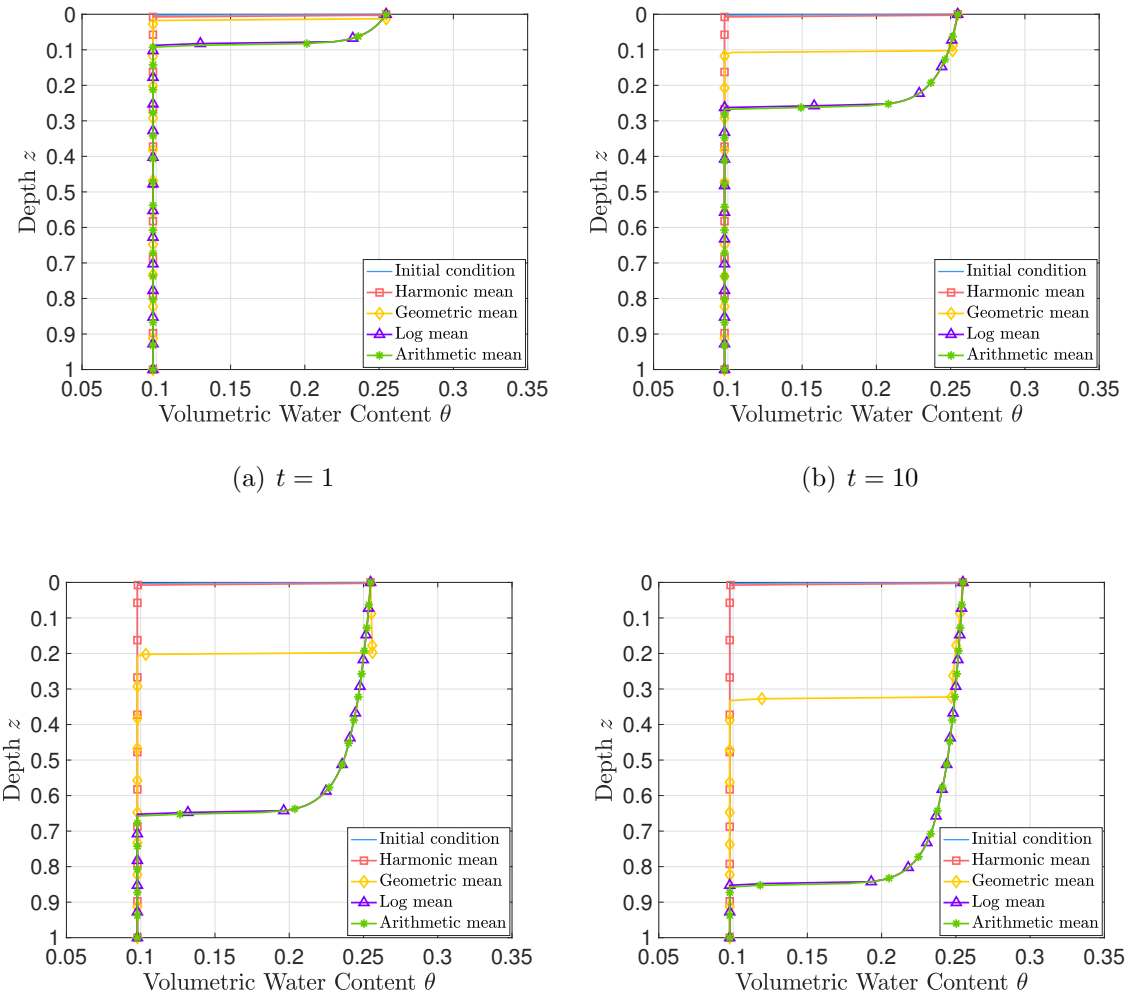

(a) $t = 1$ (b) $t = 10$

(c) $t = 60$ (d) $t = 100$

Figure 3.20: Numerical Simulations at Different Times of a 1D Infiltration Process in a Ten-Layer Soil Using the FXLR Model.

3.3 Numerical Results with Stochastic Soil Hydraulic Parameters

The Monte Carlo simulations are performed based on a normal distribution of $b = \ln(\beta) \sim \mathcal{N}(\bar{b}, \sigma_b^2)$ (Carsel and Parrish, 1988; Russo and Bouton, 1992). In this work, stochastic simulations are based on the Gardner model with the geometric mean for cell-centered conductivities, in order to compare with the numerical solution of the

reduced model (2.67). Set $\bar{b} = 0$ because of non-dimensionalization of the saturated conductivity β (in Appendix C.1). Several values of the standard deviation, σ_b, are investigated. Other soil parameters in the Gardner model are assigned isotropic, $\alpha = 2$, $\theta_r = 0.1$, $\theta_s = 0.6$.

To investigate unsaturated flow in a heterogeneous unsaturated soil column, the boundary conditions are a fixed flux at the top surface $q_{\text{top}} = 0.1$ and a fixed pressure head at the bottom $h_{\text{bottom}} = -1.0$ (both dimensionless). The initial pressure head condition is $h_{\text{initial}} = -2+z, 0 \leq z \leq 1$ (linear throughout the soil). This 1D (vertical) soil column is discretized into 50 spatial finite different cells, and each cell is assigned with random $b \sim \mathcal{N}(0, \sigma_b^2)$.

For each choice of σ_b, 200 stochastic realizations are performed. Each realization is associated with an array of b values for the sequence of spatical cells, and direct numerical simulations (DNS) are implemented by solving interface problems for boundaries of all spatical cells (like in a multi-layer soil that each cell is a distinct layer).

Figures 3.21 and 3.22 demonstrate a comparison of solutions obtained from three methods:

(1) the (statistical) mean of pressure head profiles of all DNS for a given σ_b,

(2) the solution using homogenized parameters (statistical mean of all generated random b for the same σ_b),

(3) the solution of the reduced model (2.67).

As shown in Figures 3.21 and 3.22, when σ_b increases, both the mean of DNS and the solution of the reduced model show larger pressure head (higher water content) in the upper part of the soil column and smaller pressure head (lower water content) in the lower part. This indicates that using the homogenized parameters of

heterogeneous soils in the simulation of unsaturated flow results in less variation in water content. These results also show that the reduced model can capture the higher pressure head value near the soil surface in this simulation. There is less deviation near the bottom of the soil from DNS and the reduced model to the solution of homogenized parameters, due to the fact that the pressure head is fixed at the bottom of the soil column. Also notice that the top boundary condition is a fixed positive infiltration flux (Neumann condition), so it accounts for the larger values of pressure head (wetter soil) near the soil surface compared to the solution of homogenized parameters. Further, compared to the mean of DNS, the solution of the reduced model exhibits larger deviation from the solution of homogenized parameters in the upper part and less deviation in the lower part, especially for larger values of σ_b.

Figure 3.23 shows four different DNS realizations using a fixed $\sigma_b = 0.8$, corresponding to Figure 3.22(a). It demonstrates that stochastic realizations (despite the same distribution of soil parameter) can vary dramatically from each other.

Figure 3.24–3.27 show the histograms and probability density functions (PDF) of 200 DNS realizations for each choice of $\sigma_b = 0.2, 0.4, 0.8, 1.2$. It is worth noting that when σ_b is large (e.g. 0.8), the solutions obtained from homogenized soil parameters fall out of the 3σ interval of the PDF. Although the solutions of the reduced model overestimate the water content near surface when σ_b is large, they are closer to the corresponding statistical mean of DNS. Results indicate that using homogenized soil hydraulic parameters in a extensively heterogeneous soil results in large errors and underestimates the variation of water content in such an infiltration process. The reduced model, as well as DNS, produces better approximation of the infiltration pattern in heterogeneous soils because it captures the large variation of water content.

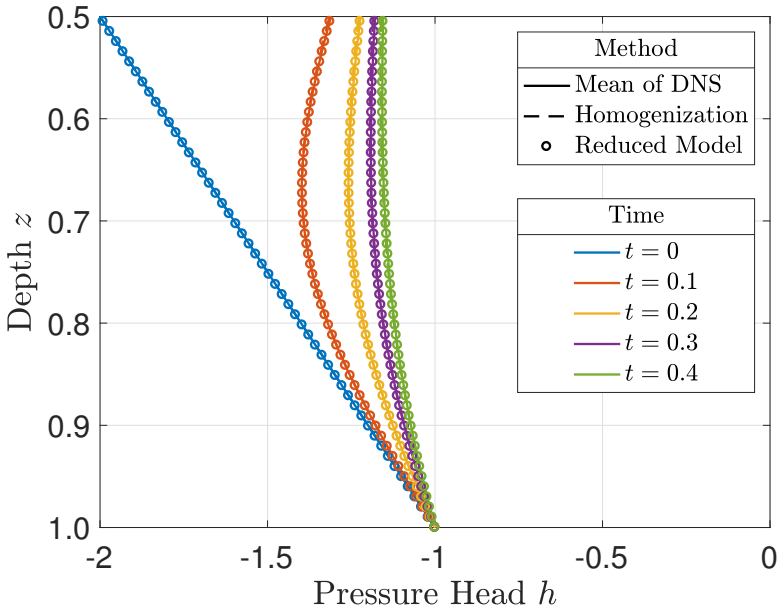

(a) $\sigma_b = 0.2$

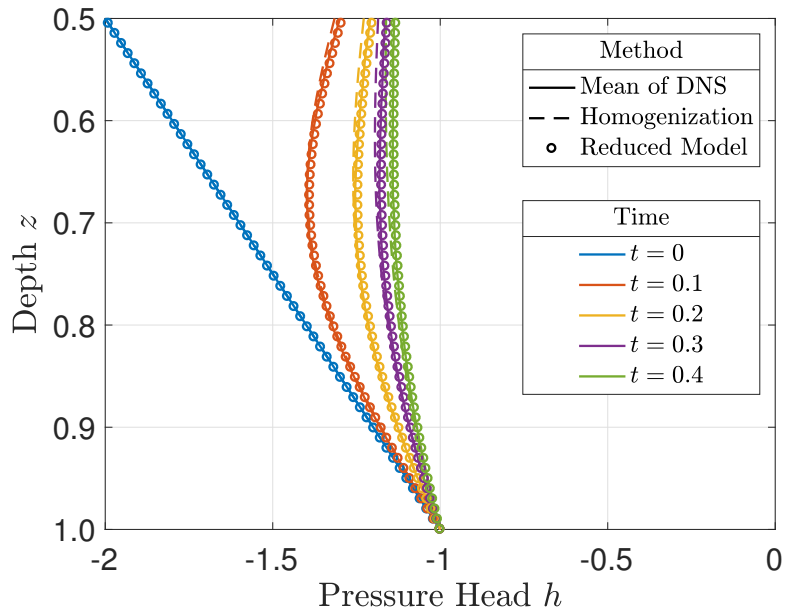

(b) $\sigma_b = 0.4$

Figure 3.21: Comparison of Mean of DNS (Solid), Solution Using Homogenized Parameters (Dashed), and Solution of the Reduced Model (Circle), for $\sigma_b = 0.2, 0.4$.

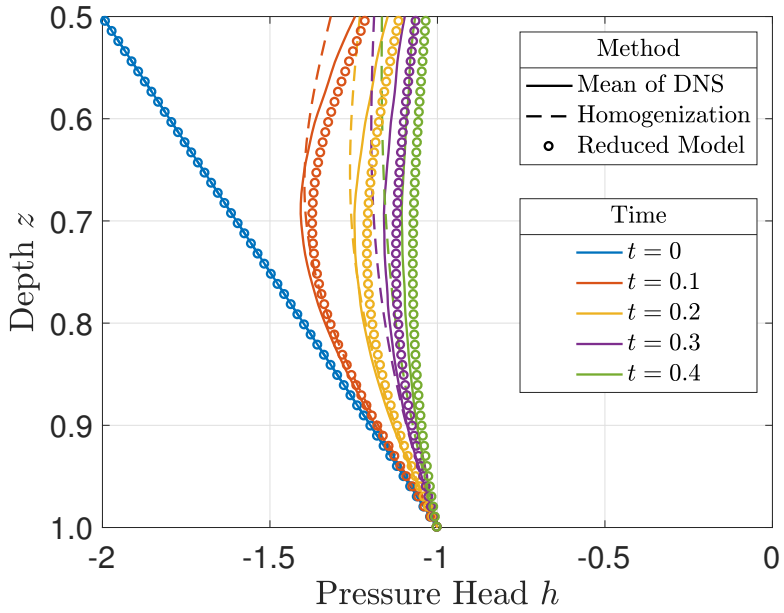

(a) $\sigma_b = 0.8$

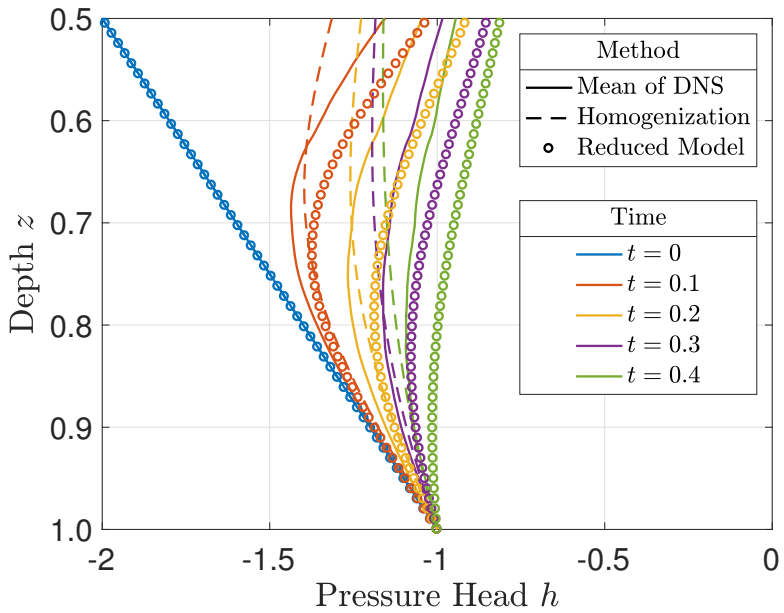

(b) $\sigma_b = 1.2$

Figure 3.22: Comparison of Mean of DNS (Solid), Solution Using Homogenized Parameters (Dashed), and Solution of the Reduced Model (Circle), for $\sigma_b = 0.8, 1.2$.

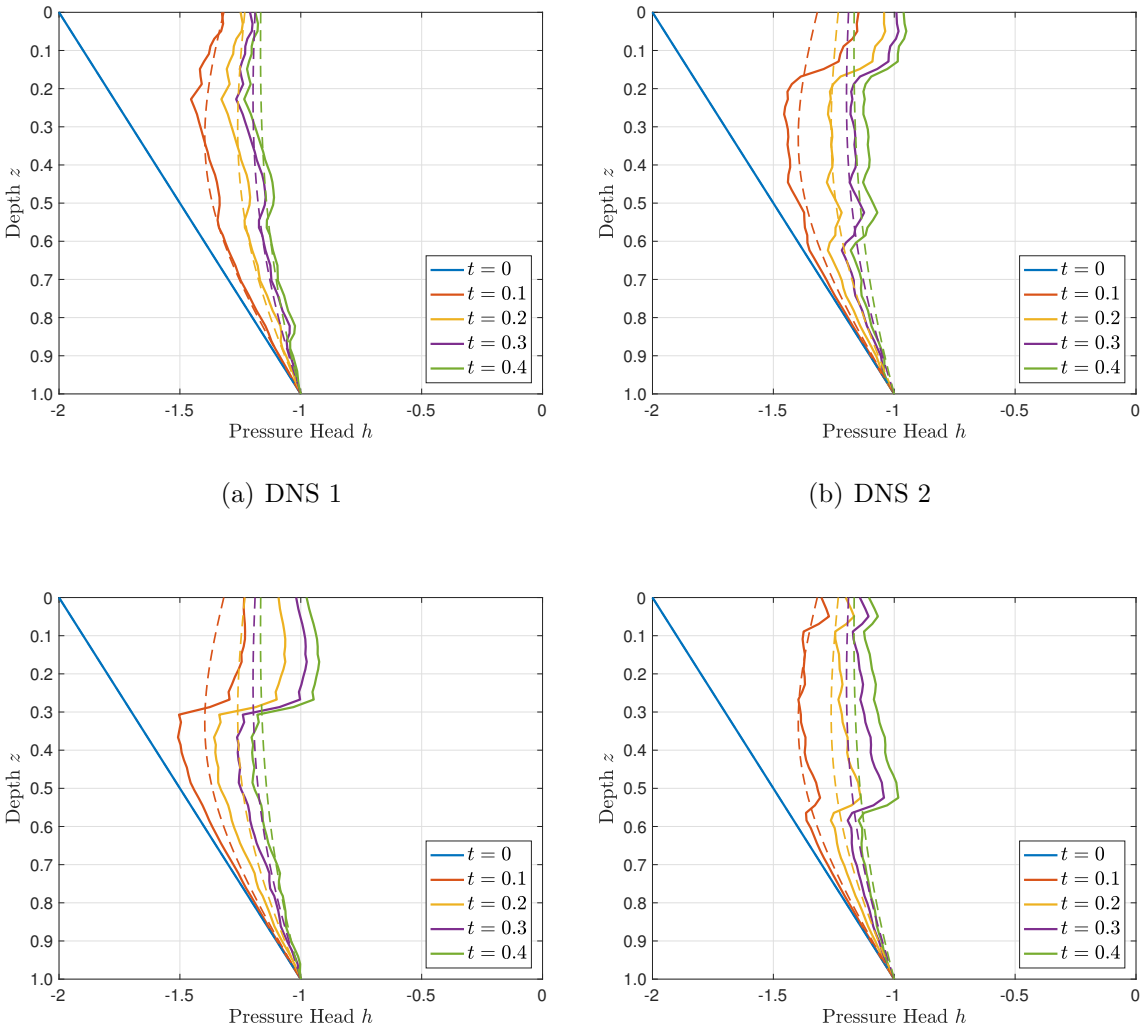

(a) DNS 1

(b) DNS 2

(c) DNS 3

(d) DNS 4

Figure 3.23: Four DNS Realizations (Solid Curves) for $\sigma_b = 0.8$, Compared with the Solution Using Homogenized Parameters (Dashed Curves), Corresponding to Figure 3.22(a).

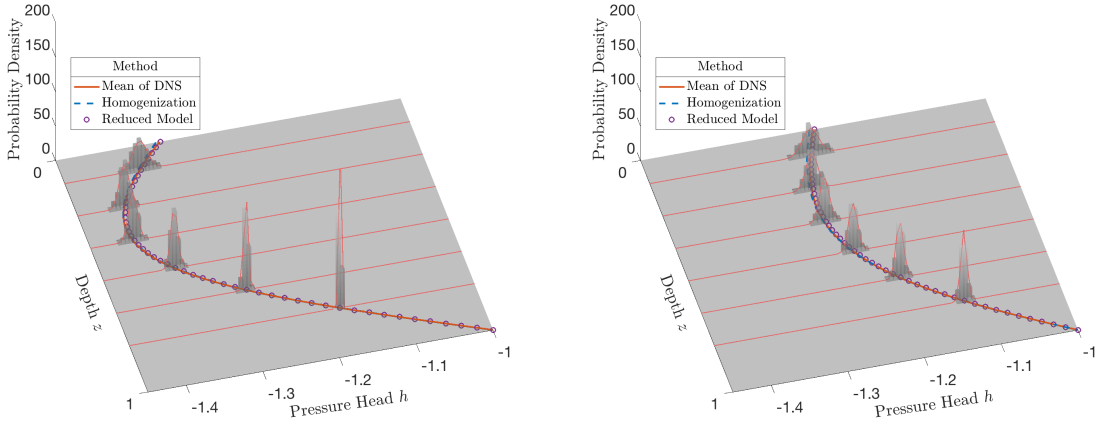

(a) $t = 0.1$

(b) $t = 0.2$

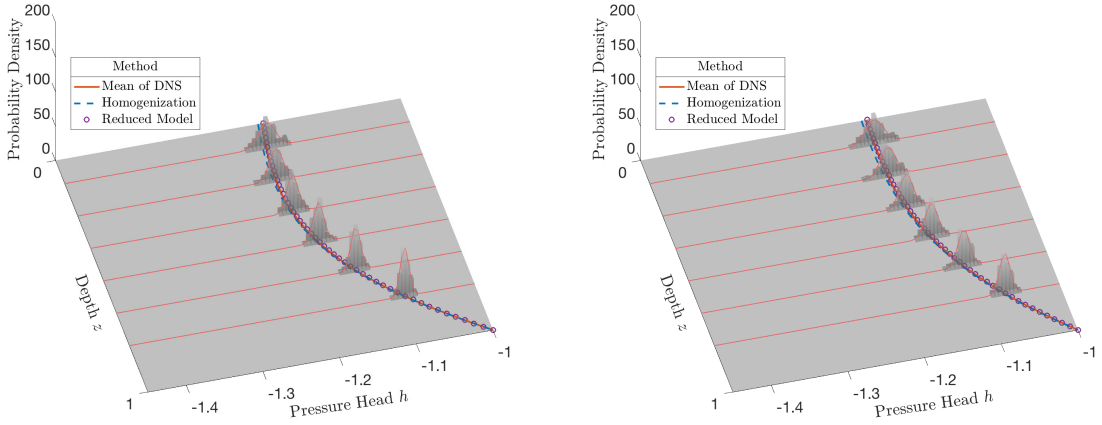

(c) $t = 0.3$

(d) $t = 0.4$

Figure 3.24: Histogram and PDF of DNS When $\sigma_b = 0.2$. The Mean of DNS Is Compared with the Solution Using Homogenized Soil Parameters or the Reduced Model.

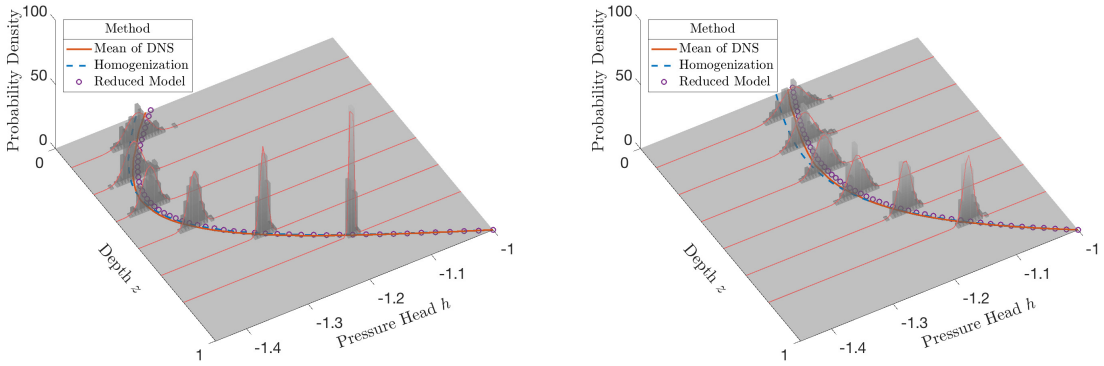

(a) $t = 0.1$

(b) $t = 0.2$

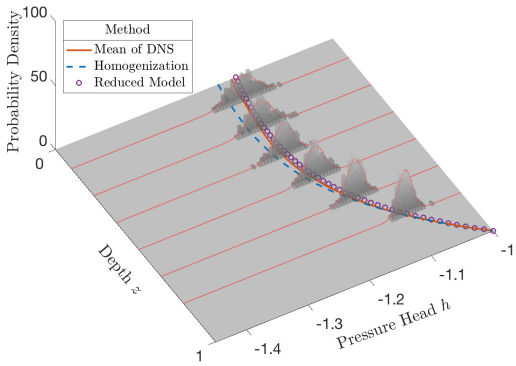

(c) $t = 0.3$

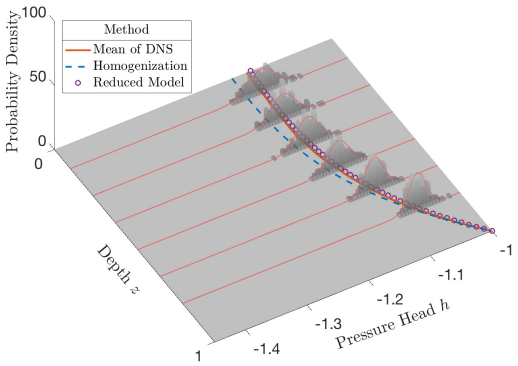

(d) $t = 0.4$

Figure 3.25: Histogram and PDF of DNS When $\sigma_b = 0.4$. The Mean of DNS Is Compared with the Solution Using Homogenized Soil Parameters or the Reduced Model.

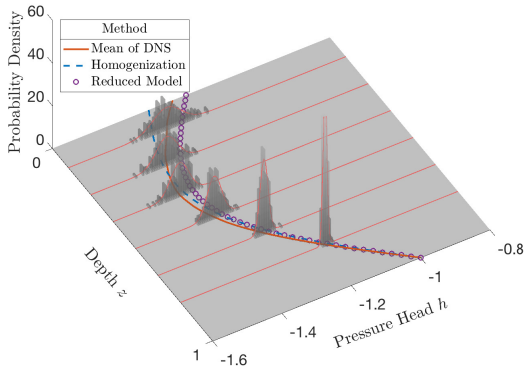

(a) $t = 0.1$

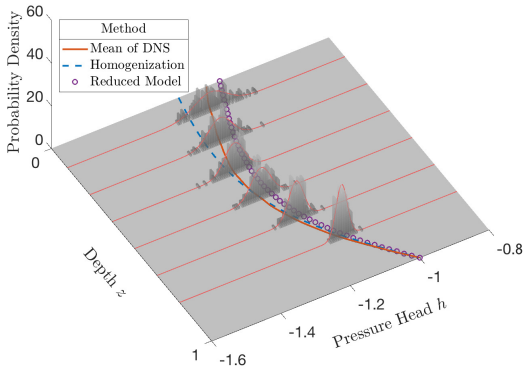

(b) $t = 0.2$

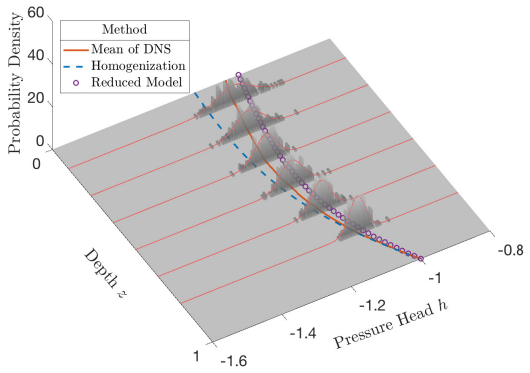

(c) $t = 0.3$

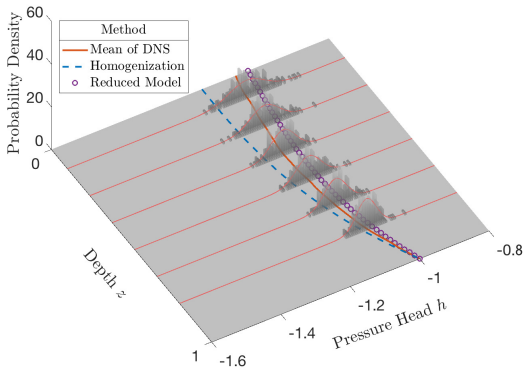

(d) $t = 0.4$

Figure 3.26: Histogram and PDF of DNS When $\sigma_b = 0.8$. The Mean of DNS Is Compared with the Solution Using Homogenized Soil Parameters or the Reduced Model.

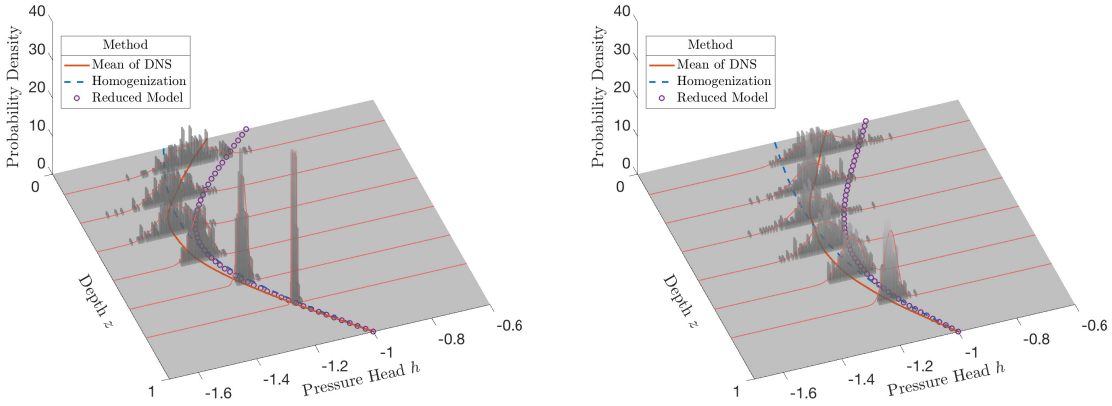

(a) $t = 0.1$ (b) $t = 0.2$

(c) $t = 0.3$ (d) $t = 0.4$

Figure 3.27: Histogram and PDF of DNS When $\sigma_b = 1.2$. The Mean of DNS Is Compared with the Solution Using Homogenized Soil Parameters or the Reduced Model.

Chapter 4

CONCLUSIONS AND FUTURE WORK

4.1 Conclusions

This research work highlights the numerical difficulties in the simulation of transient unsaturated flow in layered soils.

1. The continuity of flux across the interface of soils is often neglected in numerical (including commercial) software. This work addresses numerical difficulties of enforcement of the continuity of both pressure head and flux at soil interfaces, which yields a nonlinear interface problem. This interface problem can have multiple solutions in certain soil parameter regimes and conditions for all three soil hydraulic models (Gardner, MvG, and FXLR). Several factors affect in particular the well-posedness of the interface problem. The size of the spatial discretization around the interface between soil layers is certainly an important factor. This work presents a full mathematical analysis for the Gardner model and the geometric mean for cell-centered conductivities. Explicit criteria in terms of two parameters (μ, λ) identify *a priori* a critical mesh size Δ guaranteeing the uniqueness of the solution to the interface problem. This work shows that the parameter μ can be made small enough by reducing the cell size Δ, and eliminate the multiplicity of roots. The numerical experiments in this work also demonstrate the possibility for ill-posed interface problems using the MvG and FXLR models. The high nonlinearity of more advanced soil hydraulic models (such as MvG and FXLR) indicates difficulties in determining how small Δ should be to guarantee a unique solution to the interface problem. For some cases, especially when a grid size is not fine enough or using a small conductivity

averaging scheme (the harmonic mean), the wrong numerical ponding in simulation results is unrecoverable. In other cases, the occurrence of multiple solutions while the wetting front passes through the interface is a short-term effect that is damped once the front has passed, when pressure head differential (or gradient) gets small again, likely because of diffusive effects. The water content profile (or pressure head profile) after the multiple solutions appear dramatically differs among numerical solutions, especially on coarser grids, and it is unclear which solution makes sense physically. Practitioners who conduct numerical simulations of water flows in layered soils can *a posteriori* set a flag for the existence of multiple solutions to the interface problem during numerical simulations. In addition, use of more advanced models, such as the FXLR model that provides a good match between the hydraulic model and experimental data, can introduce additional challenges to the numerical solution. The MvG and FXLR models are used as a demonstration of this effect herein, but other more sophisticated models may also exhibit multiple roots at soil interfaces.

2. This work shows that the choice of averaging schemes for hydraulic conductivities in staggered formulations of the Richards' equations can substantially impact the numerical solution, in particular the ill-posedness of the interface problem. The harmonic averaging for cell-centered conductivities is not recommended in numerical simulations especially for sophisticated hydraulic models because of its convergency issue. Using the geometric mean, though recommended in many other studies for better accuracy (Haverkamp and Vauclin, 1979; Schnabel and Richie, 1984; Belfort and Lehmann, 2005), can lead to multiple solutions to the interface problem. Using a relatively large average conductivity (e.g., the log-mean and the arithmetic mean) is less likely to trigger the multiplicity of roots to the interface problem. The arithmetic mean of conductivities may however grossly overestimate appropriate average conductivities. The log-mean seems to be appropriate, both physically and numerically,

at least for one-dimensional simulations such as those conducted here.

3. In this work, two techniques dealing with the heterogeneity of a one-dimensional soil are proposed: (1) mean of stochastic realizations with soil hydraulic parameters defined cell-wise via solving interface problems, and (2) a reduced model for stochastic soil hydraulic parameters in the Richards' equation using the Gardner model with the geometric mean of conductivities. Results show that possible variation in pressure head profile (water content profile) can be extensively underestimated in numerical simulations via homogenization of soil hydraulic parameters. In contrast, the solution of the reduced model and the mean of stochastic realizations exhibit the same tendency of variation in pressure head in the infiltration process presented in this work. Compared to the solution using homogenized parameters, the reduced model and the mean of stochastic realizations show larger pressure head in the top part of the soil column and smaller pressure head near bottom in infiltration process. The reduced model successfully modeled variation in soil parameters, namely the saturated hydraulic conductivity, and agrees with the mean of stochastic realizations. In addition, the larger the variation in saturated hydraulic conductivity, the larger the variation in the solution of the reduced model than the mean of stochastic realizations. In addition, the large variability of flow profiles in the stochastic realizations indicates that a small change in the initial/boundary conditions or in the soil hydraulic properties can lead to large variations in flow profiles and can be visualized as "fingers" in two-dimensional or three-dimensional simulations.

4.2 Future Work

4.2.1 2D Cracked Soil

This research only focuses on one-dimensional (vertical) soils. Unsaturated flow in 1D layered soils can be generalized to two-dimensional soils. Although the simulation in 2D is similar to that in 1D, 2D models will take into account the multiple interfaces in all directions rather than merely vertically, e.g. in fractured soils. The future work will study the multiplicity of the numerical solutions and determine conditions for uniqueness of solution and stability/convergence of iterative solutions for the interface problems. We plan to apply the above interface strategies to model cracked soils (e.g. in dry areas such as Arizona) and determine how the crack pattern affects the infiltration flow of water in the soil. In turn the flow affects swelling properties and possible shifts in soils, an issue which plays an important role in geotechnical engineering, as it controls the depth of layer in remove-replace strategies for building foundations. In 1D, we use a finite difference approach, however, finite element methods can be used to model cracks in 2D, and we plan to develop a version of the interface problem in this more general setting.

4.2.2 Fingering Effect

The multiplicity of roots of the interface problem at small (but finite) discretization sizes is ultimately related to the fact that the Richards' equation is not far from being ill-posed. Another instance of instabilities triggered by small perturbations (via a fourth-order spatial derivative of the saturation) of the continuous Richards' equation has, for example, been used to model the so-called "fingering effect".

A modification of the Richards' equation to include fingering effects, associated to preferential vertical infiltration and modeled by a "correction" term involving a

fourth-order spatial derivative of the saturation, was formulated by Cueto-Felgueroso and Juanes (2008, 2009). The fingering effect is a phenomenon that the wetting front forms a finger-like contact when water infiltrates into initially dry soil.

The one-dimensional modified Richards' equation is,

$$\frac{\partial \theta}{\partial t} = -\frac{\partial}{\partial z}\left(K\left(1 - \frac{\partial h}{\partial z} - \alpha \frac{\partial^3 \theta}{\partial z^3}\right)\right), \tag{4.1}$$

where $0 < \alpha < 1$.

The last term in the modified form of the Richards' equation is a destabilizing term. For instance, assuming that h is linear with respect to z, the first and second terms vanish on the right-hand side of Equation (4.1). It yields a fourth-order partial derivative equation

$$\theta_t = \theta_{zzzz} \tag{4.2}$$

where the coefficient α can be scaled to one by multiplying the variables by constants. Assume that we can use separation of variables, i.e., $\theta(t, z) = f(t)g(z)$. The equation yields $f'(t)g(z) = f(t)g''''(z)$. Let

$$\frac{f'(t)}{f(t)} = \frac{g''''(z)}{g(z)} = \lambda, \tag{4.3}$$

then $f(t) = e^{\lambda t}$. Assuming $g(z) = e^{irz}$ with real number r, it yields $r^4 = \lambda > 0$ (a dispersion relation). It implies that the solutions $\theta(t, z)$ is unstable.

There is another way to show that θ is unstable. Define

$$E = \frac{1}{2}\int_\Omega \theta^2 \, dz, \tag{4.4}$$

where Ω is a given spatial domain with fixed θ values for boundary conditions.

Then

$$\frac{dE}{dt} = \int_\Omega \theta\theta_t \, dz = \int_\Omega \theta\theta_{zzzz} \, dz = \int_\Omega \theta_{zz}^2 \, dz > 0, \tag{4.5}$$

thus, the solution $\theta(t, z)$ is unstable.

In the modified Richards' equation, $\alpha = 0$ corresponds to the original Richards' equation and implies well-posedness with unique solution to the interface problem; but for $\alpha > 0$, instabilities and chaotic solutions may occur. This indicates a potential connection between the modified Richards' equation and the interface problems in heterogeneous soils. Similar to the large variability of flow profiles in heterogeneous soils, the impact of the extra unstable term in the modified Richards' equation can also be visualized as "fingers" in 2D/3D simulations. The "hold-back-pile-up" effect has been discussed in one-dimensional simulations using the modified Richards' equation (Eliassi and Glass, 2002). How the destabilizing term behaves and impacts the one-dimensional numerical solution is still unclear. The future work of this research will focus on the variation and instabilities of the numerical solution of the modified Richards' equation and aim to study its connection to the reduced model for stochastic soil hydraulic parameters.

REFERENCES

An, H. and S. J. Noh, "High-order averaging method of hydraulic conductivity for accurate soil moisture modeling", Journal of Hydrology **516**, 119–130 (2014).

Andersson, J. and A. M. Shapiro, "Stochastic analysis of one-dimensional steady state unsaturated flow: A Comparison of Monte Carlo and Perturbation Methods", Water Resources Research **19**, 1, 121–133 (1983).

Baker, D. L., "General validity of conductivity means in unsaturated flow models", Journal of Hydrologic Engineering **11**, 6, 526–538 (2006).

Belfort, B. and F. Lehmann, "Comparison of equivalent conductivities for numerical simulation of one-dimensional unsaturated flow", Vadose Zone Journal **4**, 4, 1191–1200 (2005).

Biggar, J. and D. Nielsen, "Spatial variability of the leaching characteristics of a field soil", Water Resources Research **12**, 1, 78–84 (1976).

Brunone, B., M. Ferrante, N. Romano and A. Santini, "Numerical simulations of one-dimensional infiltration into layered soils with the Richards equation using different estimates of the interlayer conductivity", Vadose Zone Journal **2**, 2, 193–200 (2003).

Carsel, R. F. and R. S. Parrish, "Developing joint probability distributions of soil water retention characteristics", Water Resources Research **24**, 5, 755–769 (1988).

Celia, M. A., E. T. Bouloutas and R. L. Zarba, "A general mass-conservative numerical solution for the unsaturated flow equation", Water resources research **26**, 7, 1483–1496 (1990).

Cueto-Felgueroso, L. and R. Juanes, "Nonlocal interface dynamics and pattern formation in gravity-driven unsaturated flow through porous media", Physical Review Letters **101**, 24, 244504 (2008).

Cueto-Felgueroso, L. and R. Juanes, "Adaptive rational spectral methods for the linear stability analysis of nonlinear fourth-order problems", Journal of Computational Physics **228**, 17, 6536–6552 (2009).

Dye, H. B., *Moisture movement through expansive soil and impact on performance of residential structures*, Ph.D. thesis, Arizona State University, Tempe, Arizona, USA (2008).

Eliassi, M. and R. J. Glass, "On the porous-continuum modeling of gravity-driven fingers in unsaturated materials: Extension of standard theory with a hold-back-pile-up effect", Water Resources Research **38**, 11, 16–1 (2002).

Foussereau, X., W. Graham and P. Rao, "Stochastic analysis of transient flow in unsaturated heterogeneous soils", Water resources research **36**, 4, 891–910 (2000).

Fredlund, D. G., H. Rahardjo and M. D. Fredlund, *Unsaturated soil mechanics in engineering practice* (John Wiley & Sons, 2012).

Fredlund, D. G. and A. Xing, "Equations for the soil-water characteristic curve", Canadian geotechnical journal **31**, 4, 521–532 (1994).

Gardner, W., "Some steady-state solutions of the unsaturated moisture flow equation with application to evaporation from a water table.", Soil science **85**, 4, 228–232 (1958).

Haskett, J. D., Y. A. Pachepsky and B. Acock, "Use of the beta distribution for parameterizing variability of soil properties at the regional level for crop yield estimation", Agricultural Systems **48**, 1, 73–86 (1995).

Haverkamp, R. and M. Vauclin, "A note on estimating finite difference interblock hydraulic conductivity values for transient unsaturated flow problems", Water Resources Research **15**, 1, 181–187 (1979).

Hills, R., I. Porro, D. Hudson and P. Wierenga, "Modeling one-dimensional infiltration into very dry soils: 1. Model development and evaluation", Water Resources Research **25**, 6, 1259–1269 (1989).

Kirkland, M. R., R. Hills and P. Wierenga, "Algorithms for solving Richards' equation for variably saturated soils", Water Resources Research **28**, 8, 2049–2058 (1992).

Leong, E. C. and H. Rahardjo, "Permeability functions for unsaturated soils", Journal of Geotechnical and Geoenvironmental Engineering **123**, 12, 1118–1126 (1997).

Liu, R., B. Welfert and S. Houston, "Comparison of averaging methods for interface conductivities in one-dimensional unsaturated flow in layered soils", in "VIIIth International Symposium on Stratified Flows", vol. 1 (2016a).

Liu, R., B. Welfert and S. Houston, "Numerical issues arising in determination of interlayer conductivities in layered unsaturated soils", International Journal of Geomechanics p. 04016078 (2016b).

Liu, Z., Y. Zha, W. Yang, Y.-M. Kuo and J. Yang, "Large-scale modeling of unsaturated flow by a stochastic perturbation approach", Vadose Zone Journal **15**, 3 (2016c).

Mantoglou, A. and L. W. Gelhar, "Stochastic modeling of large-scale transient unsaturated flow systems", Water Resources Research **23**, 1, 37–46 (1987).

Matthews, C. J., R. D. Braddock and G. Sander, "Modeling flow through a one-dimensional multi-layered soil profile using the Method of Lines", Environmental Modeling & Assessment **9**, 2, 103–113 (2004).

Nielsen, D., J. Biggar, K. Erh *et al.*, "Spatial variability of field-measured soil-water properties", California Agriculture **42**, 7, 215–259 (1973).

Richards, L. A., "Capillary conduction of liquids through porous mediums", Physics **1**, 5, 318–333, URL `http://dx.doi.org/10.1063/1.1745010` (1931).

Richardson, L. F., *Weather prediction by numerical process* (Cambridge, The University press, 1922).

Romano, N., B. Brunone and A. Santini, "Numerical analysis of one-dimensional unsaturated flow in layered soils", Advances in Water Resources **21**, 4, 315–324 (1998).

Russo, D. and M. Bouton, "Statistical analysis of spatial variability in unsaturated flow parameters", Water Resources Research **28**, 7, 1911–1925 (1992).

Schaudt, K. and J. Morrill, "On the treatment of heterogeneous interfaces in soil", Geophysical research letters **29**, 10, 34–1 (2002).

Schnabel, R. and E. Richie, "Calculation of internodal conductances for unsaturated flow simulations: A comparison", Soil Science Society of America Journal **48**, 5, 1006–1010 (1984).

Severino, G. and A. Santini, "On the effective hydraulic conductivity in mean vertical unsaturated steady flows", Advances in water resources **28**, 9, 964–974 (2005).

Simunek, J., M. Sejna and R. van Genuchten, "HYDRUS-1D manual of versions 2.0", US Salinity Laboratory, Riverside, CA (1998).

Socha, L., *Linearization methods for stochastic dynamic systems*, vol. 730 (Springer Science & Business Media, 2007).

Srivastava, R. and T.-C. J. Yeh, "Analytical solutions for one-dimensional, transient infiltration toward the water table in homogeneous and layered soils", Water Resour. Res **27**, 5, 753–762 (1991).

Szymkiewicz, A. and R. Helmig, "Comparison of conductivity averaging methods for one-dimensional unsaturated flow in layered soils", Advances in Water Resources **34**, 8, 1012–1025 (2011).

Ünlü, K., D. Nielsen and J. Biggar, "Stochastic analysis of unsaturated flow: One-dimensional monte carlo simulations and comparisons with spectral perturbation analysis and field observations", Water Resources Research **26**, 9, 2207–2218 (1990).

van Dam, J. C. and R. A. Feddes, "Numerical simulation of infiltration, evaporation and shallow groundwater levels with the richards equation", Journal of Hydrology **233**, 1, 72–85 (2000).

van Genuchten, M. T., "A closed-form equation for predicting the hydraulic conductivity of unsaturated soils", Soil science society of America journal **44**, 5, 892–898 (1980).

Wierenga, P., R. Hills and D. Hudson, "The las cruces trench site: Characterization, experimental results, and one-dimensional flow predictions", Water Resources Research **27**, 10, 2695–2705 (1991).

Yeh, T.-C. J., L. W. Gelhar and A. L. Gutjahr, "Stochastic analysis of unsaturated flow in heterogeneous soils: 1. Statistically isotropic media", Water Resources Research **21**, 4, 447–456 (1985a).

Yeh, T.-C. J., L. W. Gelhar and A. L. Gutjahr, "Stochastic analysis of unsaturated flow in heterogeneous soils: 2. statistically anisotropic media with variable α", Water Resources Research **21**, 4, 457–464 (1985b).

Yeh, T.-C. J., L. W. Gelhar and A. L. Gutjahr, "Stochastic analysis of unsaturated flow in heterogeneous soils: 3. observations and applications", Water Resources Research **21**, 4, 465–471 (1985c).

Zha, Y., J. Yang, L. Shi and X. Song, "Simulating one-dimensional unsaturated flow in heterogeneous soils with water content-based Richards equation", Vadose Zone Journal **12**, 2 (2013).

Zhu, J. and B. P. Mohanty, "Spatial averaging of van genuchten hydraulic parameters for steady-state flow in heterogeneous soils", Vadose Zone Journal **1**, 2, 261–272 (2002).

Zhu, J., B. P. Mohanty, A. W. Warrick and M. T. h. van Genuchten, "Correspondence and upscaling of hydraulic functions for steady-state flow in heterogeneous soils", Vadose Zone J. **3**, 527–533 (2004).

APPENDIX A

EXPLICIT CRITERIA FOR GARDNER MODEL WITH GEOMETRIC MEAN

A.1 Number of Roots of Equation (2.24)

For the Gardner model, the equation $r = g(r)$ is equivalent to

$$\varphi(r) := \ln g(r) - \ln r = \ln \lambda + \mu \, \frac{1-r}{1+r} - \ln r = 0. \tag{A.1}$$

Note that $\varphi(0^+) = +\infty$ and $\varphi(+\infty) = -\infty$ so φ vanishes at at least one value of r. The derivative

$$\varphi'(r) = -\frac{2\mu}{(1+r)^2} - \frac{1}{r}$$

vanishes for r solution of the quadratic equation $(1+r)^2 = -2\mu r$, i.e.,

$$r = r^{\pm} := -(1+\mu) \pm \sqrt{\mu(\mu+2)}. \tag{A.2}$$

For $\mu \geq 0$ both roots are real but negative, while for $-2 < \mu < 0$ the roots are complex conjugate. In both cases φ is monotonic for $r > 0$ and Equation (2.24) admits a unique solution.

If $\mu < -2$ then $0 < r^- < r^+$. Equation (2.24) therefore admits three roots if $\varphi(r^-) < 0$ and $\varphi(r^+) > 0$. These two conditions are equivalent to

$$\ln r^+ - \mu \, \frac{1-r^+}{1+r^+} < \ln \lambda < \ln r^- - \mu \, \frac{1-r^-}{1+r^-}, \tag{A.3}$$

which reduces to

$$|\ln \lambda| < \sqrt{\mu(2+\mu)} + \ln \left| 1 + \mu + \sqrt{\mu(2+\mu)} \right| \tag{A.4}$$

using $r^- r^+ = 1$. For $\mu = -2$ the function φ' vanishes at the double root $r = 1$, in which case Equation (2.24) has a single root if $\lambda \neq 1$ and the triple root $r = 1$ if $\lambda = 1$.

A.2 Stability of Fixed-Point Iteration

The fixed-point iteration (2.16) for the Gardner case (2.24) is guaranteed to converge (locally) if $|g'(r)| < 1$ for r such that $g(r) = r$, which is equivalent to

$$\frac{1}{r} > \frac{|g'(r)|}{r} = \frac{|g'(r)|}{|g(r)|} = \left|\frac{d}{dr}\ln g(r)\right| = \left|\varphi'(r) + \frac{1}{r}\right| = \frac{2|\mu|}{(1+r)^2}. \tag{A.5}$$

On the boundary of the stability domain in (μ, λ)-space the relations $(1+r)^2 = 2|\mu|r$ and $g(r) = r$ hold. The first relation yields,

$$\hat{r} = \hat{r}^{\pm} := |\mu| - 1 \pm \sqrt{|\mu|(|\mu| - 2)} > 0, \tag{A.6}$$

where

$$|\mu| = \frac{1}{2}\left(r + \frac{1}{r}\right) + 1 \geq 2.$$

The second relation yields

$$\ln\lambda = \ln r - \mu\frac{1-r}{1+r}. \tag{A.7}$$

If $\mu < -2$, $\hat{r}^{\pm}$ is equivalent to (A.2). The stability region overlaps the region of single root condition (A.4) for $\mu < -2$.

If $\mu > 2$, substituting $\hat{r}^{\pm}$ in Equation (A.7) yields

$$|\ln\lambda| = \sqrt{\mu(\mu-2)} - \ln\left(\mu - 1 - \sqrt{\mu(\mu-2)}\right), \tag{A.8}$$

using $\hat{r}^{-}\hat{r}^{+} = 1$. It determines the boundary of the shaded region in Figure 2.7.

APPENDIX B

REDUCTION IN STOCHASTIC EQUATIONS

B.1 Reduction in Equation (2.44)

For a multi-variable function $q_i(\boldsymbol{b}, \boldsymbol{\theta})$ in Equation (2.44), its Taylor expansion about $(\bar{\boldsymbol{b}}, \bar{\boldsymbol{\theta}})$ consists of three parts – (a) only with $\boldsymbol{\delta b}$ or none, (b) only with $\boldsymbol{\delta\theta}$, and (c) with both. Because the parameter b describes the variability of soil properties and results in the variability in water content θ (and S_e, h), b is considered as the primary variable. A full expansion of the terms with $\boldsymbol{\delta b}$ (i.e., part (a)) is maintained. For the other two parts with $\boldsymbol{\delta\theta}$, the expansion is truncated up to second-order, because the probability distribution of θ is unknown and the reduced model only includes covariances involving θ.

Notice that the expression of part (a) is equivalent to the Taylor expansion of $q_i(\boldsymbol{b}, \bar{\boldsymbol{\theta}})$ about $\bar{\boldsymbol{b}}$ with

$$q_i(\boldsymbol{b}, \bar{\boldsymbol{\theta}}) = \exp\left\{\frac{b_i + b_{i+1}}{2}\right\}\sqrt{(\bar{S}_e)_i(\bar{S}_e)_{i+1}}\left(1 - \frac{\bar{h}_{i+1} - \bar{h}_i}{\Delta}\right). \tag{B.1}$$

By the local scheme used in this research, q_i is only dependent on b_i and b_{i+1}. As stated in Section 3.3, b_i and b_{i+1} are independent and have the same normal distribution $\mathcal{N}(\bar{b}, \sigma_b^2)$. It notes that, for the lognormal distribution defined as $X = e^{\mu+\sigma Z}$ with Z a standard normally distributed variable, the expectation is $E[X] = e^{\mu+\sigma^2/2}$. Considering $b_i/2, b_{i+1}/2 \sim \mathcal{N}(\bar{b}/2, \sigma_b^2/4)$,then

$$E[e^{b_i/2}] = E[e^{b_{i+1}/2}] = e^{\bar{b}/2}e^{\sigma_b^2/8}. \tag{B.2}$$

Therefore,

$$\begin{aligned} E[q_i(\boldsymbol{b}, \bar{\boldsymbol{\theta}})] &= \sqrt{(\bar{S}_e)_i(\bar{S}_e)_{i+1}}\left(1 - \frac{\bar{h}_{i+1} - \bar{h}_i}{\Delta}\right)E[e^{b_i/2}]E[e^{b_{i+1}/2}] \\ &= e^{\bar{b}}\sqrt{(\bar{S}_e)_i(\bar{S}_e)_{i+1}}\left(1 - \frac{\bar{h}_{i+1} - \bar{h}_i}{\Delta}\right)e^{\sigma_b^2/4} \\ &= q_i(\bar{\boldsymbol{b}})e^{\sigma_b^2/4}. \end{aligned} \tag{B.3}$$

This provides an expression for part (a), i.e., the first term in (2.44). The other two terms in (2.44) correspond to truncated parts (b) and (c), respectively.

B.2 Reduction in Equation (2.63)

To find a closed-form expression for

$$\sum_{k_1+\cdots+k_n\geq 1} \frac{1}{k_1!k_2!\cdots k_n!}\left(D_{b_1^{k_1}\cdots b_n^{k_n}} q_i(\bar{\boldsymbol{b}},\bar{\boldsymbol{\theta}})\right) E\left[(\delta b_1)^{k_1}\cdots(\delta b_n)^{k_n}(\boldsymbol{\delta b})\right], \tag{B.4}$$

separate the first term (i.e., for $k_1+\cdots+k_n=1$) and estimate the sum of the rest.

With the assumption that b_i and b_{i+1} are independent and have the same normal distribution,

$$\overline{\delta b_i^{k_1+1}\delta b_i^{k_2}} = \overline{\delta b_i^{k_1+1}}\cdot\overline{\delta b_i^{k_2}}, \quad \overline{\delta b_i^{k_1}\delta b_i^{k_2+1}} = \overline{\delta b_i^{k_1}}\cdot\overline{\delta b_i^{k_2+1}}.$$

By the fact that odd central moments of a normal distribution are zero and even central moments are $\sigma_b^{2k}(2k-1)!!$ for any positive integer k (the expressions of the central moments can be found, for example, in Socha (2007)), also notice that q_i only depends on index i and $i+1$, the first term yields

$$\sum_{j=1}^{n}\left(D_{b_j} q_i(\bar{\boldsymbol{b}},\bar{\boldsymbol{\theta}})\right) E\left[(\delta b_j)(\boldsymbol{\delta b})\right] = \sigma_b^2 D_{\boldsymbol{b}} q_i(\bar{\boldsymbol{b}},\bar{\boldsymbol{\theta}}), \tag{B.5}$$

and by (2.36), the rest of (B.4) yields,

$$\begin{bmatrix} \vdots \\ 0 \\ \displaystyle\sum_{k_1+k_2\geq 2} \frac{q_i(\bar{\boldsymbol{b}},\bar{\boldsymbol{\theta}})}{k_1!k_2!2^{k_1+k_2}}\,\overline{\delta b_i^{k_1+1}\delta b_{i+1}^{k_2}} \\ \displaystyle\sum_{k_1+k_2\geq 2} \frac{q_i(\bar{\boldsymbol{b}},\bar{\boldsymbol{\theta}})}{k_1!k_2!2^{k_1+k_2}}\,\overline{\delta b_i^{k_1}\delta b_{i+1}^{k_2+1}} \\ 0 \\ \vdots \end{bmatrix}. \tag{B.6}$$

Here

$$\begin{aligned} &\sum_{k_1+k_2\geq 2} \frac{q_i(\bar{\boldsymbol{b}},\bar{\boldsymbol{\theta}})}{k_1!k_2!2^{k_1+k_2}}\,\overline{\delta b_i^{k_1+1}\delta b_{i+1}^{k_2}} \\ =\;& q_i(\bar{\boldsymbol{b}},\bar{\boldsymbol{\theta}})\sum_{p=1}^{\infty}\sum_{q=1}^{\infty}\frac{\sigma_b^{2p+2q}(2p-1)!!(2q-1)!!}{(2p-1)!(2q)!2^{2p+2q-1}} \\ =\;& q_i(\bar{\boldsymbol{b}},\bar{\boldsymbol{\theta}})\sum_{p=1}^{\infty}\sum_{q=1}^{\infty}\frac{\sigma_b^{2p+2q}}{(2p-2)!!(2q)!!2^{2p+2q-1}} \\ =\;& q_i(\bar{\boldsymbol{b}},\bar{\boldsymbol{\theta}})\sum_{p=1}^{\infty}\sum_{q=1}^{\infty}\frac{\sigma_b^{2p+2q}}{(p-1)!q!2^{3p+3q-2}} \\ =\;& q_i(\bar{\boldsymbol{b}},\bar{\boldsymbol{\theta}})\sum_{m=2}^{\infty}\sum_{p=1}^{m-1}\frac{\sigma_b^{2m}}{(p-1)!(m-p)!2^{3m-2}}. \end{aligned} \tag{B.7}$$

For the last double series,

$$\begin{aligned}
&\sum_{m=2}^{\infty}\sum_{p=1}^{m-1}\frac{\sigma_b^{2m}}{(p-1)!(m-p)!2^{3m-2}} \\
=\;&\sum_{m=2}^{\infty}\frac{\sigma_b^{2m}}{(m-1)!2^{3m-2}}\sum_{p=1}^{m-1}\frac{(m-1)!}{(p-1)!(m-p)!} \\
=\;&\sum_{m=2}^{\infty}\frac{\sigma_b^{2m}}{(m-1)!2^{3m-2}}(2^{m-1}-1) \\
=\;&\sum_{m=1}^{\infty}\frac{\sigma_b^{2m+2}}{m!2^{3m+1}}(2^m-1) \\
=\;&\frac{\sigma_b^2}{2}\sum_{m=1}^{\infty}\frac{\sigma_b^{2m}}{2^{2m}m!}-\frac{\sigma_b^2}{2}\sum_{m=1}^{\infty}\frac{\sigma_b^{2m}}{2^{3m}m!} \\
=\;&\frac{\sigma_b^2}{2}\left(e^{\sigma_b^2/4}-1\right)-\frac{\sigma_b^2}{2}\left(e^{\sigma_b^2/8}-1\right) \\
=\;&\frac{\sigma_b^2}{2}\left(e^{\sigma_b^2/4}-e^{\sigma_b^2/8}\right). \qquad \text{(B.8)}
\end{aligned}$$

Similarly, the $(i+1)$-th term yields the same result, and then the expression (B.6) reduces to

$$q_i(\bar{\boldsymbol{b}},\bar{\boldsymbol{\theta}})\frac{\sigma_b^2}{2}\left(e^{\sigma_b^2/4}-e^{\sigma_b^2/8}\right)(\vec{e}_i+\vec{e}_{i+1}), \qquad \text{(B.9)}$$

with $\vec{e}_i, \vec{e}_{i+1}$ standard basis vectors.

Adding (B.5) and (B.9) makes part of the i-th column of $(\boldsymbol{\delta b})\cdot\left(\dfrac{d\boldsymbol{\delta\theta}}{dt}\right)^T$, in matrix form, it becomes

$$\frac{\sigma_b^2}{2}\left(1+e^{\sigma_b^2/4}-e^{\sigma_b^2/8}\right)P \qquad \text{(B.10)}$$

with

$$P=\begin{bmatrix}
q_1(\bar{\boldsymbol{b}},\bar{\boldsymbol{\theta}}) & 0 & 0 & \dots & 0 \\
q_1(\bar{\boldsymbol{b}},\bar{\boldsymbol{\theta}}) & q_2(\bar{\boldsymbol{b}},\bar{\boldsymbol{\theta}}) & 0 & \dots & 0 \\
0 & q_2(\bar{\boldsymbol{b}},\bar{\boldsymbol{\theta}}) & q_3(\bar{\boldsymbol{b}},\bar{\boldsymbol{\theta}}) & \dots & 0 \\
0 & 0 & q_3(\bar{\boldsymbol{b}},\bar{\boldsymbol{\theta}}) & \ddots & 0 \\
0 & 0 & 0 & \ddots & q_n(\bar{\boldsymbol{b}},\bar{\boldsymbol{\theta}}) \\
0 & 0 & 0 & \dots & q_n(\bar{\boldsymbol{b}},\bar{\boldsymbol{\theta}})
\end{bmatrix}. \qquad \text{(B.11)}$$

APPENDIX C

NUMERICAL IMPLEMENTATIONS

C.1 Non-Dimensionalization Method

The following variables/parameters are non-dimensionalized (scaled). The superscript * indicates the real measurements of the quantities.

1. The total soil depth, L, is normalized using the real total depth L^* as a reference. Then the scaled depth is
$$z = \frac{z^*}{L^*} \in [0, 1].$$

2. The volumetric water content θ and the effective saturation S_e have no units of measurements, so
$$\theta = \theta^*, \quad S_e = {S_e}^*.$$

3. The hydraulic conductivity, K, and the saturated hydraulic conductivity, β, are scaled by a reference saturated conductivity ${K_s}^*$, i.e.,
$$K = \frac{K^*}{{K_s}^*}, \quad \beta = \frac{\beta^*}{{K_s}^*}.$$
For numerical experiments presented in this work, the value of ${K_s}^*$ is determined by the real saturated conductivity value in one of the soil layers. In particular, the soil layer chosen as the reference has a scaled saturated conductivity one (i.e., $\beta = 1$).

4. The non-dimensionalized pressure head is
$$h = \frac{h^*}{L^*}.$$

5. The scaled time is
$$t = \frac{{K_s}^*}{L^*} t^*.$$

6. The parameter α in all three models used in this work (Gardner, MvG, and FXLR) is associated with h, and thus should be scaled as
$$\alpha = L^* \alpha^*.$$
Hence, $\alpha h = \alpha^* h^*$.
Other parameters, n, m and p in the MvG and FXLR models are dimensionless curve-fitting parameters. They do not need to be scaled, i.e.,
$$n = n^*, \quad m = m^*, \quad p = p^*.$$

Therefore, the mixed form of Richards' equation with real measurements
$$\frac{\partial \theta^*}{\partial t^*} = -\frac{\partial}{\partial z^*}\left(K^*\left(1 - \frac{\partial h^*}{\partial z^*}\right)\right)$$
is equivalent to the equation with non-dimensionalized quantities
$$\frac{\partial \theta}{\partial t} = -\frac{\partial}{\partial z}\left(K\left(1 - \frac{\partial h}{\partial z}\right)\right).$$

C.2 Indexing for Various Boundary Conditions

The numerical scheme proposed in this research can be easily adjusted to Dirichlet or Neumann or mixed boundary conditions. However, the discrete scheme should be used with caution, in other words, flux q must be evaluated on cell-centered grids and water content θ on nodal grids. If a layered soil is considered, soil interfaces must coincide with flux grids. The discretized mesh of a vertical soil column and its indexing should be addressed as shown in Figures C.1.

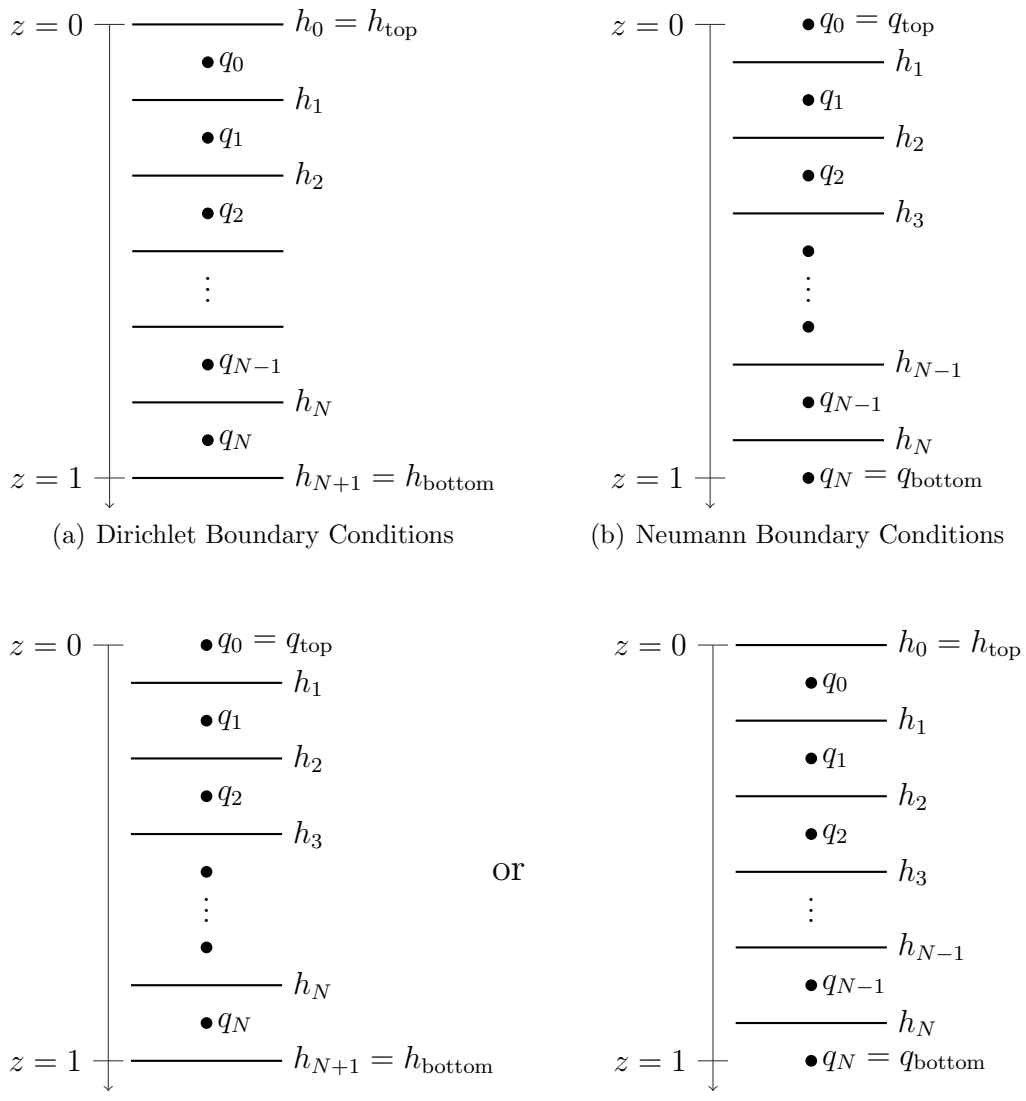

(a) Dirichlet Boundary Conditions

(b) Neumann Boundary Conditions

(c) Mixed Boundary Conditions

Figure C.1: Mesh Indexing for Various Boundary Conditions.

C.3 Solving the Interface Equation by Iterative Methods

In order to solve the interface equation (2.15), various root-finding methods can be used, for example, the "fzero" function in MATLAB. However, due to the nonlinearity of the interface equation and its propensity to have multiple roots, this work uses iterative methods instead of external root-finding packages. A Picard iteration (2.16) or a Newton iteration (2.17) is used to solve the interface equation in numerical experiments. It is also worth noting that a Picard iteration can possibly leads to a 2-cycle solution which does not converge to the correct root. Using a Newton iteration can be computational inefficient. A full analysis and comparison of the iteration methods for the Gardner model with the geometric mean of conductivities can be found in Section 2.3.2 and 3.1.1.

In this work, the iteration method (Picard or Newton) for the interface equation $r = g(r)$ starts with an initial guess $r_0 = 1$.

After the first successful time step, in general, r_0 is set to the last solution r obtained at the previous successful time integration step. If the iteration method appears to diverge, a new value of r_0 is generated automatically from a logarithmically spaced partition of r values. r_0 is then set to either of the grid values when the sign of $(r - g(r))$ changes. Then the iteration restarts with the new r_0.

In an agent-based model of heterogeneous soils (cell-wise layers), $r_0 = 1$ is always used regardless of the previous successful r.

Setting r_0 equal to r in the last successful time step typically (but not always) avoids positive extrapolated pressure heads h_j^+, h_{j+1}^-.

The existence of multiple solutions to Equation (2.15) is examined in each time iteration step by locating (μ, λ) in Figure 2.7 for the Gardner model. For the MvG or FXLR model, a fixed logarithmically spaced partition of r from 10^{-5} to 10^5 (or 10^{-10} to 10^{10}) is used to count sign changes of $(r - g(r))$. If the number of sign changes is greater than one, Equation (2.15) exhibits multiple solutions.

In addition, the existence of multiple solutions can lead to positive extrapolated pressure heads in Equation (2.11). To isolate the impact of multiple solutions, suitable hydraulic parameters and spatial discretization size is chosen to exclude positive extrapolated pressure heads in the numerical examples unless specifically pointed out otherwise.

C.4 Using DVODE

The Variable-coefficient Ordinary Differential Equation solver (VODE) is a Fortran 90 package to solve the initial value problem of first order ODEs. DVODE is the double precision version of VODE.

To avoid failure of convergence, each numerical simulation limits the maximum time integration step size (HMAX) in DVODE. The tolerance of the DVODE solver and the tolerance of the iteration method are set according to the models. Changing the tolerance of the solver can affect adaptive time integration steps and thereby influence the existence of multiple solutions to the interface problem, since the occurrence of the multiple solutions may be transient. This work only focus on comparing numerical solutions with and without multiple solutions by changing the spatial discretization size for fixed tolerance settings. This work does not deal with integration time step size in solving the Richards' equation because DVODE uses an adaptive time stepping strategy.

C.5 Using OpenMP

The Open Multi-Processing (OpenMP), specifically PARALLEL DO, is used in the following situations:

1. Evaluating volumetric water content θ, pressure head h, hydraulic conductivity K and effective saturation S_e based on the specified hydraulic model associated with different layers. The soil hydraulic properties are distinct for each layer, so are the soil hydraulic functions. The combined parallel work-sharing constructs for do-loop are applied.

2. Solving more than one interface equations with parallel regions. Notice that the parallel regions must be used with caution. In the parallel regions, set private attribute to variables $r, h_j, h_{j+1}, h_j^+, h_{j+1}^-, k_j, k_{j+1}, k_j^+, k_{j+1}^-, q_{j+\frac{1}{2}}$ and other local variables associated with individual interfaces.

3. When evaluating cell-centered conductivity values in the multi-layer soil case, although the array expressions and array intrinsic functions are applied inside each layer, parallel regions are used in the do-loop for multiple layers.

4. Specifically, OpenMP is also used for evaluation of the log-mean since the log-mean fails if the two conductivities are very close, in the sense that a near zero denominator is involved. An if condition is added to the log-mean subroutine to exclude the case when the difference of two neighboring conductivities is less than 10ϵ, where ϵ is the machine epsilon. Otherwise, use the smaller value of them for the cell-centered conductivity. Under this condition, an array-type expression is not available for the log-mean, thus parallel regions are used.